

國立交通大學

電子物理研究所

博士論文

液態晶體表面配向之新方法及其特性研究

Study of Liquid Crystal Surface Alignment: New
Methods and the Properties

The logo of National Tsing Hua University is a circular emblem with a blue border. Inside the circle, there is a stylized representation of a building or a traditional Chinese architectural element, with the letters 'NTHU' and '1911' visible within the design.

研究生：林雅峰

指導教授：趙如蘋 教授

中華民國九十六年七月

液態晶體表面配向之新方法及其特性研究
Study of Liquid Crystal Surface Alignment: New Methods and
the Properties

研究生：林雅峰

Student : Yea-Feng Lin

指導教授：趙如蘋

Advisor : Ru-Pin Pan

國立交通大學

電子物理研究所

博士論文



Submitted to Institute of Electrophysics
College of Science

National Chiao Tung University
in Partial Fulfillment of the Requirements

for the Degree of
Doctor of Philosophy

In

Electrophysics

July 2007

Hsinchu, Taiwan, Republic of China

中華民國九十六年七月

液態晶體表面配向之新方法及其特性研究

研究生：林雅峰

指導教授：趙如蘋 博士

國立交通大學電子物理研究所

摘要



玻璃基板表面在液晶物理扮演一個重要角色。被摩擦過的聚合物層被廣泛的使用來控制液晶分子的排列。新一代的液晶設備與當前設備比較，其體積將會進一步縮減並且基板將會更薄和精美。傳統摩擦方法不能做小區域或不同區域(微米範圍)的配向。所以，新的表面配向方法將是極必要的。另外，摩擦刷的過程產生的纖維殘渣和殘留靜電可能會限制住良率的提升。如果能以一般的半導體微影製程和活性離子蝕刻(RIE)方式來做基板配向處理，液晶的應用將可進一步延伸。利用此製程，不但可達到小區域或不同區域的配向，而且可提高包含液晶組件的微機電系統(MEMS)的功能。

我們研究線狀 5CB 液晶 (4'-n-Octyl-4-Cyanobiphenyl) 在表面有平行溝槽的玻璃基板上的配向性質。我們是以半導體活性離子蝕刻的方法(Reactive Ion Etch)，直接在玻璃基板蝕刻出不同深度與週期的平行 U 型溝槽。再以原子力顯微鏡檢視其表面溝槽寬度、深度、及形狀。然後將兩片具有相同方法處理且有平行溝槽的玻璃基板做成上下平行的液晶盒，灌入有左旋添加物 5CB 液晶

(4'-n-Octyl-4-Cyanobiphenyl)。利用光學方法測量表面方位角定向強度，研究玻璃基板對液晶分子的配向能力，觀察溝槽週期、深度對配向強度的影響。我們觀察到溝槽間距少於 4 微米和深度大於 50 奈米時，表面方位角定向強度可達 10^{-4} J/m^2 。

我們也研究溫度對 5CB 液晶方位角定向強度的影響。我們使用光學方法，在 5CB 液晶相溫度範圍，測量液晶扭轉角度以得到不同溫度的方位角定向強度。為了避免一些特別實驗條件(尤其是波長)的限制，我們使用二個不同波長的雷射光。我們發現，當溫度增加時表面方位角定向強度穩地減少。我們也發現了液晶扭轉角度和螺距在很寬溫度範圍中不改變，因此表面方位角定向強度與 K_{22} 是成比例的，除非溫度很靠近臨界溫度。

我們也研究其他配向方法，譬如原子力量顯微鏡來修飾鍍有配向膜的玻璃的方法。我們使用原子力量顯微鏡修飾表面鍍有聚合物配向膜的玻璃基板。再以原子力顯微鏡檢視其表面結構。我們研究被修飾過表面的玻璃基板對液晶分子配向性質與修飾條件的關係。我們發現修飾密度是一個控制配向的主要條件。



Study of Liquid Crystal Surface Alignment: New Methods and the Properties

Student : Yea-Feng Lin

Advisor: Dr. Ru-Pin Pan

Department of Electrophysics
National Chiao Tung University



ABSTRACT

The surface of glass substrate plays an important role in LC physics. Rubbed polymer layers are widely used to control the alignment of LC molecules. New generations of LC device will be much further reduced and the substrates will be much thinner and more delicate compare to present devices. The conventional rubbing method can not pattern orientations over small areas or multi-domain. New surface alignment methods will be necessary in urgent. The fiber residues and static charges introduced by rubbing process can cause trouble for devices with fine patterns. The application of LC will be much further extended, if the alignment can be achieved with common semiconductor lithography process. With this process, the small area and multi-domain alignment can be achieved and the functionality of Micro-electromechanical system (MEMS) can be increased by including LC

components.

The alignment property of the nematic liquid crystal (LC) 4'-n-pentyl-4-cyanobiphenyl (5CB) on glass substrates with parallel grooves are studied. The U-shaped grooves with a variety of depths and periods are prepared by the reactive ion etch method. Surface morphology of the grooved glass is examined by Atomic Force Microscope. Two parallel grooved substrates with chiral doped 5CB sandwiched in between were used to form a LC cell. The alignment quality for LC is studied by measuring its surface azimuthal anchoring strength using an optical method. The effect of the groove period and depth are studied. Strong anchoring strength of 10^{-4} J/m² is observed for groove spacing less than 4 μ m and depth large than 50 nm.

Temperature dependence of the azimuthal anchoring strength of the nematic liquid crystal 5CB on parallel grooved glass substrates has been also studied. We measured the azimuthal anchoring strength in the nematic temperature range by measuring the twist angle in the LC cells using an optical method. Two lasers with different wavelengths were used to avoid the limitations of either wavelength in particular conditions. We found the anchoring strength decreases steadily with increasing temperature. We found that the twist angle and pitch of LC do not change significantly in a wide temperature range, resulting in that the anchoring strength is proportional to K_{22} , unless the temperature is close to T_c .

Other alignment methods, such as atomic force microscope (AFM) modifying method has been used to modify the polyimide films on glass substrates. The surface morphology of the PI films was then probed with the AFM operating in the non-contact mode. The properties of these films for liquid crystal alignment and their relations to the modifying conditions have been studied. The modifying density is a dominant factor in the conditions we have studied.

致謝

歷經波折，終於將論文順利完成，由衷地感謝指導老師 趙如蘋教授在此研究上給予最大的協助與耐心的指導，讓我能渡過重重難關，在生活上也使我對人生態度有不同的體認與啟發。特別感謝家榮學長，與洪天河先生在實驗上不盡餘力的指導與幫助。曾經一起熬夜奮戰的伙伴易駿、明釗與欣穎，感謝你們能一起分享寶貴的經驗。也感謝昭遠、信穎、阿達、家任、卓帆與宇泰在實驗上的支援，讓我能順利完成工作。感謝清大貴儀的伙伴們在實驗上的幫助與指導。

最後將此論文獻給我的家人，感謝你們對我的支持與鼓勵。



Contents

中文摘要	i
英文摘要	iii
致謝	v
Content	vi
List of Figure	ix
Chapter 1	Introducion.....	1
1-1	Rubbing Method.....	1
1-2	Non-rubbing Methods.....	2
1-2-1	Oblique Evaporation Method.....	2
1-2-2	Surface Active Agents.....	2
1-2-3	Photoalignment.....	3
1-2-4	Ion Beam Bombardment.....	3
1-2-5	AFM Modifying Method.....	4
1-3	Molecular Alignment and Alignment Mechanisms of LC.....	4
1-3-1	Molecular Alignment of Nematic LC.....	4
1-3-2	Alignment Mechanisms of LC.....	4
1-3-3	Pretilt Mechanisms of LC.....	5
1-4	Temperature effect.....	5
1-5	Our Works.....	6
1-5-1	Reactive Ion Etching (RIE) Method.....	6
1-5-2	AFM Modifying Method.....	7
	Reference.....	8

Chapter 2	Alignment of Liquid Crystals by Ion Etched Grooving Glass Surface.....	12
2-1	Substrate Preparation.....	12
2-2	Azimuthal Anchoring Strength Measurement.....	13
2-2-1	Cell Gap Measurement.....	13
2-2-2	Natural Pitch Measurement.....	14
2-2-3	Azimuthal Anchoring Strength Measurement.....	14
2-3	Results and Discussion.....	16
2-4	Conclusions.....	17
	Reference.....	18
Chapter 3	Temperature Dependence of Azimuthal Anchoring Strength of Liquid Crystal on Microgrooved Glass Substrate.....	19
3-1	Substrate and LC Cell Preparation.....	19
3-2	Temperature dependent of Anchoring Strength Measurement.....	20
3-3	Results and Discussion.....	22
3-4	Conclusions.....	24
	Reference.....	26
Chapter 4	Liquid Crystal Alignment by Surface Modification on Polyimide Film with Atomic Force Microscope Probes.....	28
4-1	Substrate and LC Cell Preparation.....	28
4-2	Optical properties and Anchoring Strength Measurement.....	29
4-3	Results and Discussions.....	30

4-4	Conclusions.....	33
	Reference.....	35
Chapter 5	Summary and Future Scope.....	36
5-1	Summary.....	36
5-2	Future Scope.....	37
Figures	38
Appendix A	Refractive Indices of 5CB as a Function of Temperature.....	73
Appendix B	Temperature Dependence of K_{11} , K_{22} , and K_{33} for 5CB.....	74
Appendix C	Anchoring Strength for Different Depths and Periods.....	75
Appendix D	Refractive Indices of 5CB (for Wavelength 632.8nm and 532.55nm) as a Function of Temperature.....	77
Brief Biography	79
List of Publications	80

List of Figure

Fig.1-1-1	(a) A structural sketch of a rubbing machine. (b) A cross sectional view of a polymer film in contact with a moving fiber of buffing material.	38
Fig.1-2-1	Surface structure of the oblique evaporated film.	39
Fig.1-2-2	(a) N, N-dimethyl-N-octadecyl-3-aminopropyltrimethoxysilyl chloride (DMOAP). (b) N-methyl-3-aminopropyltrimethoxysilane (MAP).	40
Fig.1-2-3	A low energy beam of argon ions is used to bombard the surface of a polyimide film. The argon beam produces directional alignment when the beam is at an angle other than perpendicular to the polyimide film surface.	41
Fig.1-2-4	The AFM tip modifying methods.	41
Fig.1-3-1	Typical orientations are shown. These orientations are classified into two groups. (a)~(c) The directors of the LC molecules in homogeneous, tilted and homeotropic cases are aligned in one fixed direction, while (d)~(h), the director of LC molecules in the splay, twist, bend, hybrid and super-twisted nematic cases are not fixed in one direction.	42
Fig.1-3-2	Schematic geometry of sinusoidal grooves is shown. Berreman suggested the elongated LCs prefer to align parallel to the induced micro size grooves to reduce the total surface free energy.	45
Fig.1-3-3	A polymer chain alignment model (a) before rubbing, (b) after rubbing.	46
Fig.2-1-1	AFM image of parallel grooved glass surface, which were	

	prepared by RIE method with depth of 13.6 ± 0.3 nm and period of $7.0\ \mu\text{m}$. (a) Section analysis: the root mean square roughness for the top surfaces and bottom surfaces are 0.37 nm and 0.46 nm, respectively. (b) The AFM surface topology of the sample.	47
Fig.2-2-1	Rotational interferometric method of LC cell gap measurement. The sketch for optical path through a cell.	48
Fig.2-2-2	Rotational interferometric method of LC cell gap measurement. An example of the transmittance through an empty cell ($\theta_1=31.0^\circ$, $\theta_2=26.4^\circ$, $\Delta m=1$, $\lambda=632.8$ nm), from which we can obtain $d=8.2\ \mu\text{m}$.	48
Fig.2-2-3	(a) The chemical structure of ZLI-811. (b) Cano-Wedge method (c) Disclination lines.	49
Fig.2-2-4	The planar alignment and the uniformity of alignment of LC in the cells were confirmed by using a polarizing microscope with crossed polarizers attached. (P1, P2).	50
Fig.2-2-5	Setup for anchoring strength measurement. L1, L2, L3: lenses; AP: aperture; P: polarizer; A: analyzer; PD: photo-detector; PC: personal computer.	51
Fig.2-2-6	(a) The relationship among θ , Ψ_o , and Ψ_{pol} (b) The LC cell and the analyzer are rotated to vary Ψ_o and Ψ_{pol} simultaneously with a ratio of 1 to 2.	52
Fig.2-2-7	The relationship among $d\Delta n/\lambda$, Ψ_o , and Ψ_{pol} . When $d\Delta n/\lambda$ is close 0.5, 1.5, ..., as shown in Fig.2-2-6(a), the conditions are not suitable for anchoring strength measurement. When $d\Delta n/\lambda$ is the other values, as shown in Fig.2-2-6(b) and (c), there is a minimum condition which allows Ψ_{pol} to be determined easily.	53

Fig.2-2-8	The transmitted intensity versus the angle between the polarizer and analyzer, Ψ_{pol} . The minimum is obtained by a curve fitting. In this example, we obtain a minimum intensity angle, $\Psi_{pol} = -117.46^\circ$.	54
Fig.2-3-1	AFM image of parallel grooved glass surface, which were prepared by RIE method with period of 5.0 μm .	55
Fig.2-3-2	AFM image of parallel grooved glass surface, which were prepared by RIE method with period of 6.0 μm .	56
Fig.2-3-3	AFM image of parallel grooved glass surface, which were prepared by RIE method with period of 7.0 μm .	57
Fig.2-3-4	AFM image of parallel grooved glass surface, which were prepared by RIE method with period of 8.0 μm .	58
Fig.2-3-5	AFM image of parallel grooved glass surface, which were prepared by RIE method with period of 9.0 μm .	59
Fig.2-3-6	Anchoring strength of RIE 1 minutes substrates with Different groove periods (2 $\mu\text{m} \sim 9 \mu\text{m}$). The depth of grooves is $21 \pm 5 \text{ nm}$.	60
Fig.2-3-7	Anchoring strength versus periods of grooves for various groove depth.	60
Fig.3-1-1	AFM measured surface profile of parallel grooved glass substrate, which is prepared by RIE method with depth of $26 \pm 5 \text{ nm}$ and period of 4 μm .	61
Fig.3-2-1	Setup for anchoring strength measurement. Laser 1 ($\lambda_1=632.8\text{nm}$): He-Ne laser; Laser 2 ($\lambda_2=532.55\text{nm}$): laser pointer; M1, M2: mirrors; L1, L2, L3: lenses; AP: aperture; P: polarizer; A: analyzer; PD1, PD2: photo-detectors; PC: personal computer.	62
Fig.3-2-2	(a) An example of calculated optical transmittance as a function of	

	Ψ_o and Ψ_{pol} for $\theta = 15^\circ$, $d\Delta n/\lambda=3.5$. (b) An example of transmitted intensity versus cell angle, where the minimum does not exist.	63
Fig.3-2-3	The relation of the refractive index and temperature.	64
Fig.3-3-1	Pitch versus temperature relation.	65
Fig.3-3-2	Twist angle versus temperature measured with two samples (S_1 and S_2) and two light sources (Red laser and Green laser). Close circle: S_1 -Red laser; close triangle: S_1 -Green laser; open circle: S_2 -Red laser; open triangle: S_2 -Green laser.	65
Fig.3-3-3	K_{22} versus temperature.	66
Fig.3-3-4	Anchoring strength versus temperature. Close circle: S_1 -Red laser; close triangle: S_1 -Green laser; open circle: S_2 -Red laser; open triangle: S_2 -Green laser.	66
Fig.4-3-1	The microscope picture of a parallel cell with modifying density 6.4-lines/ μm and the modified area is $80 \times 80 \mu\text{m}^2$ while the cell is between two crossed polarizers. (a) The modifying direction is parallel to the first polarizer; this is the darkest situation. (b) The modifying direction is with an angle of 45° from the polarizer direction, which gives the brightest situation. The white square in (b) is drawn to delineate the border of the modified region.	67
Fig.4-3-2	The microscope picture of a TN cell made with same substrates as in Fig.4-3-1. The cell is between two parallel polarizers, and the modifying direction is parallel to the first polarizer.	68
Fig.4-3-3	The transmission of two parallel cells between a pair of crossed polarizers vs. the angle of modifying direction with respect to the polarizer. The transmission is normalized at 1 for the case without sample and the two polarizers parallel to each other.	68

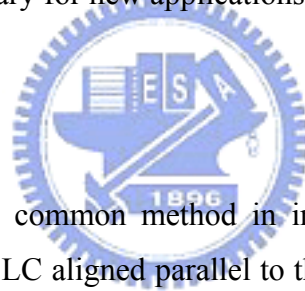
- Fig.4-3-4 $R = (T_{max} - T_{min}) / (T_{max} + T_{min})$. (a) R vs. modifying density. The observing regions are modified only once. (b) The ratio R vs. number of times of modifying at same region. While the modifying density is kept at 12.8 lines per μm . 69
- Fig.4-3-5 The anchoring strength, A . (a) The value of A vs. modifying density. When the observed regions are modified only once. (b) The value of A vs. number of times of modifying at same region. While the modifying density is kept at 12.8 lines per μm . The “*” mark by a data point indicates that point is measured with a parallel cell with chiral dopant in LC. 70
- Fig.4-3-6 The AFM surface topology of the sample modified with line density 5.12 lines per μm . The scanning line density is 82.58 lines per μm , which is 16.1 times of the modify density. (a) 2-D surface topology (b) 3-D surface topology. 71
- Fig.4-3-7 The Fourier analysis results for the sample shown in Fig. 6. If there were grooves formed by tip modifying, a peak for the “perpendicular” curve would appear at $n=16$. 72

Chapter 1

Introduction

Surface alignment is a major process for the fabrication of liquid crystal (LC) devices, such as LC display (LCD). This process provides an initial condition for LC molecular orientations. For a device working in particular modes, e.g., twisted nematic (TN) and vertical alignment (VA) modes, reliable control for LC orientation near the surfaces is most important. Many alignment methods have been utilized in LC research and industry, including rubbing and non-rubbing methods. [1] The basic alignment principles are all related to the molecular interaction between LC and the alignment materials and the interaction within the LC molecules (LCs). Understanding the specific mechanism for each method and developing new alignment methods are necessary for new applications of LCs in the future.

1-1 Rubbing Method



Rubbing is still the most common method in industry to make large areas of homogeneous alignment with LC aligned parallel to the rubbing direction, although it has been a long time since Mauguin reported this method to align LCs many years ago. [2] Fig.1-1-1(a) shows a structural sketch of a rubbing machine and a cross sectional view of a polymer film in contact with a moving fiber of buffing material is shown in Fig.1-1-1(b). Almost all of the present LCD manufactures adopted the rubbing process to control the LC alignment. If the alignment of the LC is not uniform or the alignment strength is weak, alignment-related defects appear, such as disclination lines, reverse twist, and reverse tilt. [3] These defects have large effects on the image quality of the LCDs because of either light reflection from the defect interfaces or the electro-optical characteristic differences. Therefore, controlling the alignment defects is a very important issue for LCD manufacturing. However, the fiber residues and static charges introduced by rubbing can also cause trouble for devices with fine patterns. And, it is expected that the size of new generations of LC device will be much further reduced and the substrates will be much thinner and more delicate comparing to present devices. Novel surface alignment method will be necessary and

searching for new method is in urgent. The study for alignment mechanism is the most important for guiding the search.

1-2 Non-rubbing Methods

There are many problems on rubbing process as mentioned above. To overcome these problems caused by the buffing mechanism, several LC alignments have been developed. These methods can be divided into two categories. [3] One uses surface alignment caused by the anisotropy of the surface. The other method aligns the LCs based on the electric or magnetic field outside the cell, and the surface of the substrate becomes joined to the aligned LC. After the electric or magnetic field is removed, the aligned LC on the surface aligns the bulk of the LC. Recently other alignment methods such as photo-radiation, ion beam bombardment and atomic force microscope (AFM) modifying method have been also intensively studied.

1-2-1 Oblique Evaporation Method

Oblique evaporate SiO on to a substrate, a micro columnar structure is realized on the substrate surface. [4] LC alignment direction depends on incident angle. The surface structure of the obliquely evaporated film is illustrated schematically in Fig.1-2-1. When nematic LC contact such a surface, elastic deformation of the LC along the surface induced interaction energy between the surface and nematic LC. This is thought to be the driving force for alignment of the nematic director. The surface structure of the obliquely evaporated film changes with the evaporation angle (the angle between evaporation beam and substrate normal).

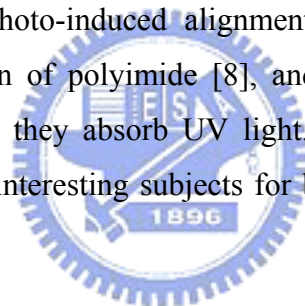
1-2-2 Surface Active Agents

It is well known that surface active agents with hydrophobic groups such as long alkyl chains with hydroxyl or carboxy groups form monomolecular films on the surface of water. By removing the formed film onto a substrate, the monomolecular film can exist on the substrate. The monomolecular layers can also be stacked to form multi-layers with several molecular layers. The monomolecular film is named a Langmuir-Blodgett film (LB film). [4]

Two particular alkoxy silane materials include N, N-dimethyl-N-octadecyl-3-aminopropyltrimethoxysilyl chloride (DMOAP) and N-methyl-3-aminopropyl-trimethoxysilane (MAP) are shown in Fig.1-2-2(a) and (b). [5] For practical alignment layers for LCDs, polyimides have been used because of their efficiency in the rubbing treatment and their thermal and chemical resistance. [6]

1-2-3 Photoalignment

The photo-induced alignment for LC has been studied for many years. As early as in 1991, Gibbons et al. had shown that the direction of the homogeneous alignment of LC molecules on specially designed optically controlled alignment polymers can be established and even be altered using polarized light. [7] Recently, the ultra-violet sensitive polyimide (PI) has been studied intensively. [8-11] The alignment mechanisms including the photo-induced alignment of dye molecules [7], photo induced cross-linking reaction of polyimide [8], and photo-induced decomposition [9-11] of some groups when they absorb UV light. The mechanism, process, and potential applications are all interesting subjects for basic understanding of LCs and useful for related industries.



1-2-4 Ion Beam Bombardment

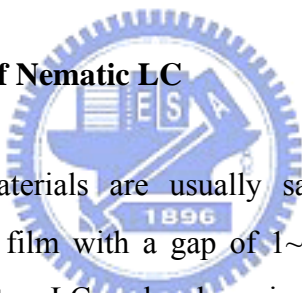
A low energy beam of argon ions is used to bombard the surface of a polyimide film and illustrated schematically as in Fig.1-2-3. [12] The argon beam produces directional alignment when the beam is at an angle other than perpendicular to the polyimide film surface. The advantages of atomic beam induced alignment over the other techniques are (1) non-contact alignment, (2) a low energy beam ensures that only the surface layers are affected so that the number of radicals induced by broken bonds, as for example under UV radiation, is a minimum. This avoids charge build up when a voltage is applied across a LC cell, (3) large area uniform and parallel beams can be readily obtained which is a problem with oblique deposition of SiO_x , and (4) atomic beams are well known to the electronics manufacturing community and are compatible with a clean room environment.

1-2-5 AFM Modifying Method

The atomic force microscope (AFM) modifying method has been studied recently for controlling the anchoring strength among various surfaces or small area alignment techniques. The AFM tip modifying methods are illustrated schematically as in Fig.1-2-4. Ruetschi et al. [13] showed that AFM in contact mode can induce the alignment of LC on polymer surface. This method has been demonstrated in areas such as special patterns of LC alignment [14], LC optical waveguide [15], LC grating [15], controllable gray scale [16], and bistability property. [17] Recently, the mechanism of LC alignment has been studied on submicron AEM patterned surface. [18] The atomic force imprinting tip systems have been developed to control the polyimide surface topology by Lee et al.. [19] The width and depth are both in nano-scale.

1-3 Molecular Alignment and Alignment Mechanisms of LC

1-3-1 Molecular Alignment of Nematic LC



In LCD devices, LC materials are usually sandwiched between two glass substrates carrying alignment film with a gap of 1~10 μ m. By the influence of the alignment film on the substrates, LC molecular orientations are determined. Typical orientations are shown in Fig.1-3-1(a)~(h). These orientations are classified into two groups.[3] The directors of the LC molecules in homogeneous, tilted and homeotropic cases are aligned in one fixed direction (Fig.1-3-1(a)~(c)), while, the directors of LC molecules in the splay, twist, bend, hybrid, and super-twisted nematic cases are not fixed in one direction (Fig.1-3-1(d)~(h)). In the latter orientation, the LCs are under stress.

1-3-2 Alignment Mechanisms of LC

It has been shown that there are two major mechanisms for the alignment of LC by rubbed PI films. The first one was suggested by Berreman, the elongated LCs prefer to align parallel to the induced micro size grooves to reduce the total surface free energy [20]. Schematic geometry of sinusoidal grooves is shown in Fig.1-3-2.

On the other hand, Geary et al. suggested that LCs is anchored by buffed polymer chains of the polymer surfaces. The alignment of LCs then follows in an epitaxial manner [21]. Fig.1-3-3 shows a polymer chain alignment model, (a) before rubbing, (b) after rubbing. Several processes to produce surfaces with micro size grooves structures for LC alignment have been proposed, for example: reactive ion etching (RIE) on glass surfaces with chromium mask [22], the photolithographic technique for photoreactive polymers using holographic exposure and reactive etching on the SiO₂ surface [23], the development and metal evaporation of photoreactive material onto the epoxy resin layer [24], and the exposure of UV light onto photocurable polymer film through masks with a grating pattern. [25]

1-3-3 Pretilt Mechanisms of LC

The rubbing generates not only an azimuthal alignment but also a polar directional alignment. The small tilt angle exists for the LC director called the pretilt angle. The pretilt angle is very important in electrooptic applications when an electric field is applied to the cell to reorient the LC director. The dominant mechanism of the pretilt angle generation of the LC might be the tilt angle of the polymer main chains. The asymmetric distribution of the side chains might be a side effect. [26] However, Shirota et al. believed that the asymmetric distribution of the side chains was the main mechanism for the pretilt angle of the LC based on the results of the SHG measurements. [27]

1-4 Temperature effect

Almost all of the nematic liquid crystals used in industry is thermotropic; all of the basic physical properties depend on temperature. As temperature increases, all of the birefringence, elastic constant, and viscosity decrease, only at different rates. [28] Obviously, temperature also affects the performance of LCD and other LC devices, such as transmittance and the response time. Up to now, the variations of the anchoring strength with temperature have been studied with different experimental techniques for a variety of aligning substrates. The majority of the experiments were performed using an external electric or magnetic field.[29-35] The temperature dependence of anchoring strength at a solid-nematic interface (MBBA on DTAC

coated glass) was first systematically investigated by Rosenblatt [29] using the application of Fréedericksz transition theory. The anchoring strength showed a reduction with temperature remarkably, especially in the vicinity of clearing point. Faetti et al. [36] measured the azimuthal anchoring energy for a nematic 5CB on obliquely evaporated SiO interface using a torsion pendulum technique. They also found the azimuthal anchoring coefficient decreases rapidly as the nematic-isotropic transition is approached. Vilfan et al. [37] measured the azimuthal anchoring strength of 5CB on rubbed Nylon by using a dynamic light scattering method, where the equilibrium LC configuration is not distorted during the measurement. They found the azimuthal anchoring coefficient decreases steadily as the nematic-isotropic transition is approached.

1-5 Our Works

However, the application of LC will be much further extended, if the alignment processes can be carried out with common semiconductor lithograph process. The characteristic small area and multi-domain properties of this process can allow LC devices being integrated with other devices such as micro-electromechanical system (MEMS). The functionality of these devices can also be much increased by including LC components.

In LC display technology, anchoring strength is an important parameter for designing the display mode. There are two types of surface anchoring involved: polar and azimuthal anchorings. The polar anchoring is about the out-of-plane tilt of the LC director on the surface from the easy axis and the azimuthal anchoring is about the in-plane angle displacement. In our work, the alignment quality for LC on grooved glass surface is studied by measuring its azimuthal anchoring strength.

1-5-1 Reactive Ion Etching (RIE) Method

In our work, we study the alignment of nematic 4'-n-pentyl-4-cyanobiphenyl (5CB) on etched bare glass substrates without any coating. The U-shaped grooves are formed on the substrate with variable depths and spacings by using reactive ion etching (RIE) method and anchoring strength were measured for each condition. [38]

We also study the temperature dependence of the azimuthal anchoring strength of nematic 5CB on these parallel grooved glass substrates without any coating. [39] We used a method that a chiral agent is doped into LC to provide a torque turning the director away from the easy direction supplied by the grooves on substrates. Azimuthal anchoring strength was calculated from the measured twist angle in the LC cells. Due to the limitation of the optical characteristics, we used two lasers with different wavelengths in order to obtain the complete data in the chosen temperature range.

1-5-2 AFM Modifying Method

In this work we also use the small tip of an AFM *to rub* or to modify the PI film on the glass substrate in contact mode, i.e., touching the tip closely to the film and running through a specified region of the film. The alignment properties of the rubbed surface, including contrast ratio and anchoring strength, are studied. The surface topology change is studied also by AFM but in non-contact mode and then investigated by Fourier analysis. The alignment mechanism will be discussed.

In chapter 2, the alignment of liquid crystals by ion etched grooving glass surfaces are described. Temperature dependence of azimuthal anchoring strength of liquid crystal on microgrooved glass substrate is described in chapter 3. The AFM modifying method is described in chapter 4. The summary and future scope is given in the last chapter.

Reference

- [1] B. W. Lee, N. A. Clark, "Alignment of liquid crystals with patterned isotropic surface", *Science*, **291**, pp.2576-2580 (2001), and references therein.
- [2] C. Mauguin, "On the liquid crystals of Lehmann", *Bull. Soc. Fr. Min.*, **34**, pp. 71-117 (1911).
- [3] K. Takatoh, M. Hasegawa, M. Koden, N. Itoh, R. Hasegawa, and M. Sakamoto, "*Alignment Technologies and Applications of Liquid Crystal Devices*", (Taylor & Francis, 2005).
- [4] J. L. Janning, "Thin film surface orientation for liquid crystals", *Appl. Phys. Lett.*, **21**, pp.173-174 (1972).
- [5] F. J. Kahn, "Orientation of liquid crystals by surface coupling agents", *Appl. Phys. Lett.*, **22**, No. 8, pp.386-388 (1973).
- [6] Y. Kawanishi, T. Takimiya, and K. Ichimura, "Photochemical control of nematic liquid crystalline orientation by the anisotropic photochromism of surface azobenzenes", *Polym. Mater. Sci. Eng.*, **66**, pp.263-264 (1992).
- [7] W. M. Gibbons, P. J. Shannon, S. T. Sun, and B. J. Swetlin, "Surface-mediated alignment of nematic liquid crystals with polarized laser light", *Nature (London)*, **351**, pp.49-50 (1991)
- [8] M. Schadt, H. Seiberle, and A. Schuster, "Optical patterning of multi-domain liquid-crystal displays with wide viewing angles", *Nature (London)*, **381**, pp. 212-215 (1996)
- [9] H. Endo, T. Shinozaki, H. Fukuro, Y. Iimura, and S. Kobayashi, *Proceedings of the Active-Matrix Liquid Crystal Display 96*, p.341, (1996)
- [10] Y. Wang, C. Xu, A. Kanazawa, T. Shiono, T. Ikeda, Y. Matsui, and Y. Tsuchi, "Generation of nematic liquid crystal alignment with polyimide exposed to linearly polarized light of long wavelength", *J. Appl. Phys.*, **84**, pp.181-188 (1998)
- [11] Y. Wang, C. Xu, A. Kanazawa, T. Shiono, T. Ikeda, Y. Matsui, and Y. Tsuchi, "Alignment of a nematic liquid crystal induced by anisotropic photo-oxidation of photosensitive polyimide films", *J. Appl. Phys.*, **84**, pp.4573-4578 (1998)
- [12] P. Chaudhari, J. A. Lacey, A. Lien, and J. L. Speidell, "Atomic beam alignment of

- liquid crystals”, *Jpn. J. Appl. Phys. Pt. 2*, **37**, L55 (1998).
- [13] M. Rüetschi, P. Grütter, J. Fünfschilling, and H. J. Güntherodt, “Creation of liquid crystal waveguides with scanning force microscopy”, *Science*, **265**, pp. 512-514 (1994).
- [14] M. Rüetschi, J. Fünfschilling, and H. J. Güntherodt, “Creation of submicron orientational structures in thin liquid crystal polymer layers”, *J. Appl. Phys.*, **80**, pp.3155-3161 (1996)
- [15] A. J. Pidduck, S. D. Haslam, G. P. Bryan-Brown, R. Bannister, and I. D. Kitely, “Control of liquid crystal alignment by polyimide surface modification using atomic force microscopy”, *Appl. Phys. Lett.*, **71**, pp.2907-2909 (1997)
- [16] B. Wen, M. P. Mahajan, and C. Rosenblatt, “Ultrahigh-resolution liquid crystal display with gray scale”, *Appl. Phys. Lett.*, **76**, pp.1240-1242 (2000)
- [17] J. H. Kim, M. Yoneya, J. Yamamoto, and H. Yokoyama, “Surface alignment bistability of nematic liquid crystals by orientationally frustrated surface patterns”, *Appl. Phys. Lett.*, **78**, pp.3055-3057 (2001)
- [18] A. Rastegar, M. Sksrabot, B. Blij, and T. Rasing, “Mechanism of liquid crystal alignment on submicron patterned surface” *J. Appl. Phys.*, **89**(2), pp.960-964 (2001)
- [19] C. D. Lee, H. M. Liu, C. K. Lee, S. M. Shen, H. Y. Wu, H. D. Chang, and C. P. Hein, “Effect of polyimide microgrooves on liquid crystal alignment”, *Eurodisplay*. pp.461-464 (2002)
- [20] D. W. Berreman, “Solid surface shape and the alignment of an adjacent nematic liquid crystal”, *Phys. Rev. Lett.*, **28**, pp.1683-1686 (1972).
- [21] J. M. Geary, J. W. Goodby, A. R. Kmetz, and J. S. Patel, “The mechanism of polymer alignment of liquid-crystal materials”, *J. Appl. Phys.*, **62**, pp.4100-4108 (1987).
- [22] D. C. Flanders, D. C. Shaver, and H. I. Smith, “Alignment of liquid crystals using submicrometer periodicity gratings”, *Appl. Phys. Lett.*, **32** (10), pp.597-598 (1978)
- [23] A. Sugimura, N. Yamamoto, and T. Kawamura, “High surface ordering of nematic liquid crystal using periodicity grating”, *Jpn. J. Appl. Phys.*, **20** (7), pp. 1343-1344 (1981)
- [24] K. Toda, N. Watanabe, T. Takemoto, and T. Nakamura, *Sharp Tech. Rep.*, **39**, p.68 (1988)

- [25] E. S. Lee, T. Uchida, M. Kano, M. Abe, and K. Sugawara, Proceedings of Japan Display '92, p.880 (1992).
- [26] R. Arafune, K. Sakamoto, D. Yamakawa, and S. Ushioda, "Pretilt angles of liquid crystals in contact with rubbed polyimide films with different chain inclinations", Surface Science, **368**, pp.208-212 (1996).
- [27] K. Shirota, M. Yaginuma, T. Sakai, K. Ishikawa, H. Takezoe, and A. Fukuda, "Orientational relationship among polyimide alignment layer, liquid crystal monolayer, and bulk pretilt angle", Appl. Phys. Lett., **69**, pp.164-166 (1996).
- [28] S. T. Wu, and D. K. Yang, "*Reflective Liquid Crystal Displays*", (Wiley, 2001).
- [29] C. Rosenblatt, "Temperature dependence of the anchoring strength coefficient at a nematic liquid crystal-wall interface", J. Phys. (Paris), **45**, pp.1087-1091 (1984).
- [30] H. Yokoyama, S. Kobayashi, and H. Kamei, "Temperature dependence of the anchoring strength at a nematic liquid crystal-evaporated sio interface", J. Appl. Phys., **61**, pp.4501-4517 (1987).
- [31] D.-S. Seo, K.-I. Muroi, T.-R. Isogami, H. Matsuda, and S. Kobayashi, "Polar anchoring strength and the temperature dependence of nematic liquid crystal (5CB) aligned on rubbed polystyrene films", Jpn. J. Appl. Phys., **31**, pp. 2165-2169 (1992).
- [32] G. A. Dilisi, C. Rosenblatt, R. B. Akins, A. C. Griffin, and U. Hari, "Anchoring strength coefficient of a monomer and its dimer at a polymer-coated interface", Liq. Cryst., **11**, pp.63-71 (1992).
- [33] D.-S. Seo, Y. Iimura, D.-Y. Kang, and S. Kobayashi, "Temperature dependence of the polar anchoring strength of weakly rubbed polyimide films for the nematic liquid crystal (5CB)", Appl. Phys. Lett., **61(2)**, pp.234-236 (1992).
- [34] D.-S. Seo, S. Kobayashi, D.-Y. Kang, and H. Yokoyama, "Effects of rubbing and temperature dependence of polar anchoring strength of homogeneously aligned nematic liquid crystal on polyimide Langmuir-Blodgett orientation films", Jpn. J. Appl. Phys., **34**, pp.3607-3611 (1995).
- [35] D.-H. Chung, H. Takezoe, and B. Park et al., "Comparative study of anchoring strength for photo-and rubbing-aligned liquid crystals on photoisomerizable polyimide alignment films", Jpn. J. Appl. Phys., **39**, pp.1252-1253 (2000).
- [36] S. Faetti, M. Gatti, V. Palleschi, and T. Sluckin, "Almost critical behavior of the anchoring energy at the interface between a nematic liquid crystal and a SiO

- substrate”, *Phys. Rev. Lett.*, **55**, pp.1681-1684 (1985).
- [37] M. Vilfan, and M. Copic, “Temperature dependence of azimuthal anchoring strength measured by dynamic light scattering”, *Mol. Cryst. Liq. Cryst.*, **375**, pp. 155-164 (2002).
- [38] Y. F. Lin, M. C. Tsou, and R. P. Pan, “Alignment of liquid crystals by ion etched grooving glass surfaces”, *Chinese J. Phys.*, **43**, No. 6, pp.1066-1073 (2005).
- [39] Y. F. Lin, Shin-Ying Lu, and Ru-Pin Pan, “Temperature dependence of azimuthal anchoring strength of liquid crystal on micro-grooved glass substrate”, *Jpn. J. Appl. Phys.*, **44**, No. 12, pp.8552-8556 (2005).



Chapter 2

Alignment of Liquid Crystals by Ion Etched Grooving Glass Surfaces

The alignment property of the nematic liquid crystal 4'-n-pentyl-4-cyanobiphenyl (5CB) on glass substrates with parallel grooves are studied. The U-shaped grooves with a variety of depths and periods are prepared by the reactive ion etch method. Surface morphology of the grooved glass is examined by Atomic Force Microscope. A LC cell consist of a pair of parallel grooved substrates with 5CB sandwiched in between is assembled. The alignment quality for LC is studied by measuring its surface azimuthal anchoring strength. The effect of the groove period and depth is studied. Strong anchoring strength of 10^{-4} J/m² is observed for groove spacing less than 4 μ m and depth larger than 50 nm.

In section 2-1, the glass etching method, surface characterization, and LC cell preparation are described. The anchoring strength measurement and its principle are described in section 2-2. The results together with the discussion are presented in section 2-3. A conclusion is given in the section 2-4.

2-1 Substrate Preparation

Two common processes in the semiconductor integrated circuits industry, lithography and reactive ion etching (RIE), were used to create parallel grooves on uncoated glass surface. The STN LCD (super-twisted nematic liquid crystal display) grade glass was obtained by removing the Indium-tin-oxide (ITO) coating from industrial-quality ITO-coated STN LCD glasses. A positive photo-resist (FH-6400L) was then coated on the glass with a spin coater and a soft baking at 80°C afterward. An exposure process followed to induce a photochemical transformation of patterns on a mask having nine grating-like patterns with various periods by using a contact method. The exposed photo-resist was then developed for 20 seconds followed by

hard baking at 110°C for 20 minutes to form photo-resist stripes on glass. The part of glass surface uncovered by photo-resist was etched away from the bulk by using the RIE method. The etching time of RIE was varied to give different groove depths.

Surface morphology of the grooved glass was examined by a tapping-mode AFM (Digital Instruments Nanoscope 3100). Fig.2-1-1(a) and (b) shows an example of the AFM image of our etched glass surface. In this example, the groove depth is 13.6 ± 0.3 nm and period is $7.0 \mu\text{m}$. The root mean square roughness for the top surfaces and bottom surfaces are 0.37 nm and 0.46 nm, respectively.

2-2 Azimuthal Anchoring Strength Measurement

The alignment quality for LC is studied by measuring its surface azimuthal anchoring strength.

2-2-1 Cell Gap Measurement

Two substrates with parallel grooves created as mentioned in the previous section were placed together with Mylar spacer to form an empty cell. The cell gap between the two substrates was measured by a rotational interferometric method [1, 2]: A He-Ne laser beam was incident on the empty cell and the transmittance is measured as a function of the incident angle. In Fig.2-2-1, we show a sketch for the optical interference from the cell. An example of transmittance of the empty cell is shown in Fig.2-2-2. The peaks correspond to incident angles satisfying the following condition:

$$2d \cos \theta = m\lambda, \quad (2-1)$$

where m is a positive integer and d is the cell gap. We choose two peaks with angles θ_1 and θ_2 , respectively, in the transmittance curve. From eq. (2-1), d can be calculated by

$$d = \frac{\Delta m \lambda}{2(\cos \theta_2 - \cos \theta_1)}, \quad (2-2)$$

where Δm is the number of minima between the two chosen peaks. The accuracy of the cell gap measurement and the uniformity of the cell gap on each cell are both under $0.2 \mu\text{m}$. Among all of the samples used in this study, the gaps varied between 7

and 10 μm .

2-2-2 Natural Pitch Measurement

To measure the anchoring strength of the grooved substrate, nematic LC 5CB doped with a 0.15 wt% of left handed chiral dopant ZLI-811 (Merck) was filled into the gap of the above empty cell and a LC cell was formed. The natural pitch of the mixture, P_o , was measured with the Cano-Wedge method [3] and found to be 41.5 μm and 45.4 μm , respectively, for the two mixtures used in this study. The chemical structure of ZLI-811, illustration of Cano-Wedge method, and an example of disclination lines are shown in Fig.2-2-3(a) ~ (c).

The planar alignment and the uniformity of alignment of LC in the cells were confirmed by using a polarizing microscope with crossed polarizers attached (Fig.2-2-4).

2-2-3 Azimuthal Anchoring Strength Measurement

The anchoring strength was measured by an optical method [4] with a system shown in Fig.2-2-5. The temperature of LC cell was controlled at $25.5 \pm 0.3^\circ\text{C}$ during the measurements. We briefly describe our method here. At the boundary, the director deviates from the direction of the grooves by an angle Δ due to the spontaneous twisting power of the chiral doped nematic LC.

The free energy per unit area is obtained as the sum of the elastic energy F_b and the surface anchoring energy F_s as follows [4],

$$F = F_b + 2 F_s, \quad (2-3)$$

Where

$$F_b = \frac{1}{2} K_{22} \left(\frac{2\pi}{P_o} - \frac{\theta}{d} \right)^2 d, \quad (2-4)$$

$$F_s = \frac{1}{2} A \sin^2 \Delta, \quad (2-5)$$

Here, K_{22} is the twist elastic constant, P_o is natural pitch, d is the cell gap, A is the surface azimuthal anchoring strength, Δ is the deviation of the director at the surface

from the groove and θ is the twisting angle of the director in the cell. The director orientation in this cell is obtained by minimizing F , which gives the torque balance equation, and then the azimuthal anchoring strength, A , was then obtained by

$$A = \frac{2K_{22}}{\sin\theta} \left(\frac{2\pi}{P_o} - \frac{\theta}{d} \right). \quad (2-6)$$

With a total twist angle, θ , in the cell the transmission, T_r , can be written as following [5]:

$$T_r = \left[\frac{1}{\sqrt{1+u^2}} \sin(\sqrt{1+u^2}\theta) \sin(\theta - \Psi_{pol}) + \cos(\sqrt{1+u^2}\theta) \cos(\theta - \Psi_{pol}) \right]^2 + \frac{u^2}{1+u^2} \sin^2(\sqrt{1+u^2}\theta) \cos^2(\theta + 2\Psi_o - \Psi_{pol}), \quad (2-7)$$

and

$$u = \frac{\pi d}{\lambda \theta} (n_e - n_o), \quad (2-8)$$

where Ψ_o and Ψ_{pol} are the angles of LC director at the first surface and the analyzer (exit polarizer), respectively, with respect to the polarizer (entrance polarizer), n_e and n_o are the extraordinary and ordinary refractive indices of the LC, and λ is the wavelength of incident light ($\lambda=632.8\text{nm}$). The relationship among θ , Ψ_o , and Ψ_{pol} are shown in Fig.2-2-6(a). The value of T_r reaches its absolute minimum with respect to the two variables Ψ_o and Ψ_{pol} where both of the two terms in eq. (2-7) are zero, i.e., the two following conditions are satisfied,

$$\frac{1}{\sqrt{1+u^2}} \sin(\sqrt{1+u^2}\theta) \sin(\theta - \Psi_{pol}) + \cos(\sqrt{1+u^2}\theta) \cos(\theta - \Psi_{pol}) = 0, \quad (2-9)$$

and

$$\theta + 2\Psi_o - \Psi_{pol} = \pm \frac{\pi}{2}, \quad (2-10)$$

Our polarizer was parallel to the groove direction and the analyzer was perpendicular to the polarizer initially. Then we rotated the LC cell and the analyzer to vary Ψ_o and Ψ_{pol} simultaneously with a ratio of 1 to 2 (Fig.2-2-6(b)). In this way, the second term of eq. (2-7) was kept at constant. The minimum of T_r occurred when eq. (2-9) was satisfied. Then, we deduced θ from eq. (2-9) by using the indices of refraction for 5CB from ref.6. To measure the anchoring strength precisely, it is necessary to select appropriate measurement condition. [7] For this purpose, we calculated the optical transmittance T_r as a function of $d\Delta n/\lambda$, Ψ_o and Ψ_{pol} in detail. The relationship among

$d\Delta n/\lambda$, Ψ_o , and Ψ_{pol} are shown in Fig.2-2-7. When $d\Delta n/\lambda$ is close 0.5, 1.5, ..., as shown in Fig.2-2-7(a), the conditions are not suitable for anchoring strength measurement. When $d\Delta n/\lambda$ is the other values, as shown in Fig.2-2-7(b) and (c), there is a minimum condition which allows Ψ_{pol} to be determined easily. Fig.2-2-8 shows an example of transmittance measurement. The value for K_{22} (25.5°C) was obtained from ref.8.

2-3 Results and Discussion

The periods of U-shape grooves were varied from 2 μm to 9 μm in this study. We obtained three different depths by changing the etching time in the RIE process. The depths were 21 ± 5 nm, 56 ± 6 nm, and 121 ± 5 nm for etching time 1, 6 and 20 minutes, respectively. Fig.2-3-1~2-3-5 shows some example of the AFM image of our etched glass surface.

In Fig.2-3-6, we show the measured anchoring strength versus the groove periods for the samples with groove depth of 21 ± 5 nm. The anchoring strengths are within the range of $1 \times 10^{-8} \sim 2 \times 10^{-6}$ J/m² with an uncertainty less than 1%. A uniformly planar alignment was achieved, although the anchoring was weak comparing to the conventional rubbed substrate (with A around 10^{-4} J/m²).

The effect of groove depths to anchoring strength is shown in Fig.2-3-7 with samples having various etching depth. When the depths are larger than 50 nm, the anchoring strength (larger than 10^{-5} J/m²) was more than an order of magnitude larger comparing to the substrate with shallower grooves.

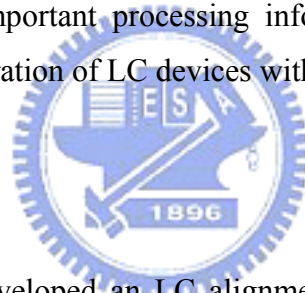
The anchoring strength of samples with groove depth of 21 ± 5 nm (Fig.2-3-6) is insensitive to its period. The effect of groove period on anchoring strength for samples with groove depths of 56 ± 6 nm and 121 ± 5 nm, on the other hand, can be clearly observed in Fig.2-3-7. The anchoring strength decreases with the groove periods and drops drastically when the period reaches 5 μm . The anchoring strength is compatible with conventional rubbed PI substrate when the groove periods are less than 4 μm and depths above 50 nm.

The major error of this measurement comes from the measurement of twist angle

and the misalignment of the two substrates. When the anchoring strength is less than 10^{-6} J/m^2 , the method for measuring anchoring strength employed here is very accurate with error less than 1%. On the other hand, for strong anchoring (anchoring strength above 10^{-4} J/m^2), the anchoring strength measuring method employed here has larger error bar. Because the surface anchoring becomes much stronger than the spontaneous twisting power caused by chiral doping in nematic LC, the director of LC molecules near the surface deviate only by a small angle (less than 0.5 degree) from the direction of grooves.

Figure 2-3-7 shows that the anchoring strengths of samples etched for 20 minutes (groove depth of 121 nm) are smaller than those etched for only 6 minutes (groove depth of 56nm). The mechanism for this phenomenon is not clear yet. It is possibly due to the roughness along the side surfaces within the grooves. Suffice to say, preparation of the surface with an etching time of 6 minutes would yield excellent alignment results. This is important processing information for the fabrication of future devices requiring integration of LC devices with MEMS.

2-4 Conclusions



In this work we have developed an LC alignment process employing standard semiconductor processing steps (do not need alignment film). This is advantageous for integrating LC devices with other devices such as MEMS. We have etched U-shape grooves of micron scale with various periods and depths and studied their alignment property and anchoring strength to LC.

The periods of the grooves are varied between 2 and 9 μm . When the depths of the grooves is small ($21 \pm 5 \text{ nm}$), the anchoring strength ($<10^{-6} \text{ J/m}^2$) are smaller than traditional rubbed polyimide surfaces. It can be increased more than an order of magnitude by varying the groove depth and period. Strong anchoring with strengths larger than 10^{-5} J/m^2 can be achieved with the depths of the grooves 56 or 121 nm and periods less than 4 μm .

Reference

- [1] H. Zhu, Q. Lin, and B. Zhang, "Analyses of system error in the measurement of liquid crystal empty cell gap by means of interferometry", *Display*, 21, pp. 121-126, (2000).
- [2] K. H. Yang, "Measurements of empty cell gap for liquid-crystal displays using interferometric methods", *J. Appl. Phys.*, **64**, No. 9, pp.4780-4781, (1988).
- [3] P. G. de Gennes, and J. Prost, "*The Physics of Liquid Crystals*", (Oxford, London, 1993)
- [4] Y. Sato, K. Sato, and T. Uchida, "Relationship between rubbing strength and surface anchoring of nematic liquid crystal", *Jpn. J. Appl. Phys.*, **31**, pp. L579-581 (1992).
- [5] A. Lien, "Optimization of the Off-States for Single-Layer and Double-Layer General Twisted Nematic Liquid-Crystal Displays", *IEEE Trans Electron Dev* 36, pp.1910-1914 (1989).
- [6] R. G. Horn, *J. Physique*, 39, p.105, (1978)
- [7] Y. Saitoh, and A. Lien, "An Improved Azimuthal Anchoring Energy measurement Method Using Liquid Crystals with Different Chiralities", *Jan. J. Appl. Phys.*, **39**, pp.1743-1746 (2000).
- [8] J. D. Bunning, T. E. Faber, and P. L. Sherrell, "The Frank constants of nematic 5CB at atmospheric pressure", *J. Physique.*, **42**, pp.1175-1182 (1981).

Chapter 3

Temperature Dependence of Azimuthal Anchoring Strength of Liquid Crystal on Microgrooved Glass Substrate

Temperature dependence of the azimuthal anchoring strength of the nematic liquid crystal (LC) 4'-n-pentyl-4-cyanobiphenyl (5CB) on parallel grooved glass substrates has been studied. The U-shaped grooves are prepared by the reactive ion etching method. Two parallel grooved substrates with chiral doped 5CB sandwiched in between are used to form an LC cell. The azimuthal anchoring strength in the nematic temperature range is determined by measuring the twist angle in the LC cells using an optical method at two laser wavelengths. The anchoring strength is found to decrease steadily with the increasing temperature. The change of the anchoring strength is attributed to the change of elastic constant K_{22} , unless the temperature is close to the clearing point.

In section 3-1, the glass surface etching, characterization, and LC cell preparation are described. The anchoring strength measurement and its principle and the limitation of the optical characteristics are described in section 3-2. The results together with the discussion are presented in section 3-3. A conclusion is given in the section 3-4.

3-1 Substrate and LC Cell Preparation

We use the common processes in semiconductor integrated circuits industry, lithography and reactive ion etching (RIE), to create parallel grooves on uncoated glass.[1] An atomic force microscope (Digital Instruments Nanoscope 3100) under tapping mode is used to examine the surface morphology and to determine the groove depth and period. Figure 3-1-1 shows an example of the surface profile of our etched

glass surface measured by AFM. Substrates used in this work have parallel grooves with depth of 26 ± 5 nm and period of 4 μm , as shown in this figure. The rms roughness for the top surfaces and bottom surfaces are 0.917 nm and 2.28 nm, respectively.

Two substrates obtained by breaking the etched glasses to two halves are placed together with grooves parallel to each other and a Mylar spacer in between to form an empty cell. The cell gap, d , between the two substrates was measured by the rotation interferometric method. [2, 3] Two cells (S_1 and S_2) with cell gaps 11.13 and 11.65 μm , respectively, are studied in this work.

To measure the anchoring strength, we fill the nematic LC 5CB (from Merck) doped with a 0.15 wt% of left handed chiral dopant ZLI-811 (Merck) into the gap to form LC cells. The natural pitch of the mixture, P_o , is measured with Cano-Wedge method. [4]

3-2 Temperature dependence of Anchoring Strength Measurement

The anchoring strength is determined by measuring the twist angle of LC in the cell by an optical method [5] with a system shown in Fig. 3-2-1. Light intensity through the arrangement from left to right in this figure detected by a photo-detector, PD1, is divided by the reference intensity measured by PD2, to eliminate the fluctuation of laser power. The temperature of the cells is controlled with temperature stability around ± 0.2 $^{\circ}\text{C}$. The measurement is carried out for temperatures from 25 $^{\circ}\text{C}$ to above T_c (about 33 $^{\circ}\text{C}$). The T_c for pure 5CB from Merck should be 35.3 $^{\circ}\text{C}$, however, it is lowered with dopant. We have observed that the T_c of our 5CB with dopant can be affected by humidity significantly. It can be varied as much as 2 $^{\circ}\text{C}$. To use the data in literature, all temperatures are expressed in terms of $T - T_c$.

At the boundary, the director deviates from the direction of groove by an angle Δ due to the spontaneous twisting power of the chiral doped nematic LC. The azimuthal anchoring strength, A , is defined with the surface free energy F_s by the following equation:

$$F_s = \frac{1}{2} A \sin^2 \theta \quad (3-1)$$

With the measured total twist angle θ in the cell, the anchoring strength A is given by

$$A = \frac{2K_{22}}{\sin \theta} \left(\frac{2\pi}{P_o} - \frac{\theta}{d} \right), \quad (3-2)$$

where K_{22} is the twist elastic constant of 5CB at the measuring temperature.[6] The principle and method for measuring θ were described in our previous work.[1] Briefly, for the setup shown in Fig. 3-2-1, the transmittance, T_r , can be written as following: [7]

$$T_r = \left[\frac{1}{\sqrt{1+u^2}} \sin(\sqrt{1+u^2}\theta) \sin(\theta - \Psi_{pol}) + \cos(\sqrt{1+u^2}\theta) \cos(\theta - \Psi_{pol}) \right]^2 + \frac{u^2}{1+u^2} \sin^2(\sqrt{1+u^2}\theta) \cos^2(\theta + 2\Psi_o - \Psi_{pol}), \quad (3-3)$$

and

$$u = \frac{\pi d}{\lambda \theta} (n_e - n_o), \quad (3-4)$$

where Ψ_o and Ψ_{pol} are the angles of LC director at first surface of the cell and the analyzer (exit polarizer), respectively, with respect to the polarizer (entrance polarizer), n_e and n_o are the extraordinary and ordinary refractive indices of the LC, and λ is the wavelength of incident light. The value of T_r reaches its absolute minimum with respect to the two variables Ψ_o and Ψ_{pol} when both of the two terms in eq. (3-3) are zero. However, to determine the twist angle θ , only the first term is needed. In our work, the polarizer is parallel to the groove direction and the analyzer is perpendicular to the polarizer at the beginning. Then we rotate the LC cell and the analyzer to vary Ψ_o and Ψ_{pol} simultaneously with a ratio of 1 to 2. In this way, the second term of eq. (3-3) is kept as a constant. The minimum of T_r is achieved when the first term of eq. (3-3) is zero, then the twist angle θ can be determined.

However, to determine θ precisely, the value for $d\Delta n/\lambda = d(n_e - n_o)/\lambda$ should be away from half integers. [8] In general, when d , λ are fixed, this value will change with temperature, because the birefringence of LC changes with temperature. In some temperature range, the value of $d\Delta n/\lambda$ becomes close to 0.5, 1.5, 2.5, the conditions not suitable for anchoring strength measurement. In Fig. 3-2-2(a) we shows an example of the calculated the transmittance T for $\theta=15^\circ$ and, $d\Delta n/\lambda=3.5$. Under this

condition, the value for T_r does not have minimum points, and the twist angle can not be determined. Experimentally, we get a flat transmittance with cell angle as shown in Fig. 3-2-2(b) as we rotate the sample and analyzer synchronously along the white line in Fig. 3-2-2(a). To avoid this optical limitation, we use two lasers in our work to obtain the complete results for the chosen temperature range. One is a He-Ne red laser and the other is a green laser pointer (second harmonic of a diode-pumped $\text{Nd}:\text{YVO}_4$ laser, Leadlight Corp., Taiwan) with wavelengths $\lambda_1=632.8$ nm and $\lambda_2=532.6$ nm, respectively. Because the laser pointer has large fluctuations in power, the reference power measurement by PD2 in Fig. 3-2-1 is necessary. The values of refractive indices (see Fig. 3-2-3) at various temperatures are interpolated from that measured by Wu et al.. [9]

3-3 Results and Discussion

From eq. (3-2), we can see that the anchoring strength is determined by P_o , K_{22} , and θ . Our measured pitch versus temperature is plotted in Fig. 3-3-1. The temperature is raised from 25°C to above T_c , and then lowered down to 25°C. Note that the pitch P_o remains a constant of 51.2 ± 0.2 μm throughout this range except for temperatures near T_c , where the pitch becomes unstable.

Two cells (S_1 and S_2) with U-shaped parallel grooves (depth= 26 ± 5 nm and period= $4 \mu\text{m}$) are studied in this work. In Fig. 3-3-2, we have plotted the twist angle θ vs. temperature for both samples. The solid points are for S_1 and the hollow points for S_2 . The circular points are measured with the red laser and the triangular ones with the green laser. We can see that the twist angle itself is essentially a constant (0.46 ± 0.01 rad) at most temperatures except when the temperature is close to the clearing point ($T_c - T < 1.74$ °C). With the total twist angle θ , and P_o measured in this work and K_{22} from literature (Fig. 3-3-3), [6] the anchoring strength A is determined by eq. (3-2). We plot the measured anchoring strength, A , as a function of temperature in Fig. 3-3-4. Because both cells S_1 and S_2 are made with similar substrates, the data are shown together in Fig. 3-3-4. The anchoring strength of either cell has values around 10^{-6} J/m² with an uncertainty less than 1% and manifests a monotonic decrease with increasing temperature. There are several temperature ranges, where the optical

limitations of $d\Delta n/\lambda$ being close to half integers are encountered: $1.0\text{ }^\circ\text{C} < T_c - T < 3.4\text{ }^\circ\text{C}$ for S_1 at λ_1 ; $1.5\text{ }^\circ\text{C} < T_c - T < 5.9\text{ }^\circ\text{C}$ for S_1 at λ_2 ; $T_c - T < 2.1\text{ }^\circ\text{C}$ for S_2 at λ_1 ; and $1.6\text{ }^\circ\text{C} < T_c - T < 4.8\text{ }^\circ\text{C}$ for S_2 at λ_2 having the $d\Delta n/\lambda$ value close to 2.5 or 3.5. As a result, A can not be determined using light of just one wavelength. With two cells of different thickness and two lasers, the anchoring strength of the grooved substrates can be determined for the whole nematic range.

The well-known Berreman model [10] of the azimuthal anchoring energy, used to model the grooved structure of the obliquely evaporated SiO film originally, is given by

$$A = \frac{2\pi^3 h^2}{l^3} K, \quad (3-5)$$

where h and l are the amplitude and period of the sinusoidal grooves, respectively, and K is an average elastic constant of LC molecules.

From eq. (3-5), the Berreman theory, the anchoring strength is proportional to the elastic constant; therefore the ratio of A to K is a constant. Following eq. (3-2), this ratio can be expressed as:

$$\frac{A}{K_{22}} = \frac{2}{\sin\theta} \left(\frac{2\pi}{P_o} - \frac{\theta}{d} \right). \quad (3-6)$$

If the pitch does not vary with temperature the twist angle θ will be a constant, which is demonstrated in this work (see Figs. 3-3-1 and 3-3-2). Therefore, it is proved that the anchoring strength is proportional to the elastic constant K_{22} , as predicted by Berreman. At a temperature close to T_c , this method for determining the anchoring strength using chiral doped nematic has larger uncertainty due to the unstable pitch near T_c .

In our case, the experimental value of the azimuthal anchoring strength is found to be several orders of magnitude higher than that predicted by applying our depth and period directly into eq.(3-5) ($1.6 \times 10^{-9} \text{ J/m}^2$). If we consider our U-shaped grooves having a square wave form, then the Fourier series for this square wave with period l and amplitude h is given by [11]

$$f(x) = \frac{4h}{\pi} \sum_{n=1,3,5,\dots}^{\infty} \frac{1}{n} \sin\left(\frac{2n\pi}{l}x\right). \quad (3-7)$$

In other words, our U-shaped periodical grooves can be considered consisting of a series of sinusoidal grooves with amplitudes $4h/n\pi$ and periods l/n , where $n=1,3,5,\dots$.

Then A becomes

$$A = K \frac{32\pi h^2}{l^3} \sum_{n=1,3,5,\dots} n, \quad (3-8)$$

which is a divergent series. Therefore, eq. (3-5) is not accurate enough to predict the value of our anchoring strength; a much larger value for A can be anticipated due to the diverging of eq. (3-8).

Lee et al. [12] have studied the A values for rubbed polyimide film and compared with Berreman's theory. The values obtained experimentally were more than two orders of magnitude higher than that obtained from Berreman's theory. The major reason was considered to be the following: a surface morphology with very fine grooves (periods less than about 15nm), or intermolecular interaction between the LC and polymer molecules. Hallam et al. [13] and Ohta et al. [14] demonstrated that the A values on sinusoidal grooved photo-resist surface is closely related to Berreman's theory for small depth/period ratio.

Recent finite element calculations [14, 15] have shown that the groove shape plays a crucial role for anchoring strength. For rectangular grooves, the anchoring strength is higher than the sinusoidal grooves. Particularly, when the groove depth is small as in our case, the rectangular grooves can give an anchoring strength more than two orders of magnitude higher than the sinusoidal grooves. Our results agree with these predictions.

3-4 Conclusions

We use an improved method for measuring the temperature dependence of azimuthal anchoring strength by using two lasers with different wavelengths. A chiral dopant is added into the nematic liquid crystal 5CB for anchoring strength measurement. The azimuthal anchoring strength of 5CB on parallel grooved glass substrates are found to decrease monotonically with the increasing temperature. The

change of A is due to the change of K_{22} at most nematic temperature range unless the temperature is very close to the clearing point, T_c . Near T_c the pitch changes and becomes unstable, therefore this method is not suitable for anchoring strength measurement at this temperature region.



Reference

- [1] Yea-Feng Lin, Ming-Chao Tsou, and Ru-Pin Pan , “Alignment of liquid crystals by ion etched grooving glass surfaces”, Chinese Journal of Physics, **43**, No. 6, pp.1066-1073 (2005).
- [2] H. Zhu, Q. Lin, and B. Zhang, “Analyses of system error in the measurement of liquid crystal empty cell gap by means of interferometry”, Display. 21, pp. 121-126 (2000).
- [3] K. H. Yang, “Measurements of empty cell gap for liquid-crystal displays using interferometric methods”, J. Appl. Phys., **64**, No. 9, pp.4780-4781 (1988).
- [4] P. G. de Gennes, and J. Prost, “*The Physics of Liquid Crystals*”, (Oxford, London, 1993).
- [5] Y. Sato, K. Sato, and T. Uchida, “Relationship between rubbing strength and surface anchoring of nematic liquid crystal”, Jpn. J. Appl. Phys., **31**, pp. L579-581 (1992).
- [6] J. D. Bunning, T. E. Faber, and P. L. Sherrell, “The Frank constants of nematic 5CB at atmospheric pressure”, J. Physique., **42**, pp.1175-1182 (1981).
- [7] A. Lien, ”Optimization of the Off-States for Single-Layer and Double-Layer General Twisted Nematic Liquid-Crystal Displays”, IEEE Trans Electron Dev 36, pp. 1910-1914 (1989).
- [8] Y. Saitoh, and A. Lien, “An Improved Azimuthal Anchoring Energy measurement Method Using Liquid Crystals with Different Chiralities”, Jan. J. Appl. Phys., **39**, pp.1743-1746 (2000).
- [9] S. T. Wu, and C. S. Wu, “Refractive index dispersions of liquid crystals”, Opt. Eng. **32**(8), pp.1775-1780 (1993).
- [10] D. W. Berreman, “Solid surface shape and the alignment of an adjacent nematic liquid crystal”, Phys. Rev. Lett., **28**, pp.1683-1686 (1972).
- [11] G. Arfken, Mathematical Method for Physicists, 3rd ed.(Orlando, FL: Academi pp.760-793 (1985)
- [12] E. S. Lee, Y. Saito, and T. Uchida, Jpn. J. Appl. Phys., **32**, Part 2, No. 12B, L1822 (1993).
- [13] B. T. Hallam, and J. R. Sambles, “Groove depth dependence of the anchoring strength of a zero order grating-aligned liquid crystal”, Liquid Crystals, **27**, No. 9,

pp.1207-1211 (2000).

- [14] Y. Ohta, N. Tanaka, M. Kimura, and T. Akahane, "Surface azimuthal anchoring energy between the grating surface and nematic liquid crystal layer studied by finite element method", *Jpn. J. Appl. Phys.*, **43**, No. 7A, pp.4310-4311 (2004).
- [15] M. Kimura, Y. Ohta, and T. Akahane, "Surface azimuthal anchoring energy between the trapezoid grating surface and nematic liquid crystal layer studied by finite element method", *Adv. In Tech. of Mat. and Mat. Proc. J. (ATM)*, **7**[2], pp. 91-96 (2005).



Chapter 4

Liquid Crystal Alignment by Surface Modification on Polyimide Film with Atomic Force Microscope Probes

Atomic force microscope (AFM) has been used to modify the polyimide films on glass substrate. The surface morphology of the films was then probed with the AFM operating in the non-contacting mode. The properties of these films for liquid crystal alignment and their relations to the modifying conditions have been studied. The modifying line density is a dominant factor in the conditions we have studied.

4-1 Substrate and LC Cell Preparation

The PI films are formed by coating a 2.5 % (volume) of Nissan SE-130B in NMP (N-methyl-2-pyrrolidinone) solution on glass substrates with a spin coater followed by thermal curing in oven. The PI film is then modified with the probe tips of an AFM (Digital Instruments Dimension 3100 with NanoScope IIIa controller) scanning through specified region with a particular scanning line density. To make a modification on the film, the AFM is operated in the contact mode, in which the tip is closely touching the PI film. The glass substrate used is the regular substrate for super-twisted-nematic liquid crystal display (STN LCD) with indium tin oxide (ITO) coating on one side. The ITO coated side of the substrates is the surface we work on, only that the ITO is removed.

Before and after the modification, the film surface morphology is measured by the same AFM, but operating in a non-contact tapping mode. In this mode, the tip does not touch the film. Therefore, it will not make further changes to the film. Besides taking the 3 dimensional images of the films, we have also carried out a Fourier analysis to see how the tip modifying process changes the surface structure.

The substrate with modified film is combined with another glass substrate with conventional mechanically rubbed PI film to form a LC cell. The cells are filled with

nematic 4'-n-pentyl-4-cyanobiphenyl (5CB) from Merck. The cell thickness is controlled with a 6 μ m-thick mylar film. Both parallel cell and twist nematic (TN) cell have been prepared.

4-2 Optical properties and Anchoring Strength Measurement

The optical properties of the cells are observed under a polarized optical microscope. The optical transmission curves of the LC cells between crossed polarizers, while rotating the cell, are also measured under the same microscope with a line filter (546nm), a CCD camera and image processing tools.

With the same setup mentioned above, we have also measured the anchoring strength of the AFM-modified film to LC with the optical method. The definition of anchoring strength is the same as being defined in chapter 2. The azimuthal anchoring strength A is defined with area surface free energy, F_s , by

$$F_s = \frac{1}{2} A \sin^2 \varphi_s, \quad (4-1)$$

Where φ_s is the angle deviation of surface director from the easy direction. The measuring has been carried out by using either a parallel or a TN cell filled with chiral doped 5CB. After measuring the twisting angle θ of LC and the surface angle φ_s , we can obtain the anchoring strength by the following eq. [1],

$$A = \frac{2K_{22}}{\sin 2\varphi_s} \left(\frac{2\pi}{P_o} - \frac{\theta}{d} \right), \quad (4-2)$$

where K_{22} is the twist elastic constant, P_o is the natural pitch of the chiral doped nematics LC.

The twisting angle and the surface deviation angle are measured by the following. We put the sample under the microscope between two polarizers (crossed for parallel cell and parallel for TN cell). We rotate the sample until the minimum is reached and then rotate the second polarizer until another minimum is reached again. This process is repeated a couple of times then the real minimum will be reached. The final angle between the two polarizers gives the twisting angle, θ . The surface deviation angle is θ for parallel cell or $90^\circ - \theta$ for TN cell, assuming the surface by rubbing has strong anchoring. The natural pitch P_o is measured using Cano wedge method [2]. While

both parallel and TN cells can be used for anchoring strength measurement, a chiral dopant must be added for the parallel cell. A left-hand dopant S811 (from Merck) is added into 5CB with weight of 0.15%.

4-3 Results and Discussions

We have modified the PI films on the glass substrate using AFM tips with line densities between 5 to 25 lines per μm . In Figs.4-3-1 and 4-3-2, we show pictures of one sample taken under the polarized microscope. In this example, the modified area is $80 \times 80 \mu\text{m}^2$ and the line density is 6.4 lines per μm . Figure 4-3-1 is for the parallel cell while Fig.4-3-2 is for the TN cell, re-made with the same substrates. In Fig.4-3-1(a), the parallel cell is between crossed polarizers with the modifying direction parallel to the first polarizer. Dark region is the modified region. In Fig.4-3-1(b), the sample has been rotated 45° , which gives the brightest situation. In Fig.4-3-2, the TN cell is between two parallel polarizers, and the modifying direction is parallel to one of the polarizers. With these results, we confirm that the AFM-rubbed PI surface aligns LC parallel to the tip moving direction.

With a line filter of wavelength 546 nm before the first polarizer in the polarizing microscope, we have measured the transmission of light through the LC cell between the crossed polarizers versus the rotation angle of the LC cell. Results for the sample shown in Fig.4-3-1 and another parallel cell with line density 12.8 lines per μm are shown in Fig.4-3-3. For an ideal parallel LC cell, the transmission T of the cell between a pair of crossed polarizers is

$$T = \sin^2(\pi \Delta n d / \lambda) \cdot \sin^2(2\varphi) = C \sin^2(2\varphi), \quad (4-3)$$

where Δn is the birefringence, λ is the wavelength and φ is the angle between the alignment direction and one of the polarizers. With fixed sample and wavelength, eq.(4-3) has a simple form as

$$T = C \cdot \sin^2(2\varphi), \quad (4-4)$$

where C is a constant. In real situation, the scattering of light, the non-uniformity of surface, and the extinction rate of the polarizers can all make the T vs. φ curve deviate from the ideal curve. The quality of the alignment is a dominant factor that determines how close the real curve is to eq.(4-4). A good approximation to the measured

transmission is

$$T = a + b \cdot \sin^2(2\varphi), \quad (4-5)$$

where a and b are constants.

A quantity R is defined as the ratio of the difference between maximum transmission (T_{max}) and minimum transmission (T_{min}) to the sum of T_{max} and T_{min} , i.e.,

$$R \equiv \frac{T_{max} - T_{min}}{T_{max} + T_{min}} = \frac{b}{2a + b} . \quad (4-6)$$

For an ideal cell, with transmission given by eq.(4-4), a is equal to 0 and hence R equal to 1. While for a non-aligned sample, b is equal to 0 and R becomes 0. Therefore we use R , which is between 0 and 1, as a quantity to indicate the alignment quality. In Fig.4-3-4(a), we compare R , for several modifying density. These samples were modified just once in any chosen region. It is clear that the R increases with line density monotonically. We have also studied the effect of multiple modifications by running the tip repeatedly in the same region with a fixed line density of 12.8 lines per μm . The results are shown in Fig.4-3-4(b), we can see that the R remains a constant value. The multiple modifying processes do not improve the alignment quality nor make it worse.

For all of the samples shown in Fig.4-3-4, we have measured their anchoring strength, which are plotted in Fig.4-3-5. The points with a “*” mark are for the samples made into parallel cells, where the chiral dopant 5CB is used. The anchoring strength is found to increase with the line density and approximately proportional to the line density [see Fig.4-3-5(a)], except for the one with chiral dopant in the cell. The difference caused by the chiral dopant is expectable, because the LC material becomes different with chiral dopant added in and the anchoring strength is a quantity that indicates the anisotropy of molecular interaction between LC molecules and the PI films.

We have varied the number of times to modify the PI films with a fixed line density (of 12.8 lines per μm). The measured anchoring strength is shown in Fig. 4-3-5(b); it does not change significantly with the number of times for multiple modifications.

In the work by Lien et al. [1], the anchoring strength for the photo-induced alignment was found to be between 10^{-5} and 10^{-4} J/m², while the anchoring strength we measured for the rubbed surface is about 10^{-4} J/m². The anchoring strength in our study is $0.8\sim 3\times 10^{-5}$ J/m², which is compatible to the strength by photo-induced alignment. Our assumption of strong anchoring by rubbed surface when determining θ and φ_s is justified.

We have used the same AFM but working on the tapping mode to study the surface topology of the samples. Figure 4-3-6 shows a typical example for the surface topology. No trace of any groove due to the AFM modification process can be seen. All other samples show similar topology, which is also similar to the one prior to AFM modification. Although some scratch-like grooves can be seen, they are not parallel to the modifying direction. They may be intrinsic fine grooves on the glass substrates while they were polished.

Even though we do not see any difference on the surface topology by directly looking at the 3- dimensional plots, some very shallow grooves may still be buried in the rough surface topology. To clarify this possibility, we have carried out a Fourier analysis of the surface topology data. The power spectrum of the topographic data is calculated according to the following equations.

For a line with data taken from L equal spaced points, the height of each point is denoted by $f(x)$ with $x=1$ to L . The function $f(x)$ can be expressed as a Fourier series,

$$f(x) = 2\pi \sum_1^L \left[A_n \cos\left(\frac{n2\pi}{L}x\right) + B_n \sin\left(\frac{n2\pi}{L}x\right) \right], \quad (4-7)$$

where

$$A_n = \frac{1}{L} \sum_1^L f(x) \cos\left(\frac{n2\pi}{L}x\right), \quad (4-8)$$

$$B_n = \frac{1}{L} \sum_1^L f(x) \sin\left(\frac{n2\pi}{L}x\right). \quad (4-9)$$

The power spectrum P_n is then calculated by

$$P_n = A_n^2 + B_n^2. \quad (4-10)$$

In Fig.4-3-7, we show a set of typical power spectrum obtained in this manner. For the sample with the modifying density 5.12 lines per μm shown in Fig.4-3-6, we have analyzed the data with a scanning density of 82.58 points per μm and a total of 256 points are scanned for each line. We have also scanned the sample with scanning directions parallel and perpendicular to the modifying direction. In this figure, the power spectra for lines parallel and perpendicular to the modifying direction are plotted. The curve for the surface before modification is also shown for comparison. While the one parallel to the modifying direction is a little different from that for the unmodified region, the result for the line perpendicular to the modifying direction is very different from both of them. From these plots, we can see that the surface has ripples of large period, i.e., small n , caused by the AFM modification. The ripples perpendicular to the modifying direction are much more profound than that parallel to.

Grooves caused by the AFM-modification are still not found. If there were grooves caused by the AFM tip during the modify processes, the spacing would be 16.1 points, which is the ratio of scanning density and modifying density. In the “perpendicular” curve, there should then be a peak at $n=16$, which is the ratio of total points in a line scan to the spacing. However, there is no clear peak at $n=16$ or its multiples.

For all of the samples we studied, none of them shows a characteristic peak for the grooving structures after Fourier analysis. The feature that lines scanned perpendicular to the modifying direction have larger values at small n is very common, although the difference may differ from sample to sample. The only exception occurs when the film has been multiply modified for three times. The results together indicate that the wide ripples are formed perpendicular to the modifying direction and possibly caused by a dragging shear force from the AFM tip.

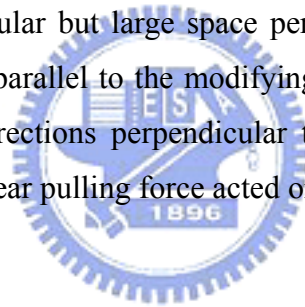
4-4 Conclusions

We have modified the PI coated glass substrate surface with AFM tip by running the tip touching the surface with various line densities. This process can make the PI film interacting with the LCs on the surface anisotropically and make the liquid

crystals aligned along the tip moving direction. The aligning property and anchoring strength to the LCs are nearly proportional to the modifying line density. On the other hand, they are not affected by how many times the same processes are repeated. Overall, the anchoring strength is compatible with that from a common rubbing process [3] and [4].

The positioning for the modified region is very fine; in principle it can be near 10 nm. However, the LC cell thickness and the LC coherence length limit the real resolution of the alignment. In our samples, which have a thickness of 6 μm , the resolution is about 3 μm .

Either by looking at the AFM topographical picture or by Fourier analysis on the topology data, no any grooving structure due to the AFM modify on the PI films is found. However, the Fourier analysis results do show changes caused by the modifying process. The irregular but large space period ripples are formed on both directions perpendicular and parallel to the modifying direction, although the ripples are more profound in the directions perpendicular to the modifying direction. We consider this caused by the shear pulling force acted on the film by the moving tip.



References

- [1] Y. Saitoh, and A. Lien, “An Improved Azimuthal Anchoring Energy measurement Method Using Liquid Crystals with Different Chiralities”, *Jan. J. Appl. Phys.*, **39**, pp.1743-1746 (2000).
- [2] P. G. deGennes, and J. Prost, “*The Physics of Liquid Crystals*”, (Oxford, London, 1993)
- [3] A. J. Pidduck, G. P. Bryan-Brown, S. D. Haslam, and R. Bannister, “Estimation of microscopic rubbing alignment parameters”, *Liq. Cryst.*, **21**, pp.759-763, (1996).
- [4] A. J. Pidduck, G. P. Bryan-Brown, S. D. Haslam, R. Bannister, and I. Kitley, T. J. McMaster, L. Boogaard, “Atomic force microscopy studies of rubbed polyimide surfaces used for liquid crystal alignment”, *J. Vac. Sci. Technol. A*, **14**, No. 3, pp. 1723-1728 (1996).



Chapter 5

Summary and Future Scope

5-1 Summary

In this work we have developed a LC alignment process employing standard semiconductor processing steps (do not need alignment film). This is advantageous for integrating LC devices with other devices such as MEMS. We have etched U-shape grooves of micron scale with various periods and depths and studied their alignment properties and anchoring strengths to LC.

The periods of the grooves are varied between 2 and 9 μm . When the depths of the grooves is small ($21 \pm 5 \text{ nm}$), the anchoring strength ($<10^{-6} \text{ J/m}^2$) are smaller than traditional rubbed polyimide surfaces. It can be increased more than an order of magnitude by varying the groove depth and period. Values larger than 10^{-5} J/m^2 can be achieved with the depths of the grooves larger than 50 nm. Strong anchoring can be obtained when the periods are less than 4 μm and depths are above 50 nm. However, grooves much deeper than 50 nm may reduce the anchoring strength.

We used an improved method for measuring the temperature dependence of azimuthal anchoring strength by using two lasers with different wavelengths. A chiral dopant is added into the nematic liquid crystal 4'-n-pentyl-4-cyanobiphenyl (5CB) for anchoring strength measurement. The azimuthal anchoring strength of 5CB on parallel grooved glass substrates was found to decrease steadily when temperature increases. The change of A is due to the change of K_{22} at most nematic temperature unless the temperature is very close to the clearing point. When temperature is very close to T_c , the pitch changes and becomes unstable, therefore this method is not suitable for anchoring strength measurement at this temperature range.

We have modified the PI coated glass substrate surface with AFM tip by running the tip touching the surface with various line densities. This process can make the PI

film interacting with the LCs on the surface anisotropically and make the liquid crystals aligned along the tip moving direction. The aligning property and anchoring strength to the LCs are nearly proportional to the modifying line density. On the other hand, they are not affected by how many times the same processes are repeated. Overall, the anchoring strength is compatible with that from a common rubbing process.

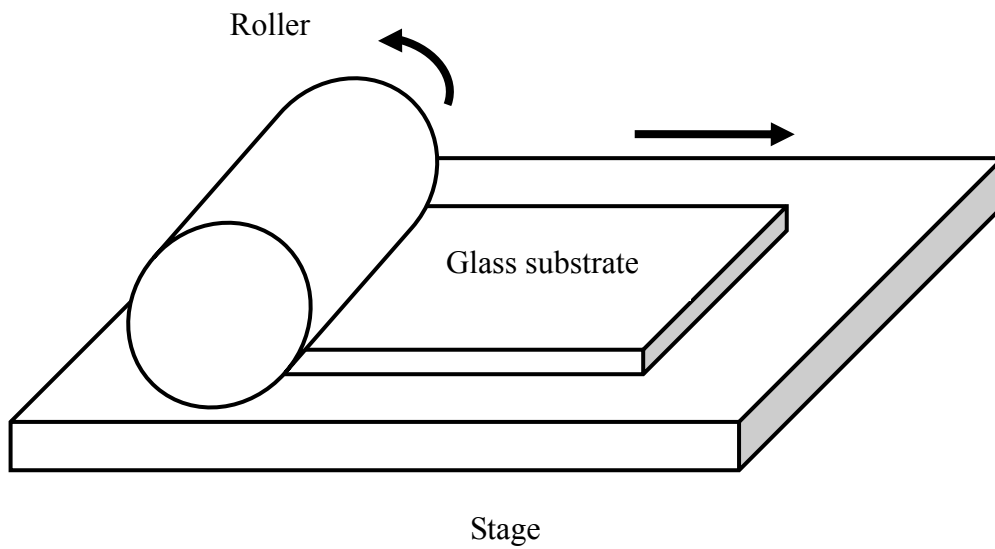
The positioning for the modified region is very fine; in principle it can be near 10 nm. However, the LC cell thickness and the LC coherence length limit the real resolution of the alignment. In our samples, which have a thickness of 6 μm , the resolution is about 3 μm .

Either by looking at the AFM topographical picture or by Fourier analysis on the topology data, no any grooving structure due to the AFM modify on the PI films is found. However, the Fourier analysis results do show changes caused by the modifying process. The irregular but large space period ripples are formed on both directions perpendicular and parallel to the modifying direction, although the ripples are more profound in the directions perpendicular to the modifying direction. We thought that this caused by the shear pulling force acted on the film by the moving tip.

5-2 Future Scope

Understanding the dependence of the shape of the grating surface on the surface azimuthal anchoring is important. We will use Nanoimprint lithography technique to create microgroove with arbitrary surface shape. And to design the surface azimuthal anchoring energy of the arbitrary surface shape of the relief grating by FEM. After tracing the real surface by using AFM, traced pattern can be directly input to FEM, and the surface azimuthal anchoring energy can be obtained by FEM.

(a)



(b)

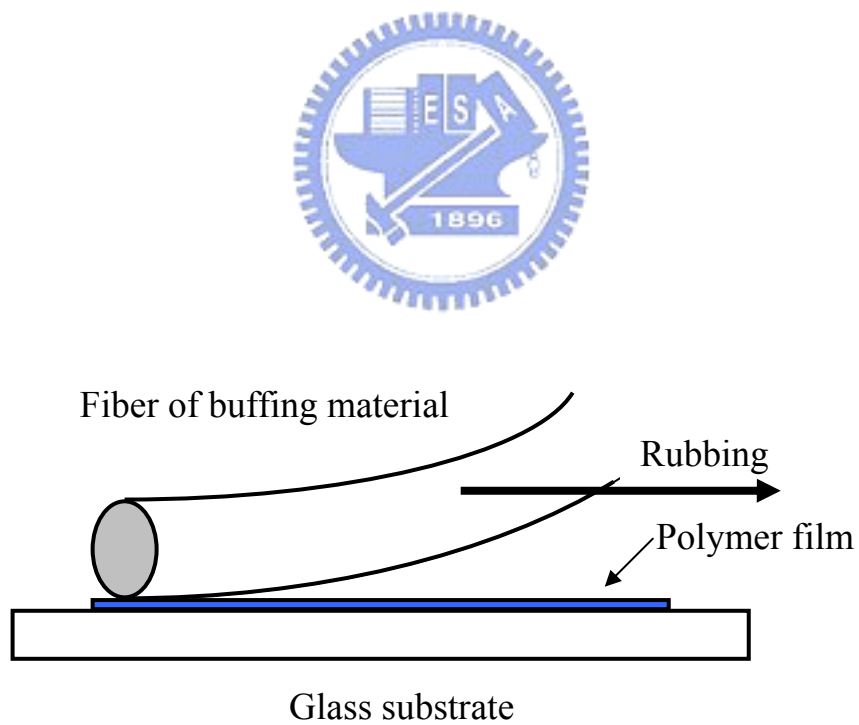


Fig. 1-1-1(a) A structural sketch of a rubbing machine. (b) A cross sectional view of a polymer film in contact with a moving fiber of buffing material.

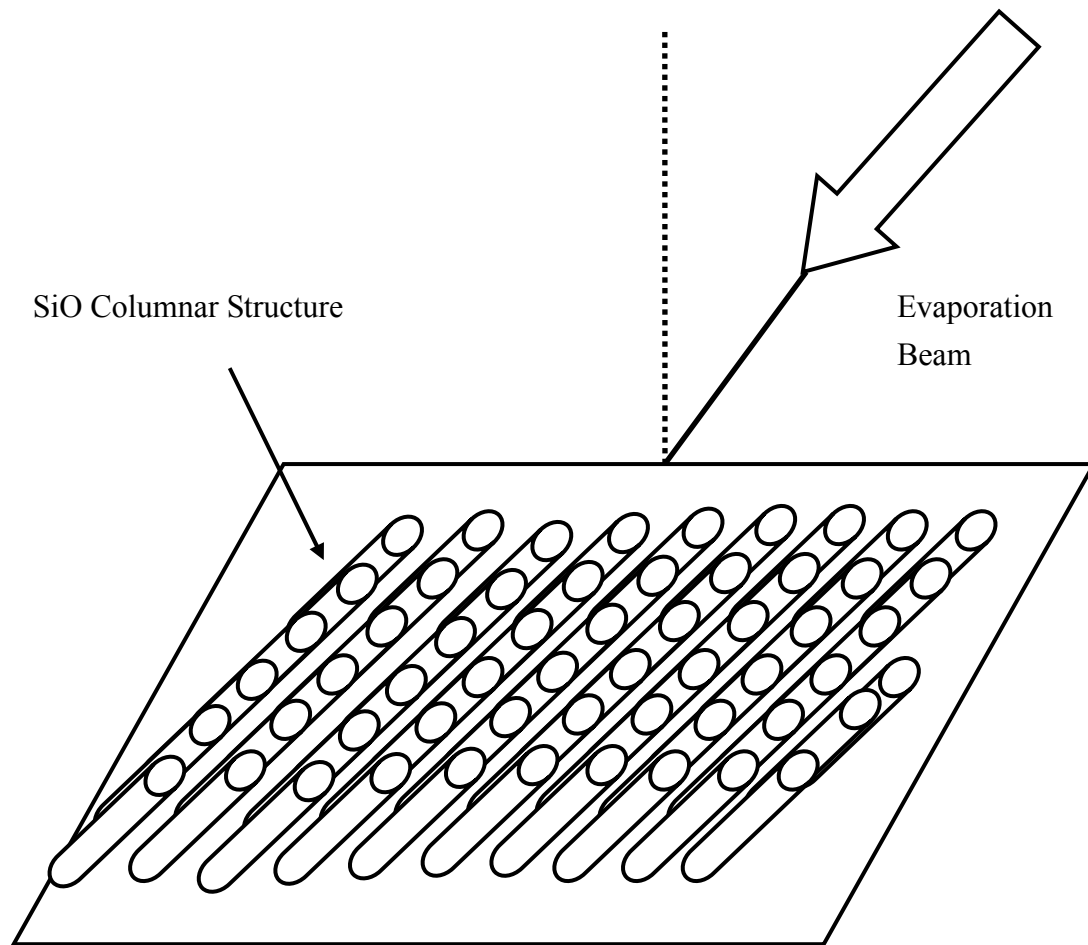
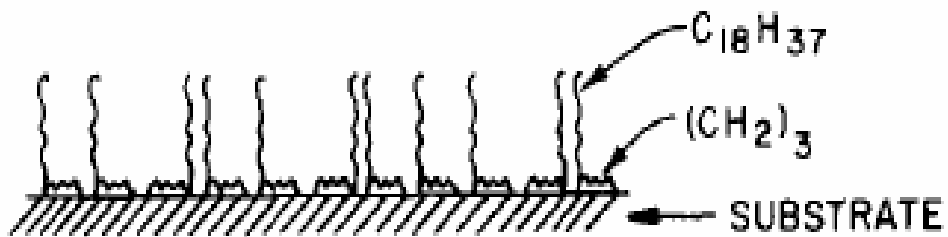
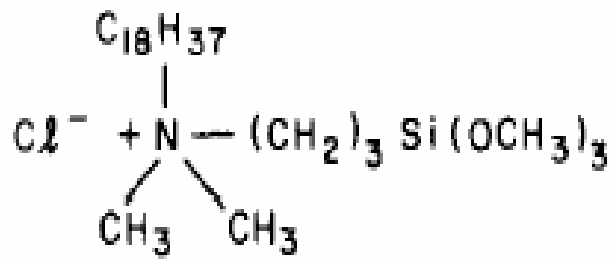


Fig.1-2-1 Surface structure of the oblique evaporated film. When nematic LC contact such a surface, elastic deformation of the LC along the surface induced interaction energy between the surface and nematic LC. This is thought to be the driving force for alignment of the nematic director. The surface structure of the obliquely evaporated film changes with the evaporation angle (the angle between evaporation beam and substrate normal). K. Takatoh, M. Hasegawa, M. Koden, N. Itoh, R. Hasegawa, and M. Sakamoto, “*Alignment Technologies and Applications of Liquid Crystal Devices*” (Taylor & Francis, 2005).

(a)



(b)

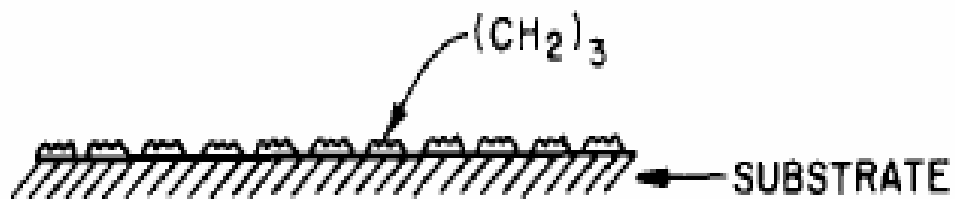
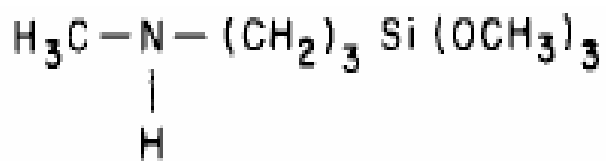


Fig.1-2-2(a) N, N-dimethyl-N-octadecyl-3-aminopropyltrimethoxysilyl chloride (DMOAP). (b) N-methyl-3-aminopropyltrimethoxysilane (map). F. J. Kahn, Appl. Phys. Lett., **22**, No. 8, pp.386-388 (1973).

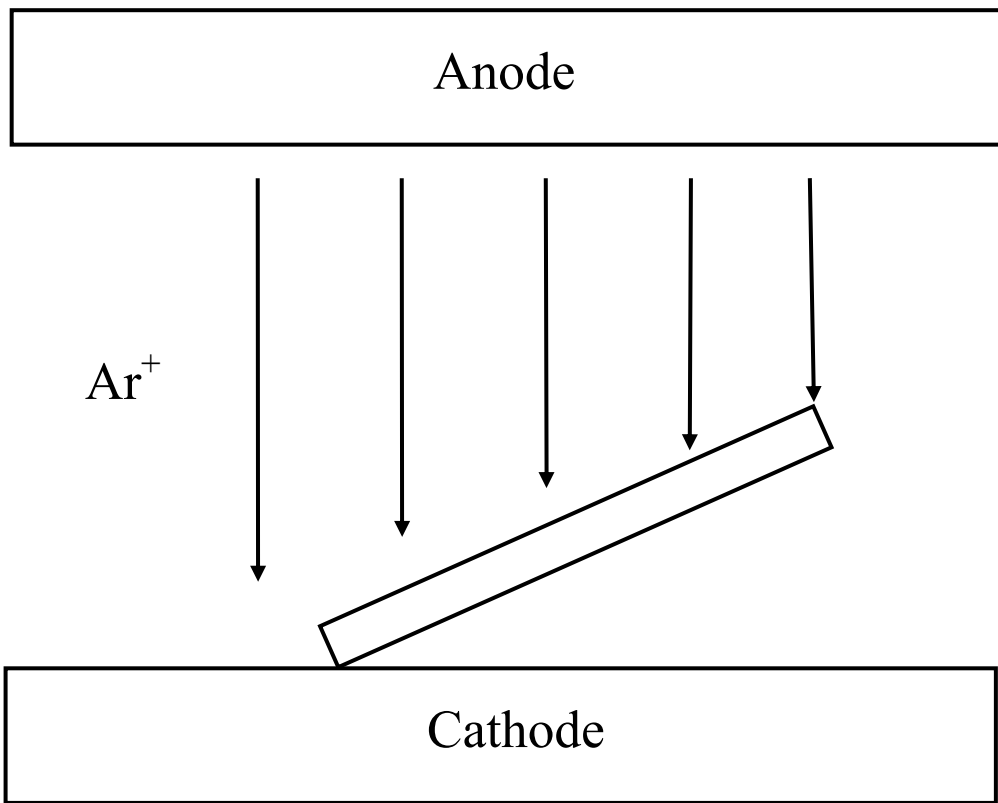


Fig.1-2-3 Low energy beam of argon ions is used to bombard the surface of a polyimide film. The argon beam produces directional alignment when the beam is at an angle other than perpendicular to the polyimide film surface.

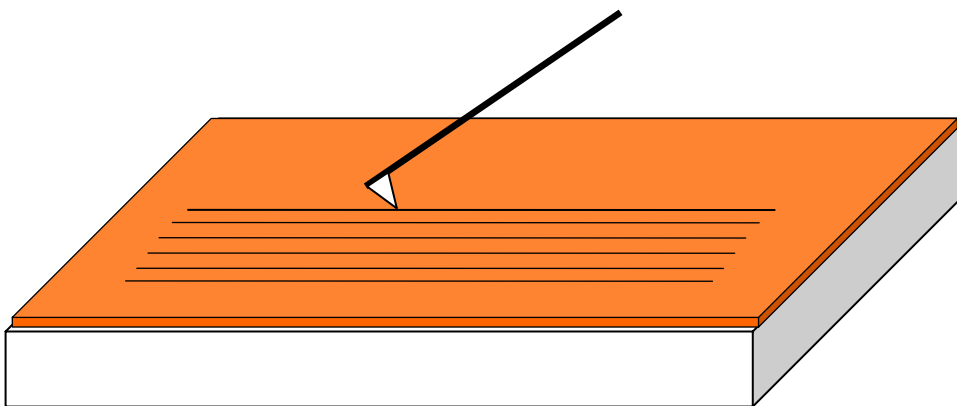
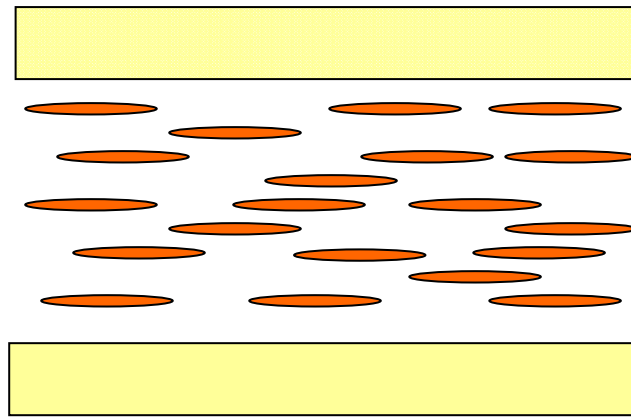


Fig.1-2-4 The AFM tip modifying methods.

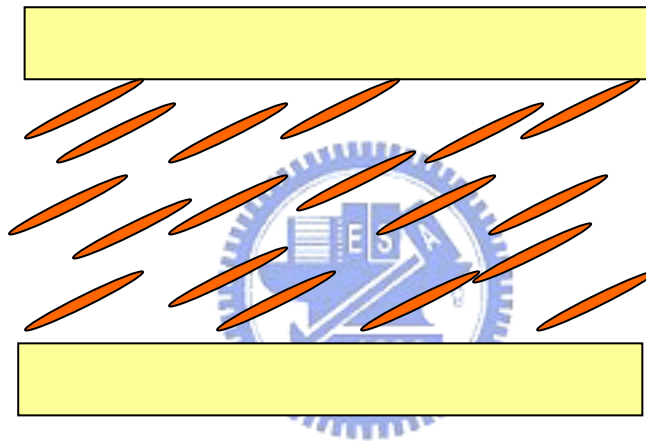
(a)

Homogeneous



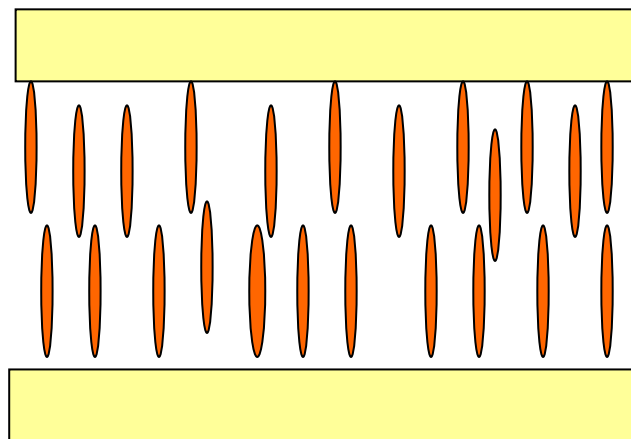
(b)

Tilted



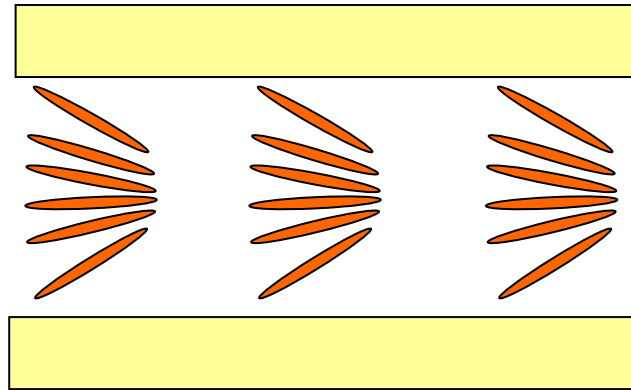
(c)

Homeotropic



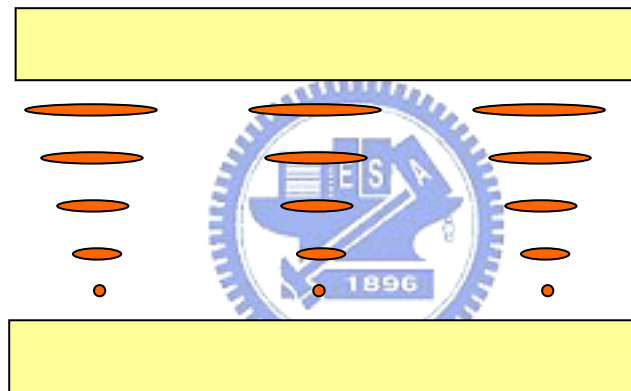
(d)

Splay



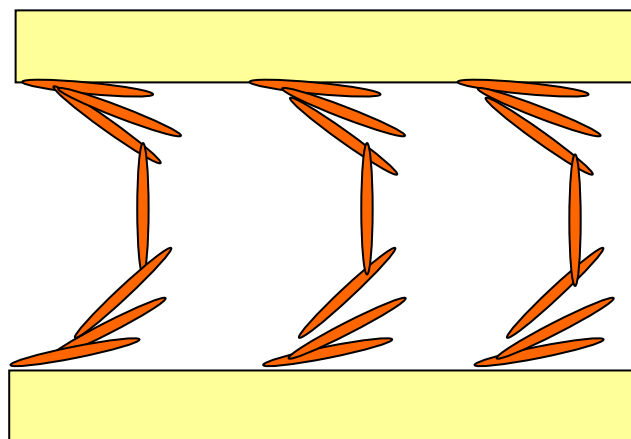
(e)

Twist



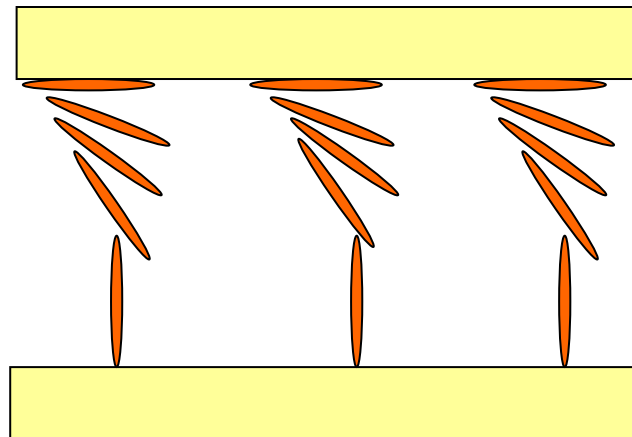
(f)

Bend



(g)

Hybrid



(h)

Super-twisted nematic

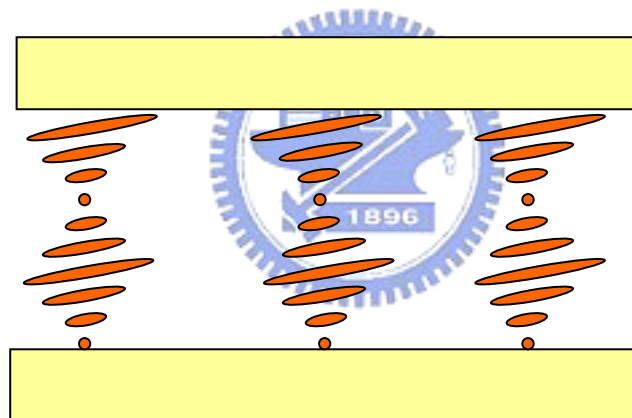


Fig.1-3-1 Typical orientations are shown. These orientations are classified into two groups. (a)~(c) The directors of the LC molecules in homogeneous, tilted and homeotropic cases are aligned in one fixed direction, while(d)~(h), the director of LC molecules in the splay, twist, bend, hybrid and super-twisted nematic cases are not fixed in one direction. K. Takatoh, M. Hasegawa, M. Koden, N. Itoh, R. Hasegawa, and M. Sakamoto, “*Alignment Technologies and Applications of Liquid Crystal Devices*” (Taylor & Francis, 2005).

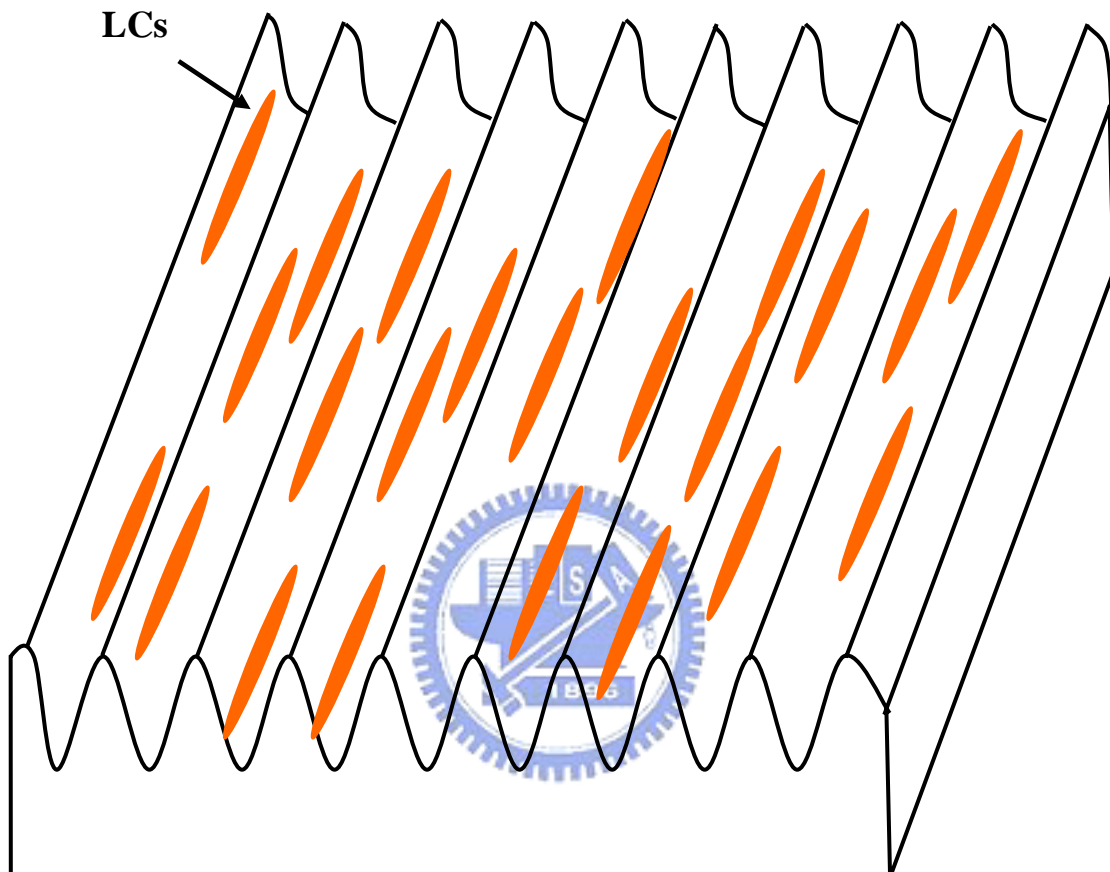
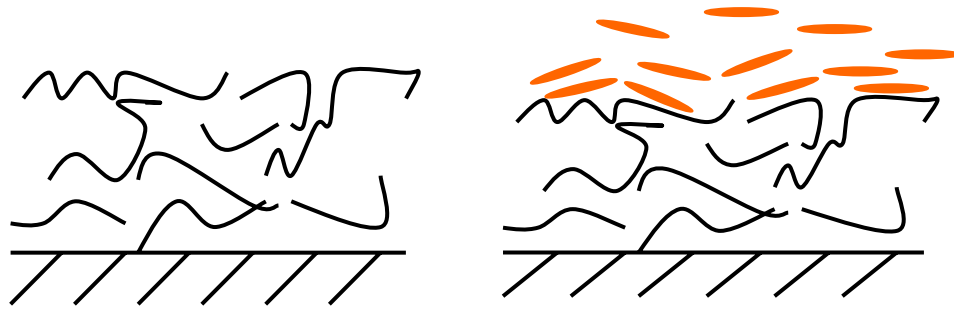


Fig.1-3-2 Schematic geometry of sinusoidal grooves is shown. Berreman suggested the elongated LCs prefer to align parallel to the induced micro size grooves to reduce the total surface free energy. D. W. Berreman, "Solid surface shape and the alignment of an adjacent nematic liquid crystal", Phys. Rev. Lett. **28**, pp.1683-1686 (1972).

(a)

Before rubbing

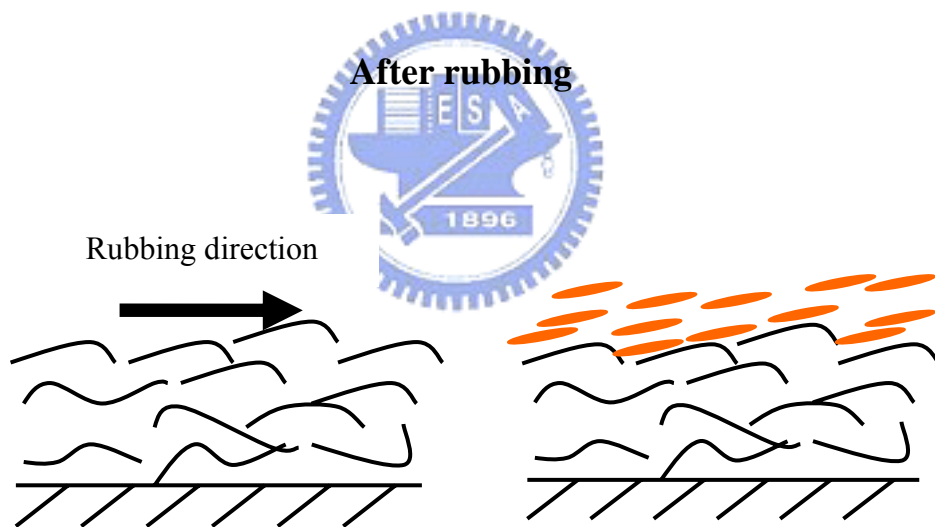


Before injection LC

After injection LC

(b)

After rubbing



Before injection LC

Aefore injection LC

Fig.1-3-3 A polymer chain alignment model (a) before rubbing, (b) after rubbing. Geary et al. suggested that LCs is anchored by buffed polymer chains of the polymer surfaces. The alignment of LCs then follows in an epitaxial manner. J. M. Geary, J. W. Goodby, A. R. Kmetz, and J. S. Patel, "The mechanism of polymer alignment of liquid-crystal materials", J. Appl. Phys. **62**, pp.4100-4108 (1987).

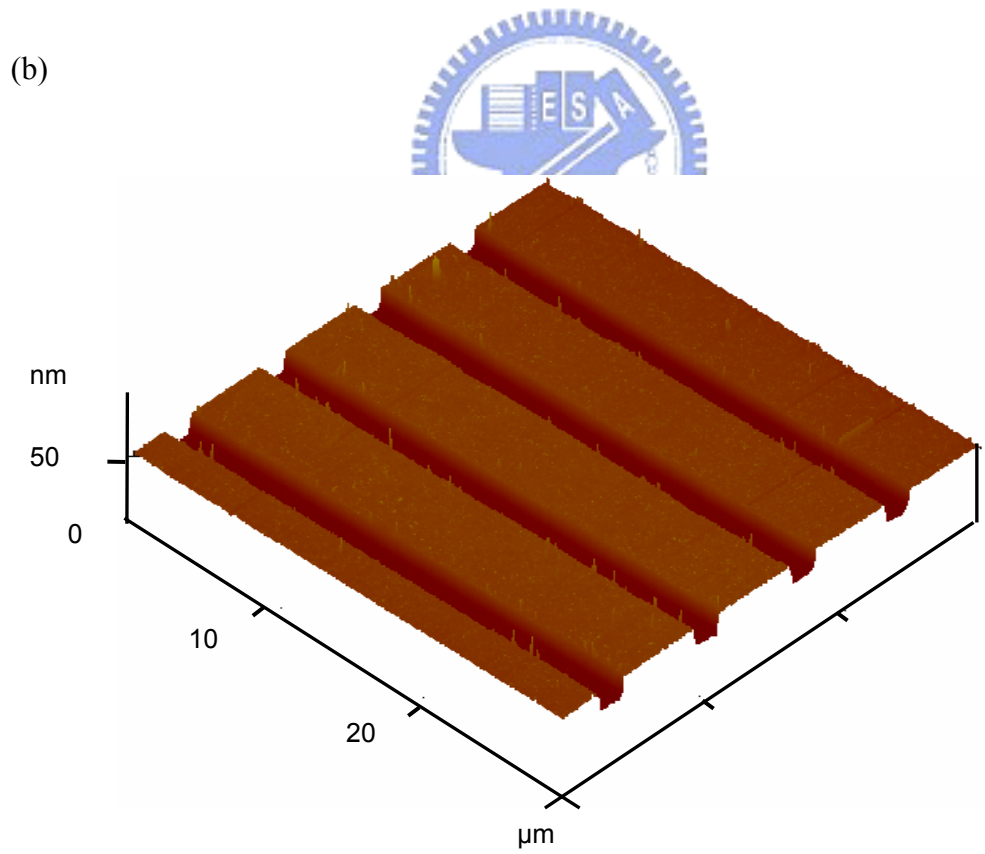
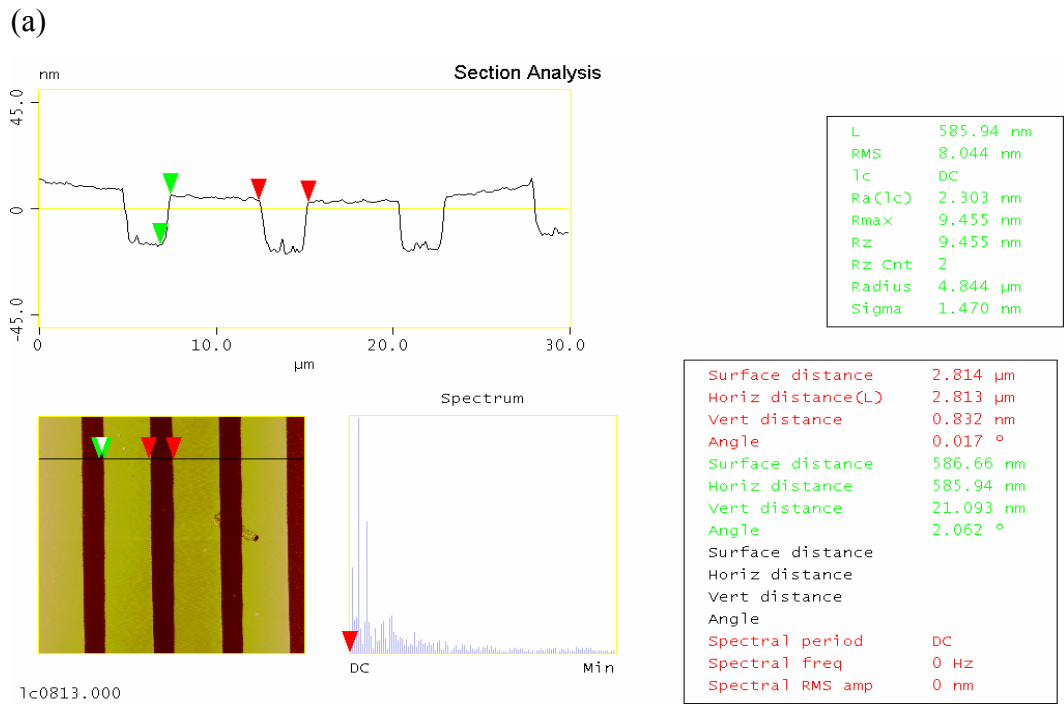


Fig. 2-1-1 AFM image of parallel grooved glass surface, which were prepared by RIE method with depth of 13.6 ± 0.3 nm and period of $7.0 \mu\text{m}$. (a) Section analysis: the root mean square roughness for the top surfaces and bottom surfaces are 0.37 nm and 0.46 nm, respectively. (b) The AFM surface topology of the sample

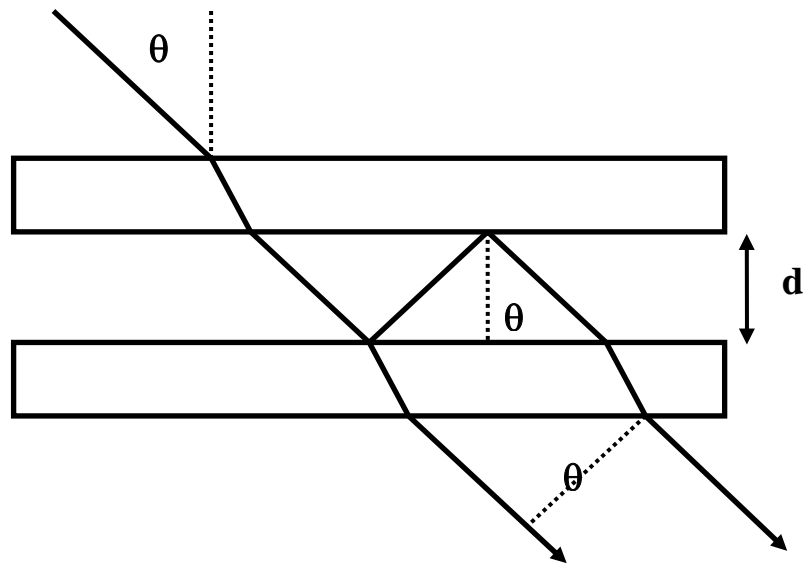


Fig. 2-2-1 Rotational interferometric method of LC cell gap measurement. A sketch for optical path goes through a cell.

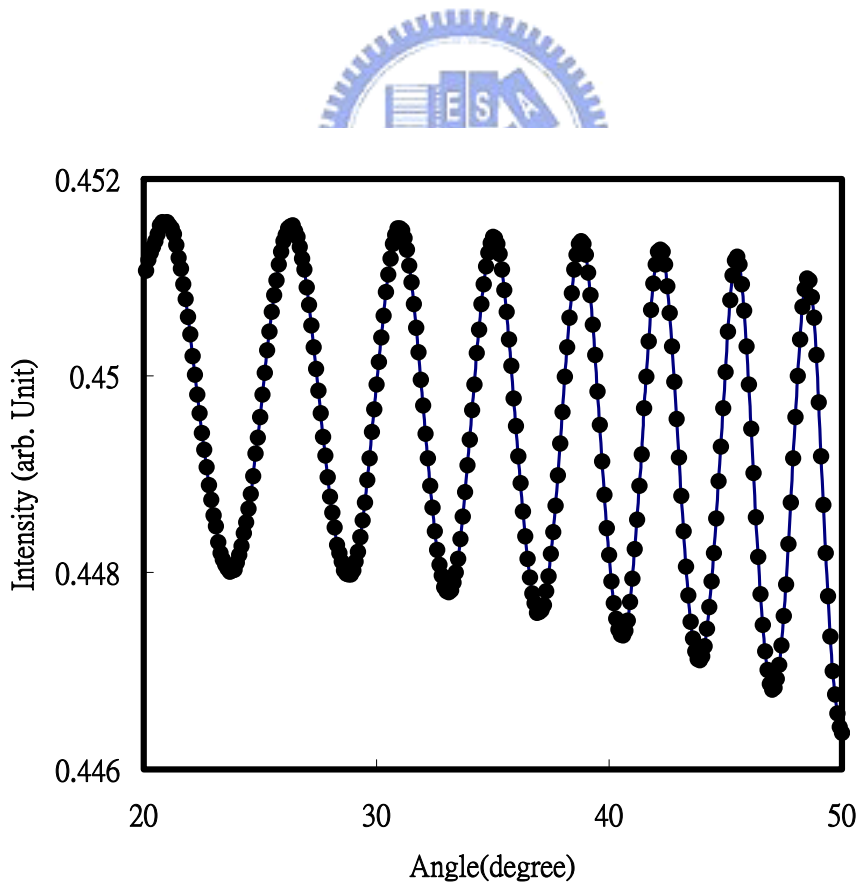
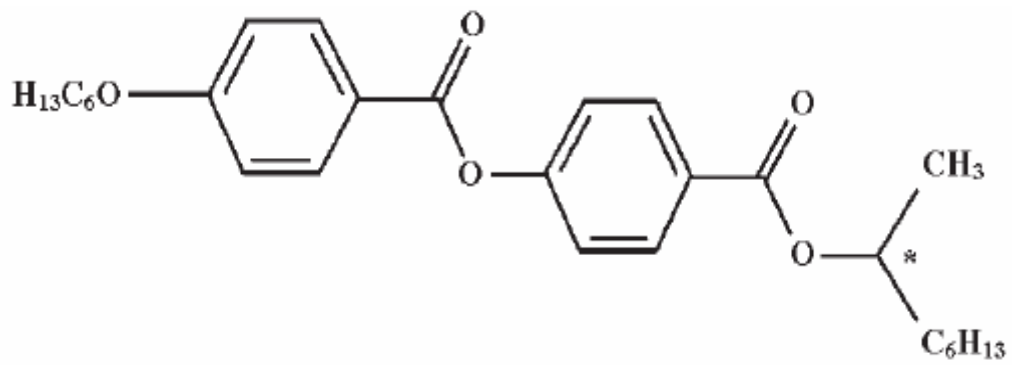
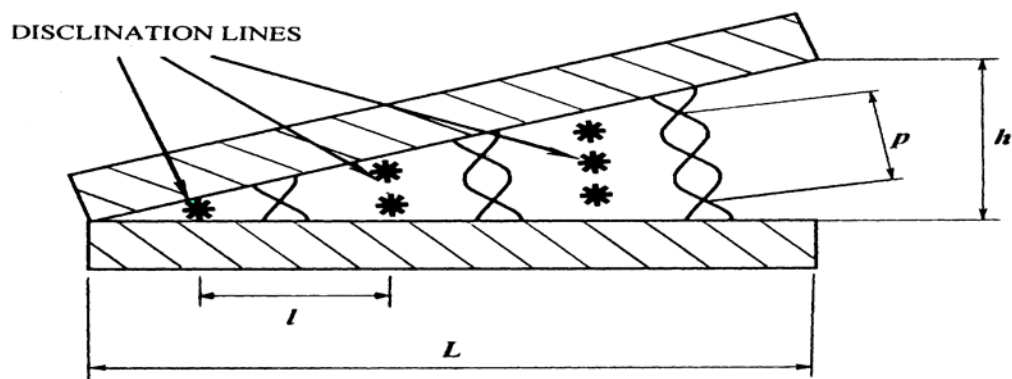



Fig. 2-2-2 Rotational interferometric method of LC cell gap measurement. An example of the transmittance through an empty cell ($\theta_1=31.0^\circ$, $\theta_2=26.4^\circ$, $\Delta m=1$, $\lambda=632.8$ nm), from which we can obtain $d=8.2$ μm .

(a)



(b)





$$\frac{p/2}{l} = \frac{h}{L} \Rightarrow p = \frac{2lh}{L}$$

(c)

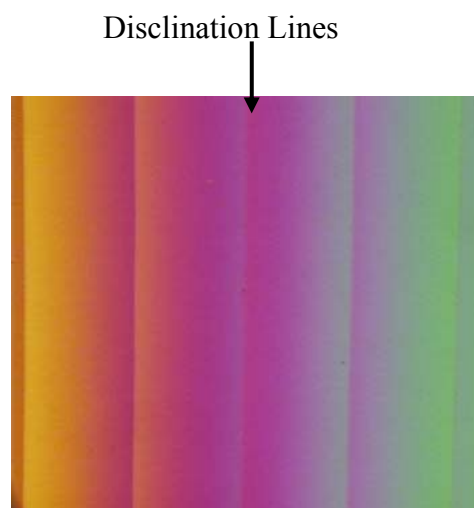


Fig.2-2-3 (a) The chemical structure of ZLI-811. (b) Cano-Wedge method. (c) Disclination lines.

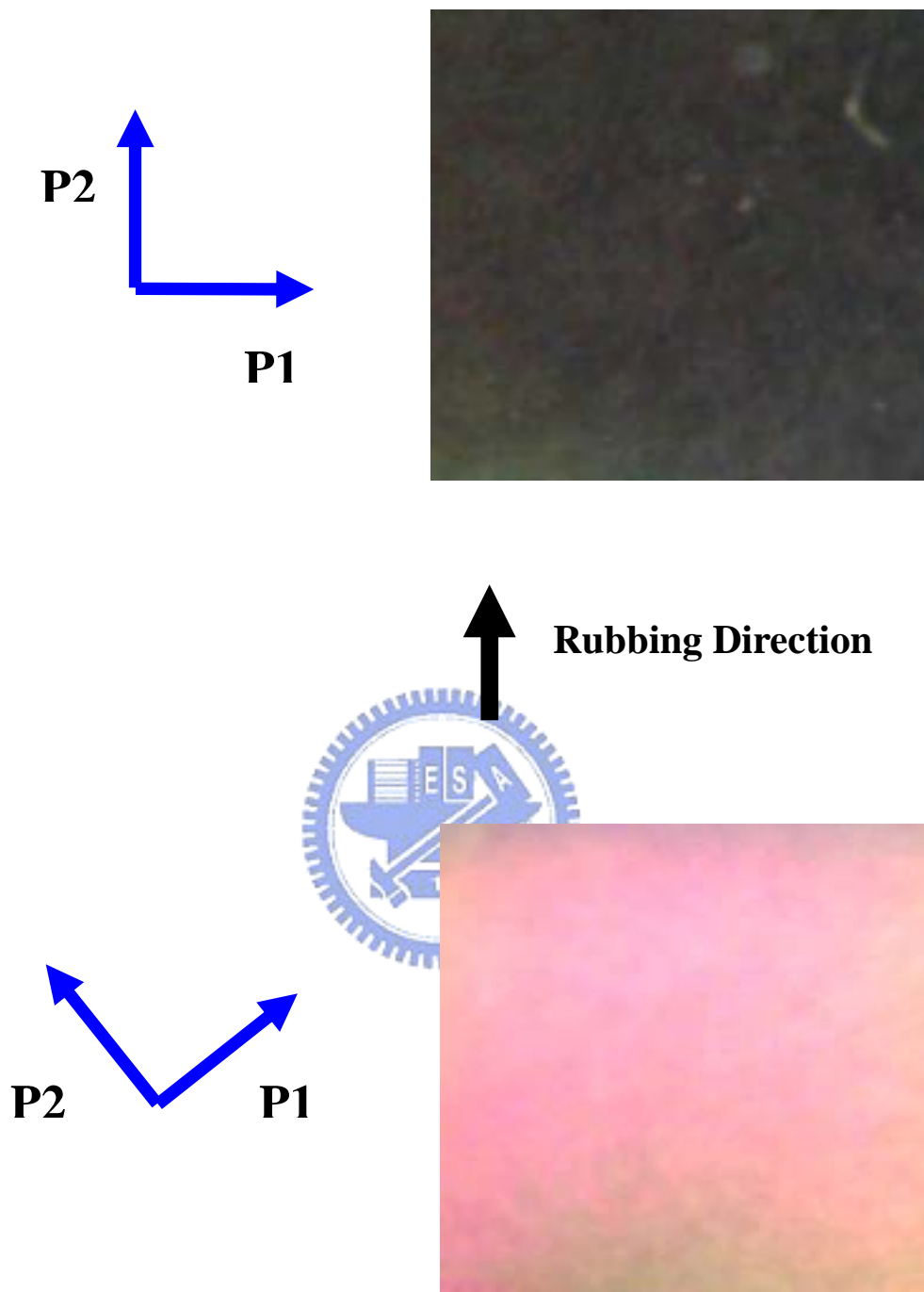


Fig.2-2-4 The planar alignment and the uniformity of alignment of LC in the cells were confirmed by using a polarizing microscope with crossed polarizers attached. (P1, P2)

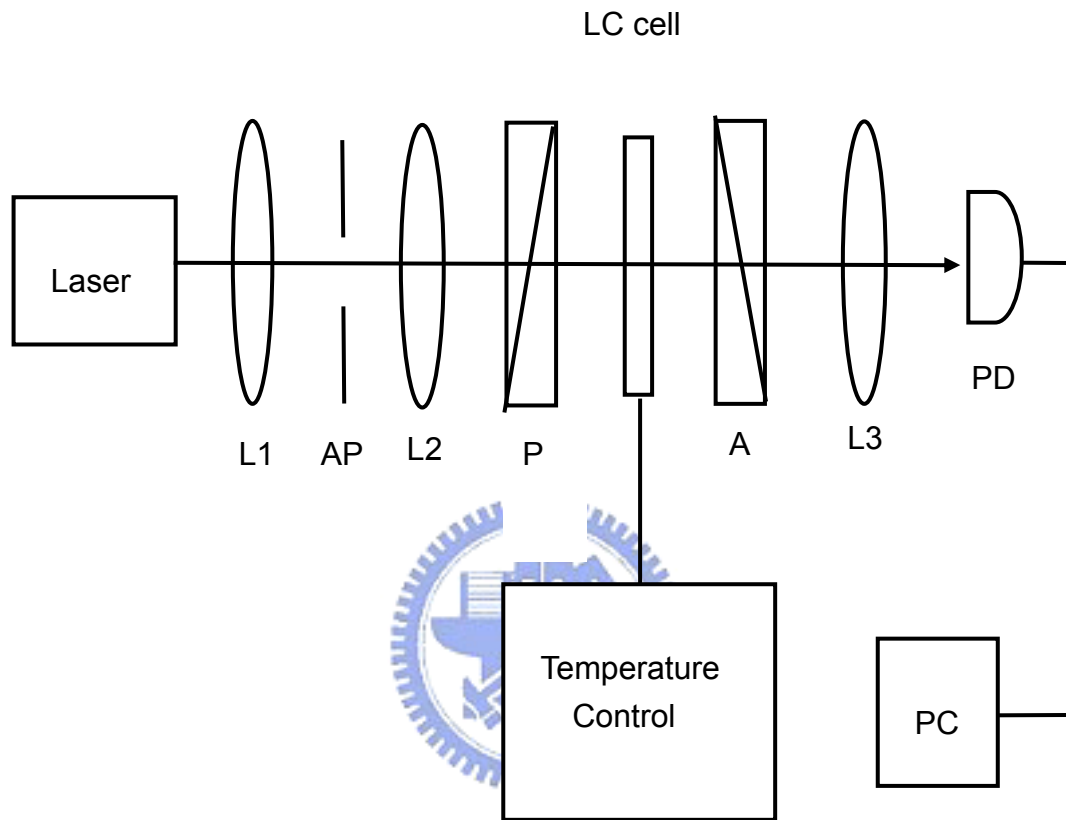
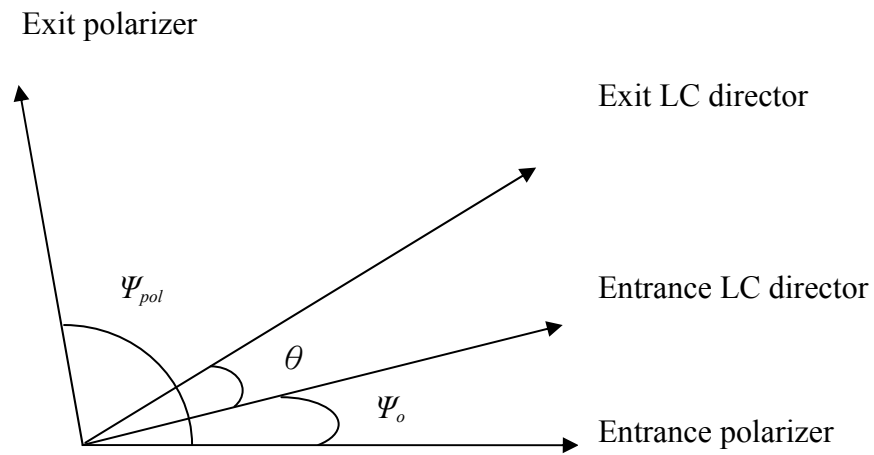


Fig. 2-2-5 Setup for anchoring strength measurement. L1, L2, L3: lenses; AP: aperture; P: polarizer; A: analyzer; PD: photo-detector; PC: personal computer. Light intensity through the arrangement from left to right in this figure detected by a photo-detector, PD1, is divided by the reference intensity measured by PD2, to eliminate the fluctuation of laser power. The temperature of the cells is controlled with temperature stability around ± 0.2 °C.

(a)



(b)

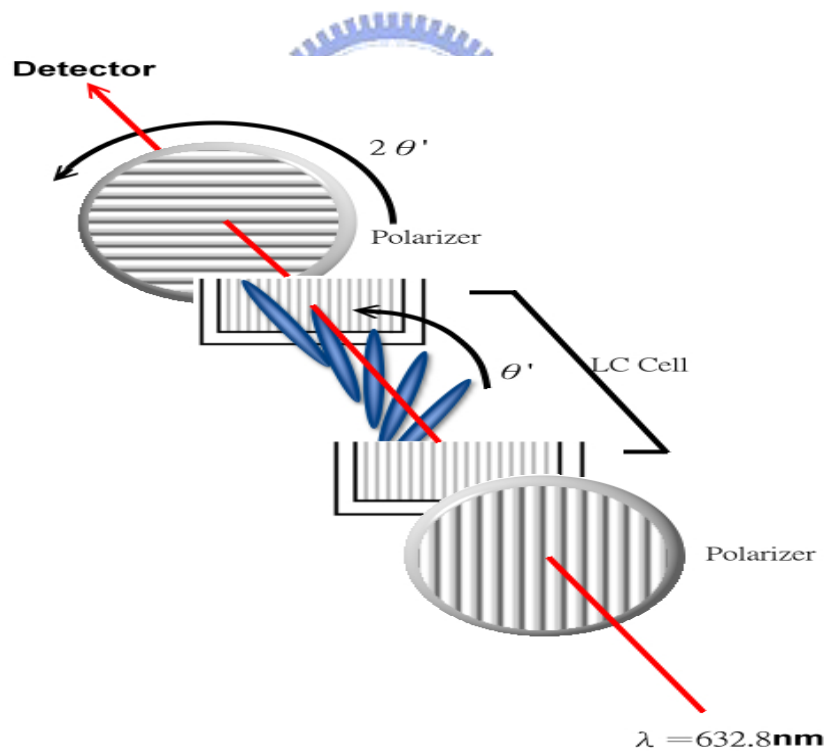
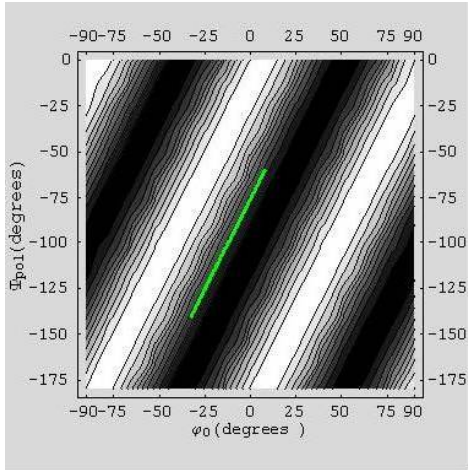
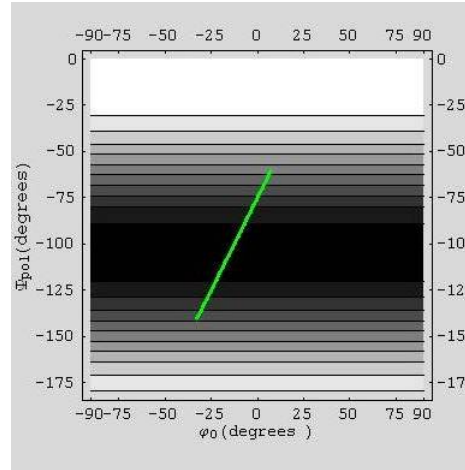


Fig.2-2-6(a) The relationship among θ , Ψ_o , and Ψ_{pol} (b)The LC cell and the analyzer are rotated to vary Ψ_o and Ψ_{pol} simultaneously with a ratio of 1 to 2.

(a) $d\Delta n/\lambda$ is close 0.5, 1.5,...



(b) $d\Delta n/\lambda$ is close 1



(c) $d\Delta n/\lambda$ otherwise

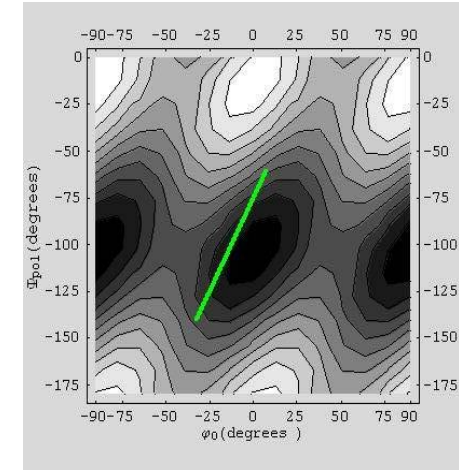


Fig.2-2-7 The relationship among $d\Delta n/\lambda$, Ψ_o , and Ψ_{pol} . When $d\Delta n/\lambda$ is close 0.5, 1.5, ..., as shown in Fig.2-2-6(a), the conditions are not suitable for anchoring strength measurement. When $d\Delta n/\lambda$ is the other values, as shown in Fig.2-2-6(b) and (c), there is a minimum condition which allows Ψ_{pol} to be determined easily. Y. Saitoh, and A. Lien, "An Improved Azimuthal Anchoring Energy measurement Method Using Liquid Crystals with Different Chiralities", Jan. J. Appl. Phys., **39**, pp.1743-1746, (2000).

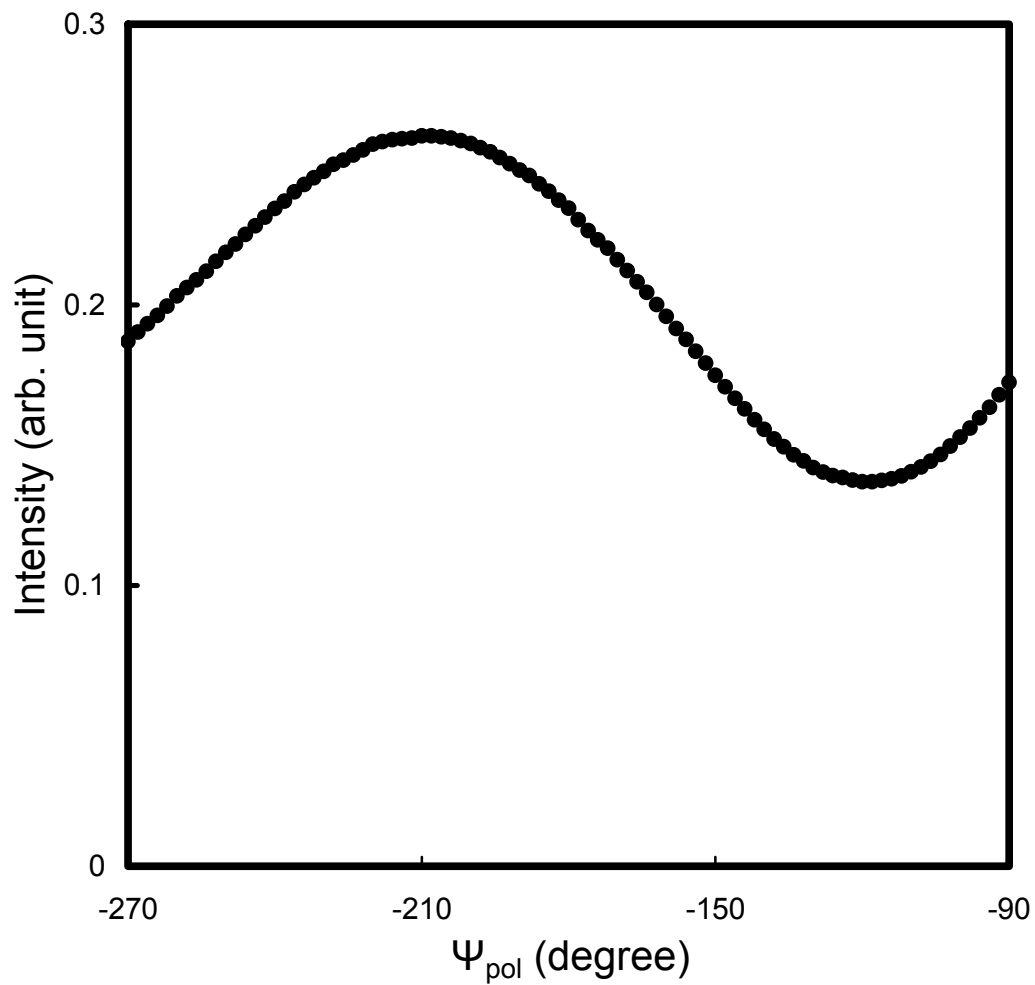


Fig. 2-2-8 The transmitted intensity versus the angle between the polarizer and analyzer, Ψ_{pol} . The minimum is obtained by a curve fitting. In this example, we obtain an angle with minimum intensity, where $\Psi_{pol}=-117.46^\circ$.

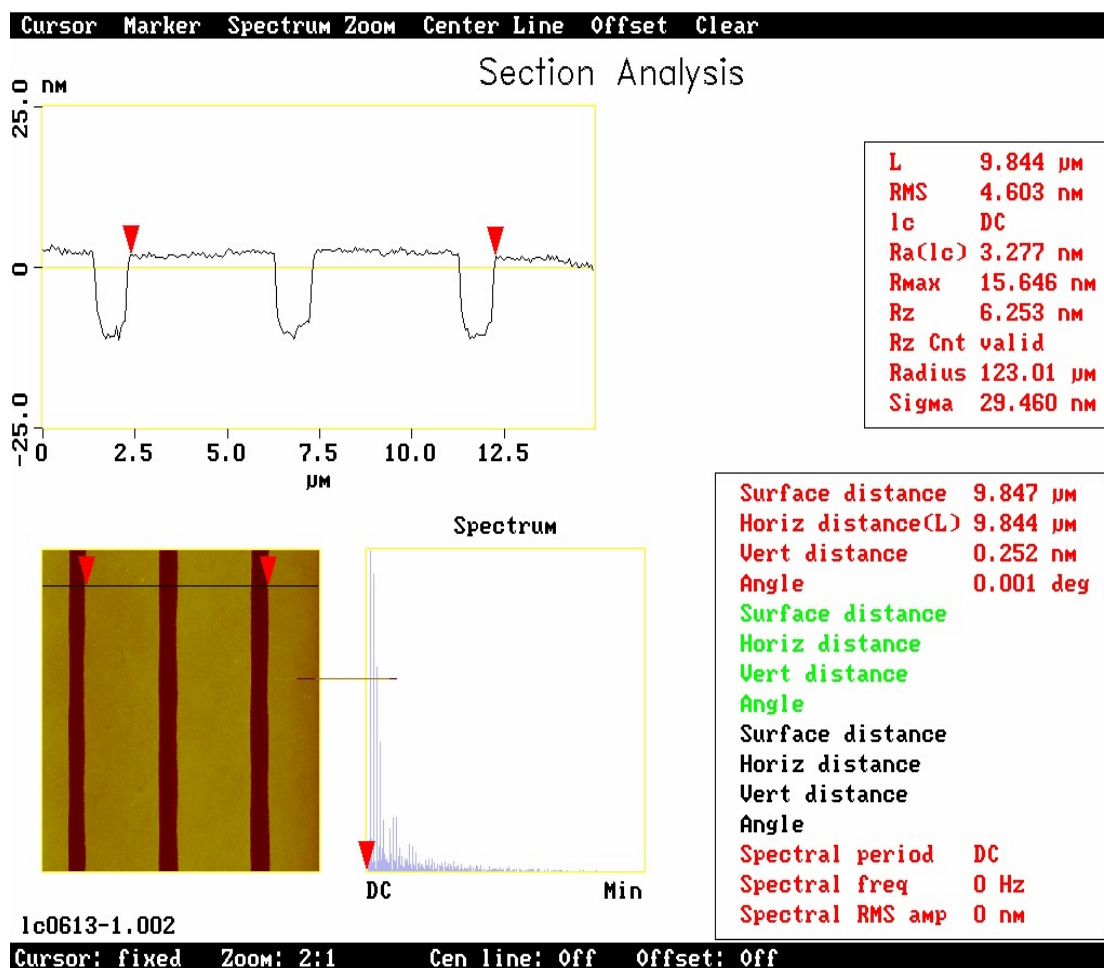


Fig. 2-3-1 AFM image of parallel grooved glass surface, which were prepared by RIE method with period of 5.0 μm .

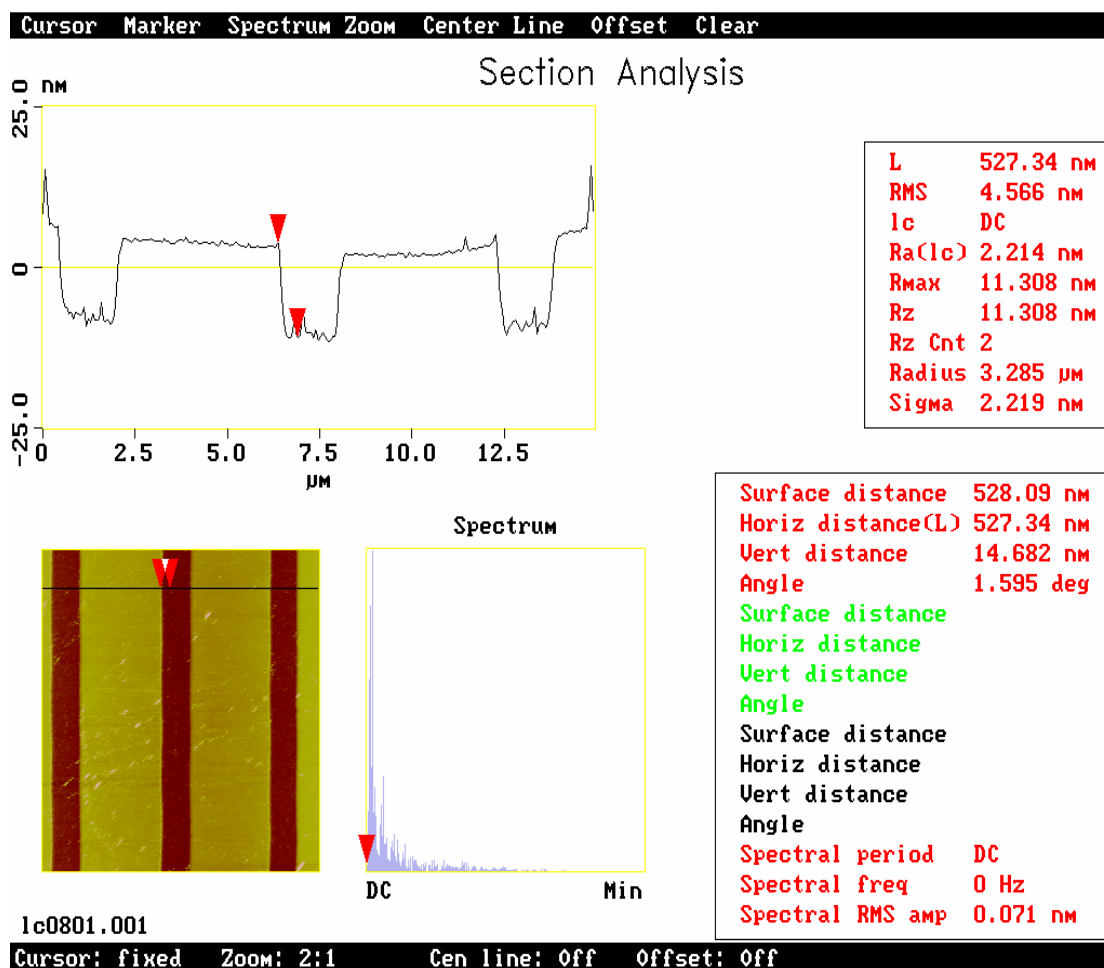


Fig. 2-3-2 AFM image of parallel grooved glass surface, which were prepared by RIE method with period of 6.0 μm.

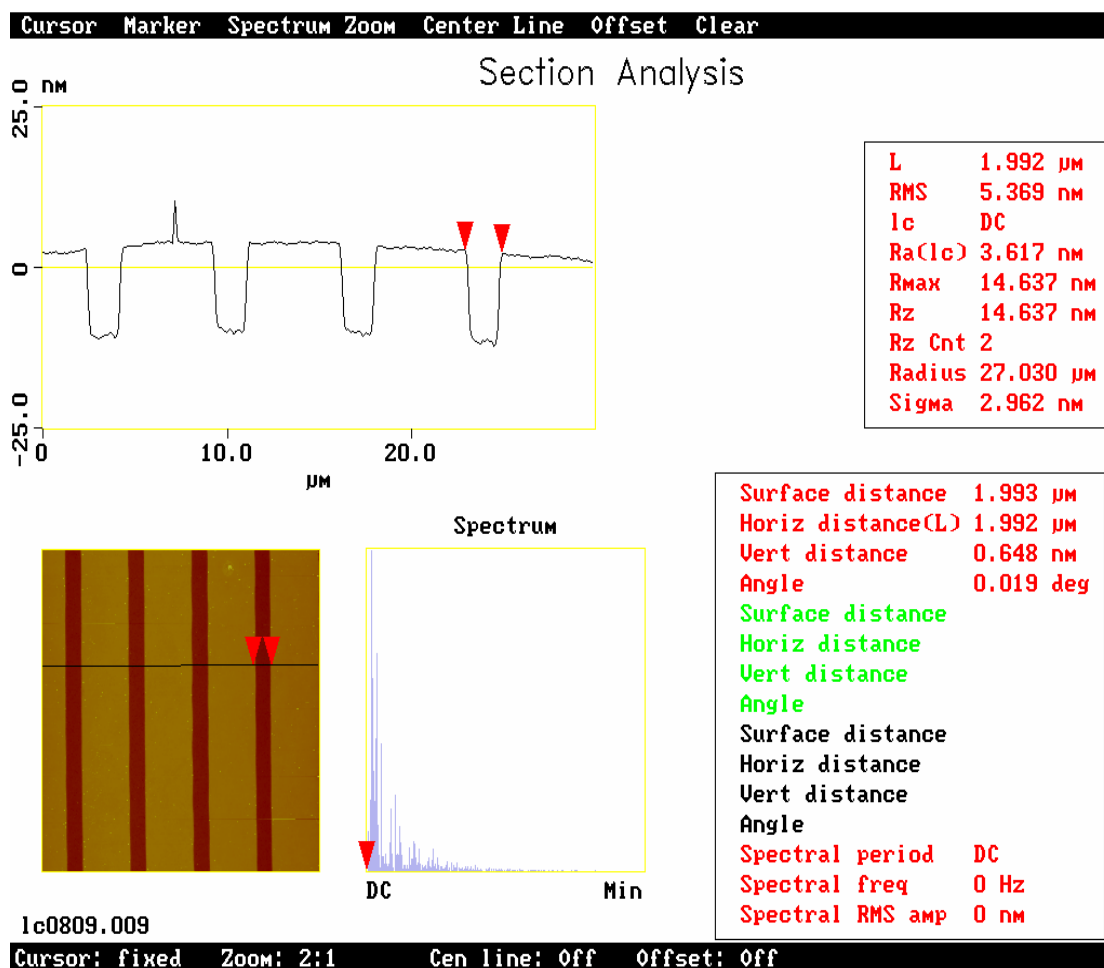


Fig. 2-3-3 AFM image of parallel grooved glass surface, which were prepared by RIE method with period of 7.0 μm.

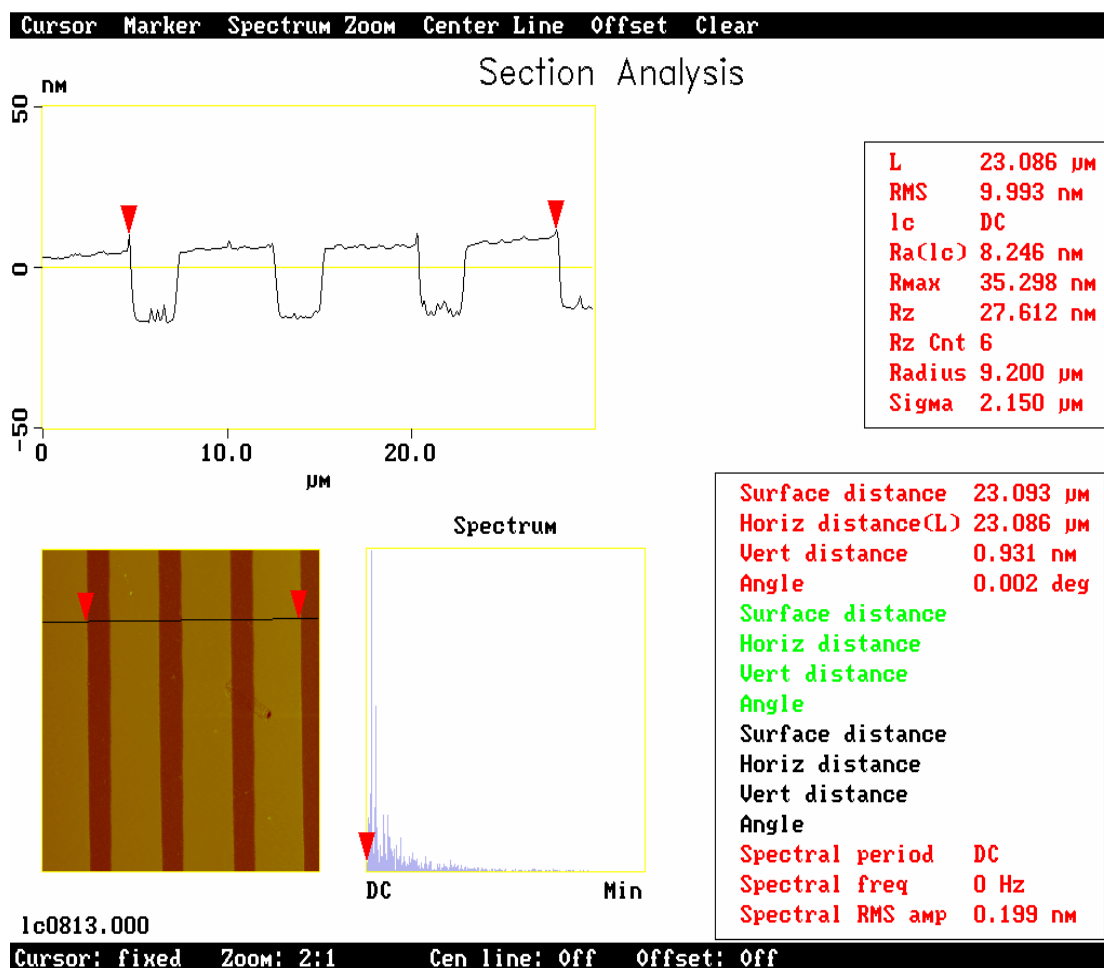


Fig. 2-3-4 AFM image of parallel grooved glass surface, which were prepared by RIE method with period of 8.0 μm.

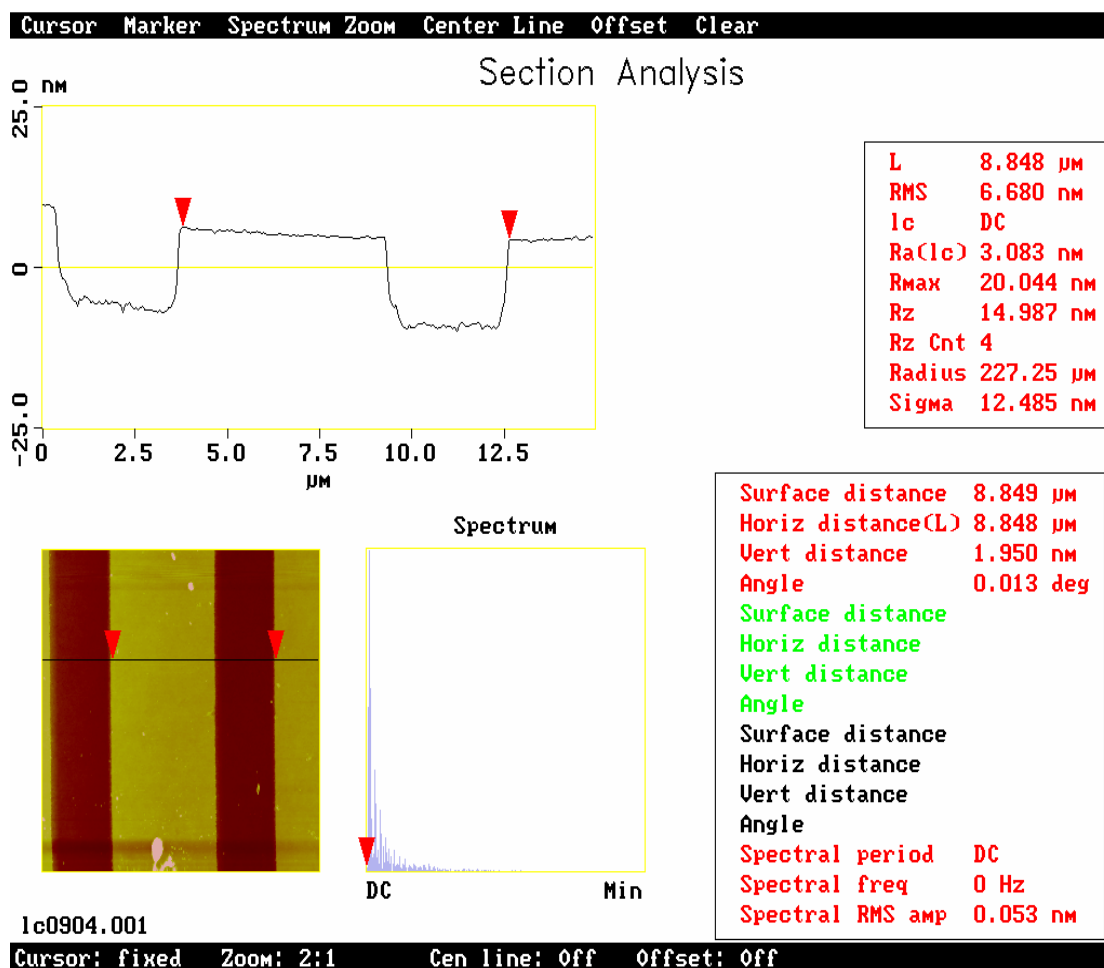


Fig. 2-3-5 AFM image of parallel grooved glass surface, which were prepared by RIE method with period of 9.0 μm.

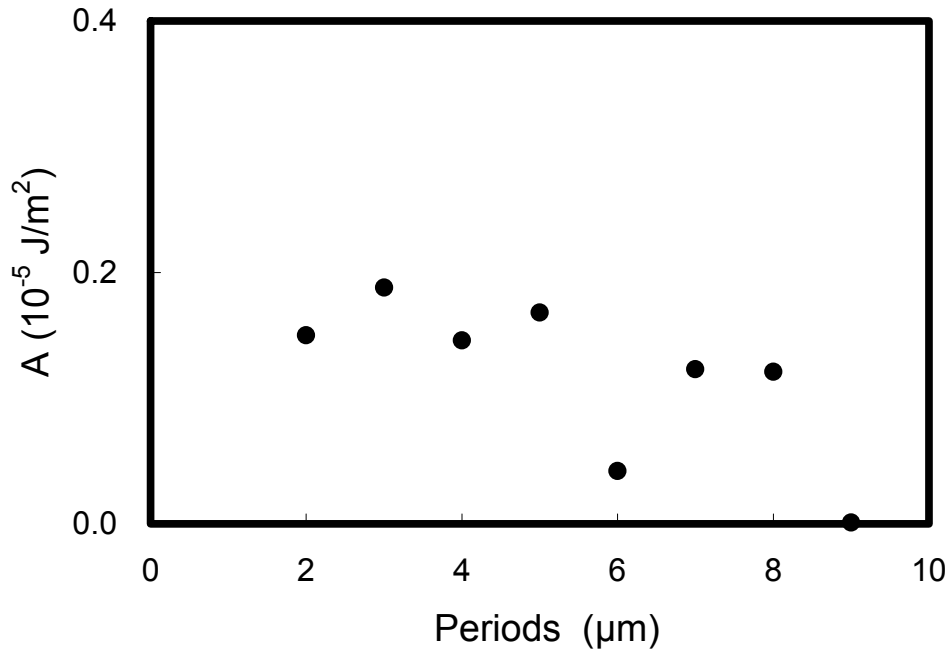


Fig. 2-3-6 Anchoring strength of RIE 1 minutes substrates with different groove periods ($2 \mu\text{m} \sim 9 \mu\text{m}$). The depth of grooves is $21 \pm 5 \text{ nm}$.

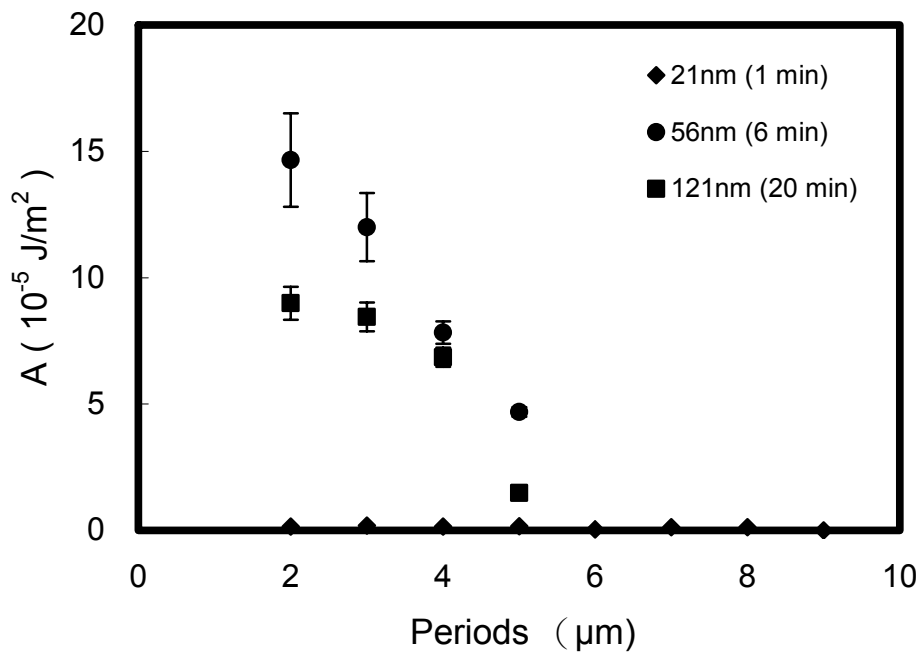


Fig. 2-3-7 Anchoring strength versus periods of grooves for various groove depth.

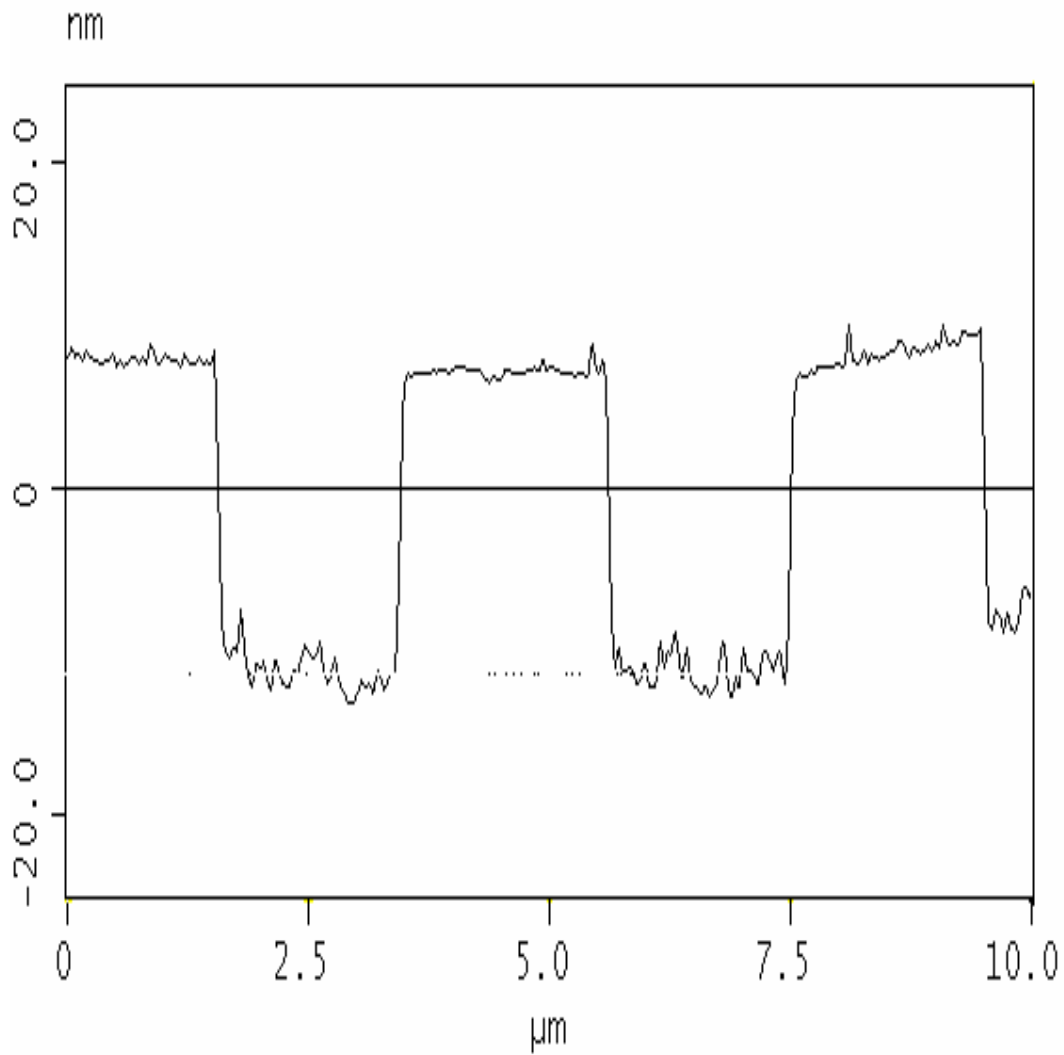


Fig. 3-1-1 AFM image of parallel grooved glass surface, which was prepared by RIE method with depth of 26 ± 5 nm and period of 4 μm .

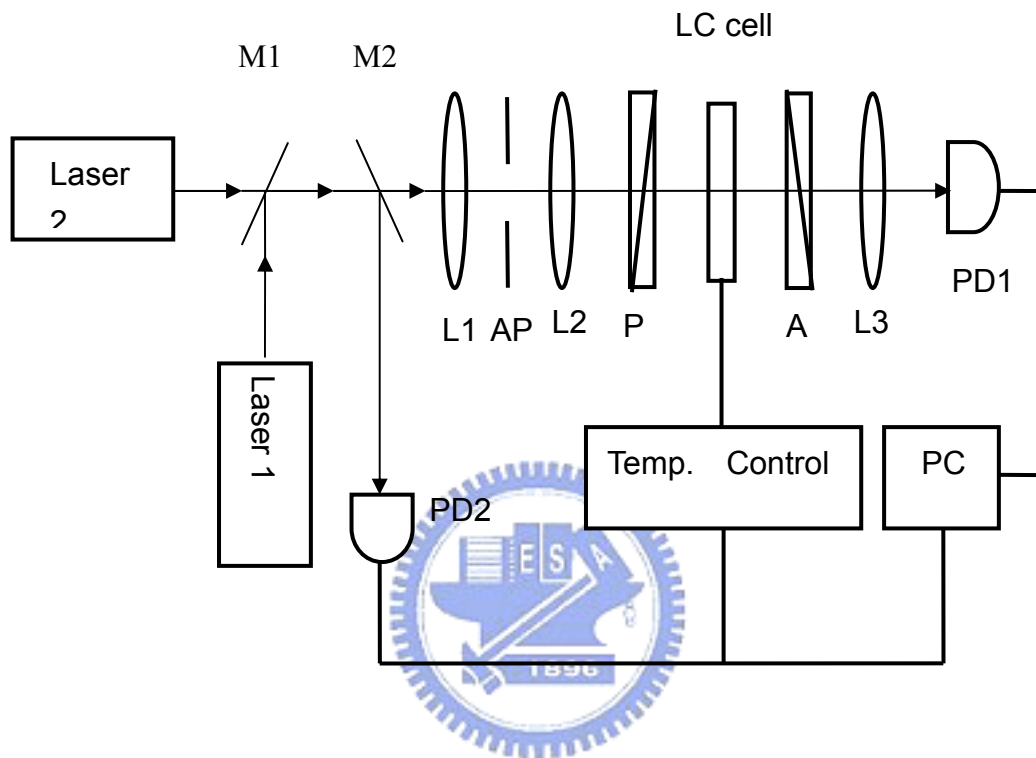
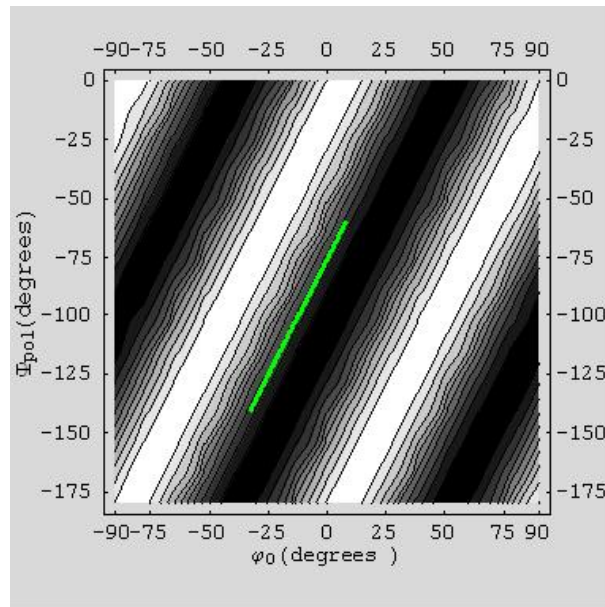


Fig. 3-2-1 Setup for anchoring strength measurement. Laser1 ($\lambda_1=632.8\text{nm}$): He-Ne laser, Laser2 ($\lambda_2=532.55\text{nm}$): Semiconductor laser, M1, M2: mirror, L1, L2, L3: lenses; AP: aperture; P: polarizer; A: analyzer; PD: photo-detector; PC: personal computer.

(a)



(b)

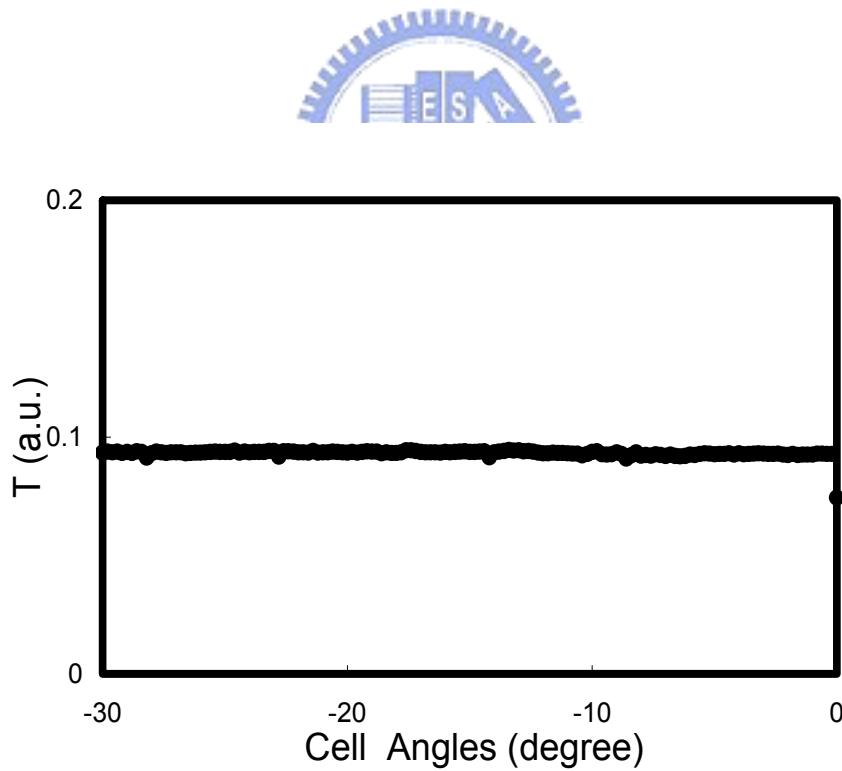


Fig. 3-2-2 (a) An example of calculated optical transmittance as a function of ψ_0 and ψ_{pol} in case where $\theta = 15^\circ$, $d\Delta n / \lambda = 3.5$. (b) The transmitted intensity versus incident angle, where the minimum does not exist.

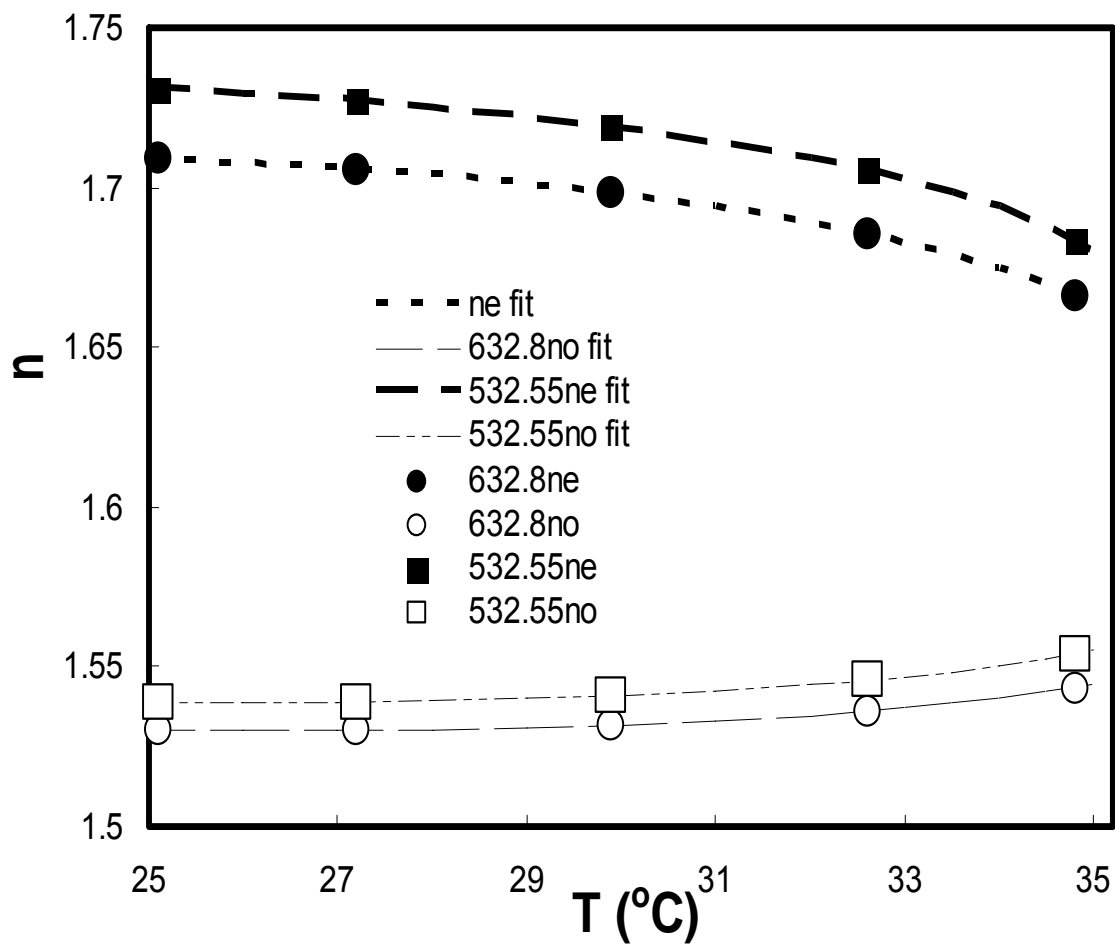


Fig.3-2-3 The relation of the refractive index and temperature. The values of refractive indices at various temperatures are interpolated from that measured by Wu et al.. S. T. Wu, and C. S. Wu, "Refractive index dispersions of liquid crystals", Opt. Eng. **32**(8), pp.1775-1780 (1993).

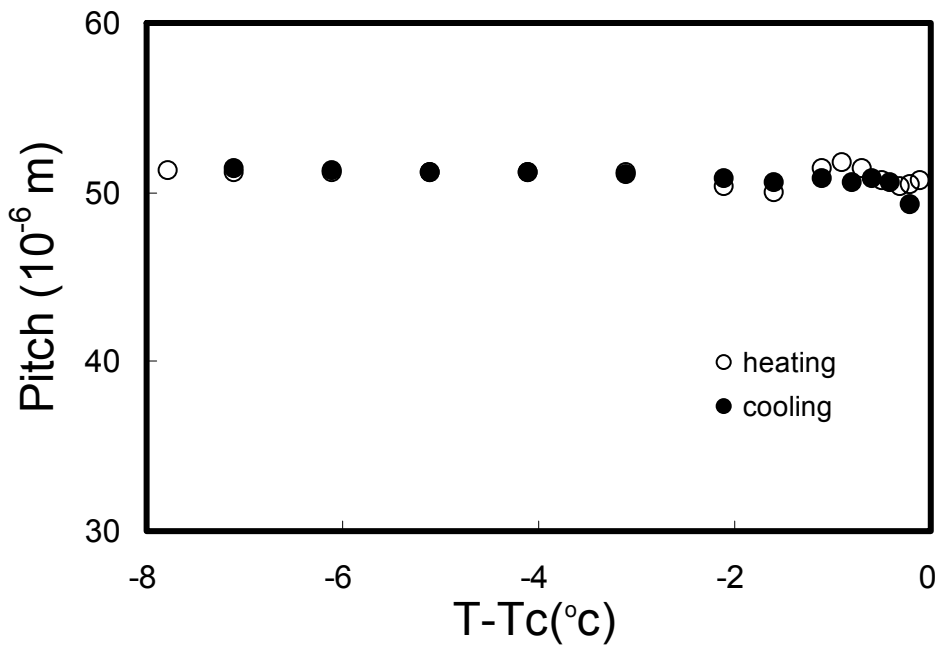


Fig. 3-3-1 Pitch versus temperature. The temperature is raised from 25°C to above T_c , and then lowered down to 25°C. Note that the pitch P_o remains a constant of $51.2 \pm 0.2 \mu\text{m}$ throughout this range except for temperatures near T_c , where the pitch becomes unstable.

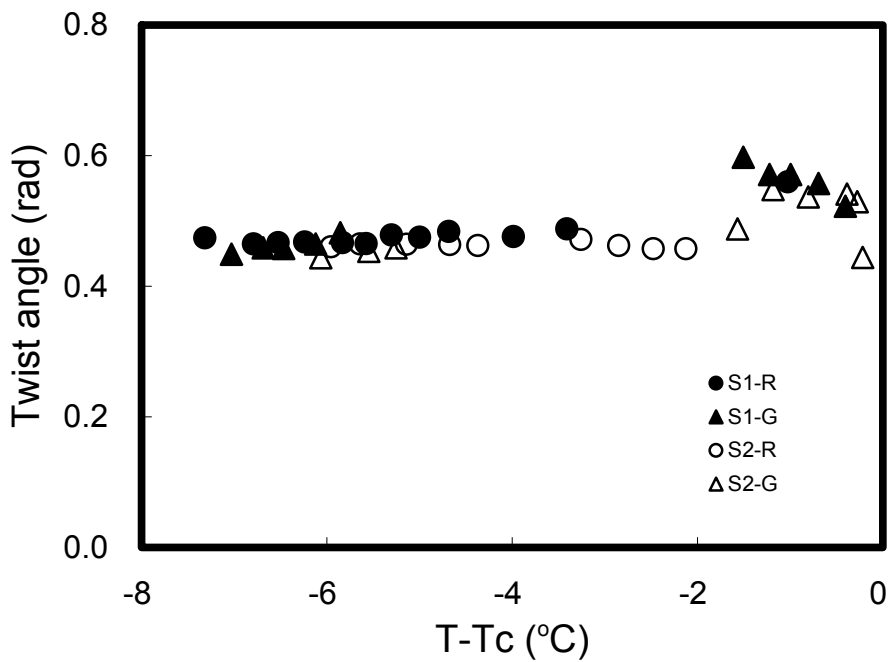


Fig. 3-3-2 Twist angle versus temperature. Circles: S1-R (λ_1); Triangle: S1-G (λ_2); Open circles: S2 (λ_1); Open triangle: S2 (λ_2).

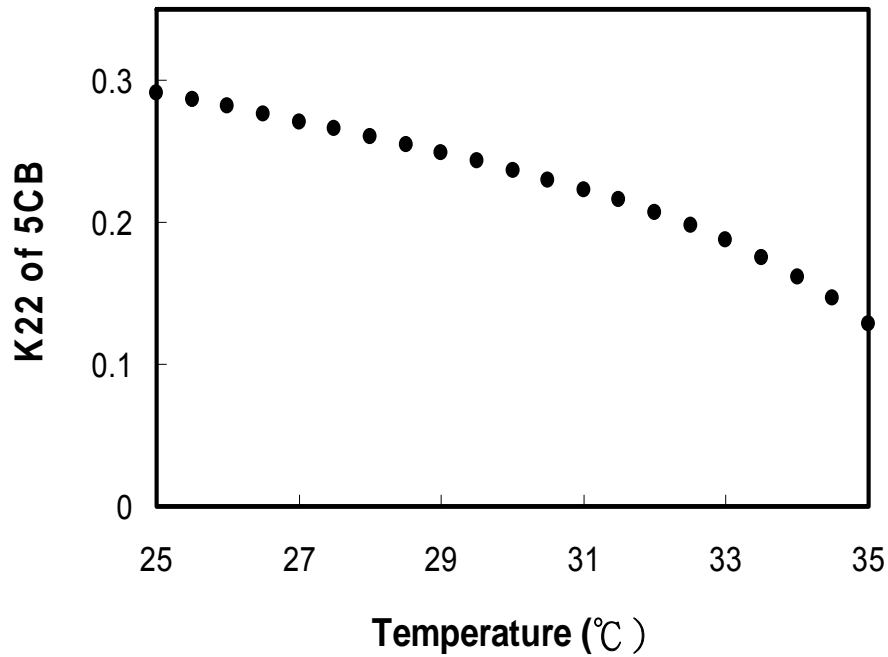


Fig. 3-3-3 K_{22} versus temperature. J. D. Bunning, T. E. Faber, and P. L. Sherrell, "The Frank constants of nematic 5CB at atmospheric pressure", J. Physique., **42**, pp. 1175-1182 (1981).

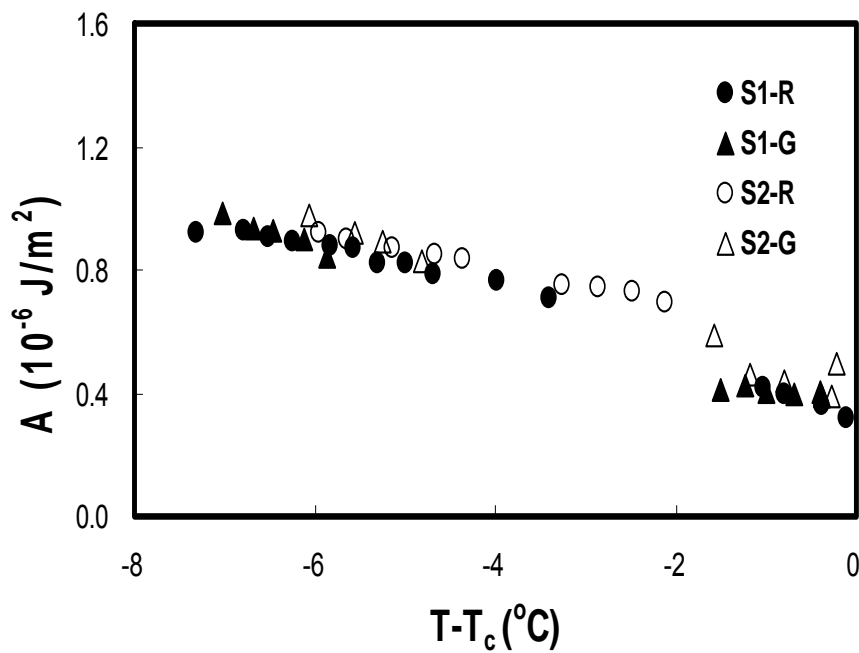
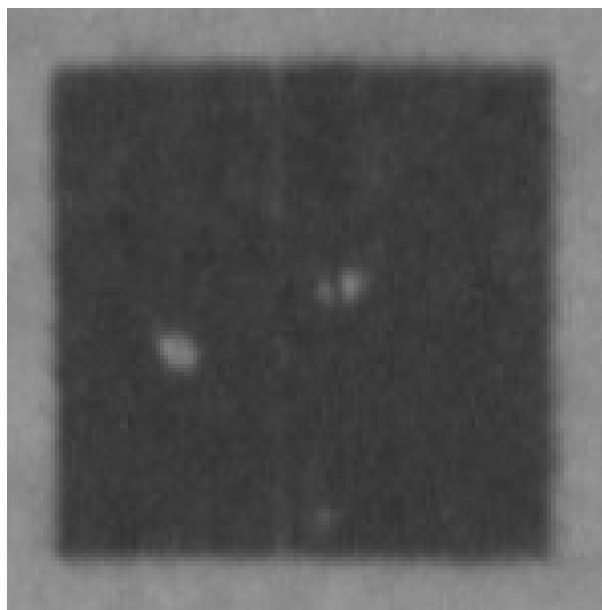


Fig. 3-3-4 Anchoring strength versus temperature . Circles: S1-R (λ_1); Triangle: S1-G (λ_2); Open circles: S2 (λ_1); Open triangle: S2(λ_2).

(a)



(b)

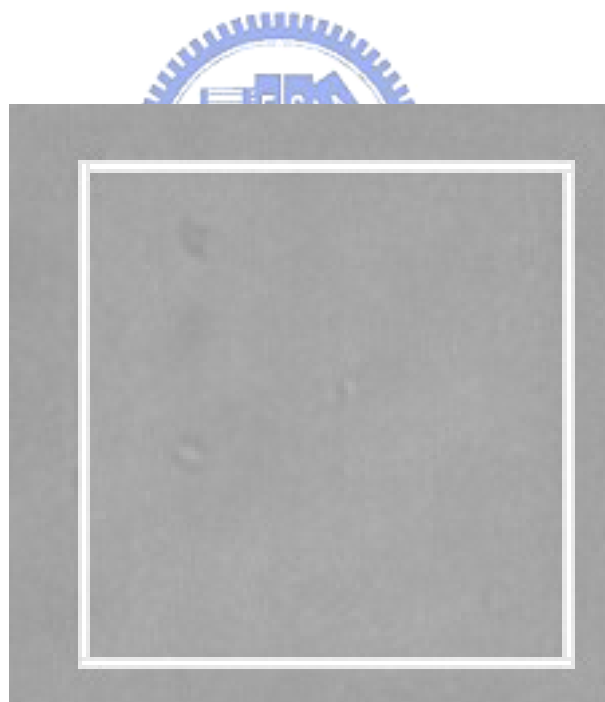


Fig. 4-3-1 The microscope picture of a parallel cell with modifying density 6.4 lines/ μm and the modified area is $80 \times 80 \mu\text{m}^2$ while the cell is between two crossed polarizers. (a) The modifying direction is parallel to the first polarizer; this is the darkest situation. (b) The modifying direction is with an angle of 45° from the polarizer direction, which gives the brightest situation. The white square in (b) is drawn to delineate the border of the modified region.

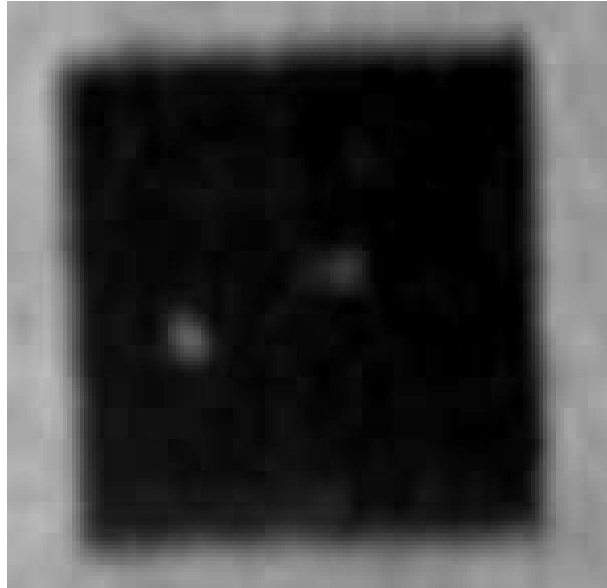


Fig. 4-3-2 The microscope picture of a TN cell made with same substrates as in Fig. 4-3-1. The cell is between two parallel polarizers, and the modifying direction parallel to the first polarizer.

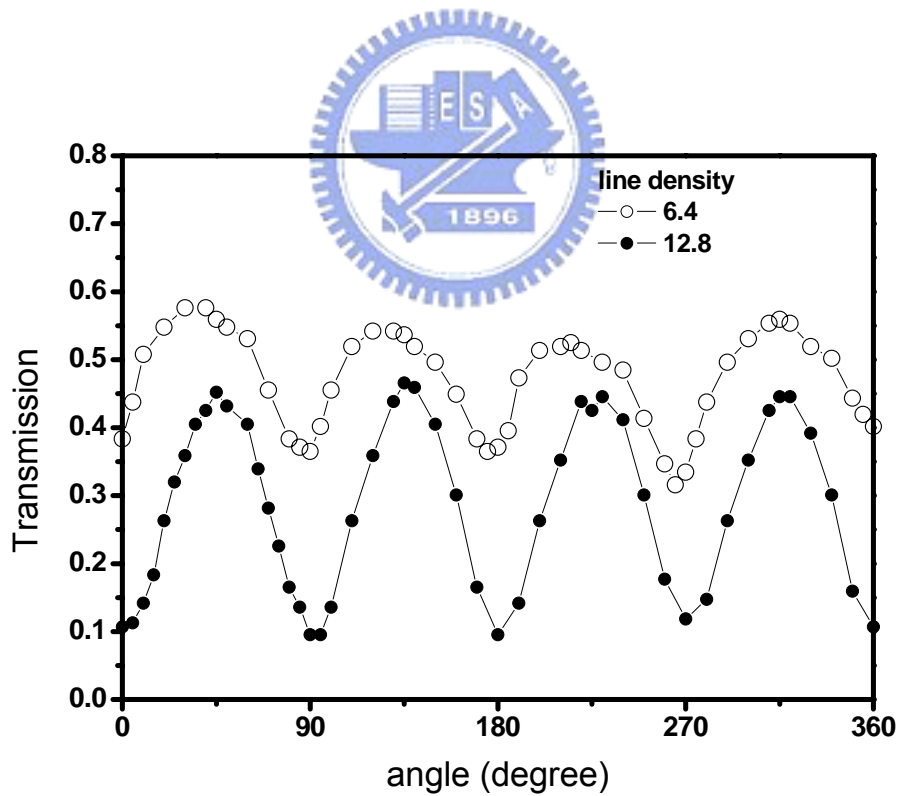
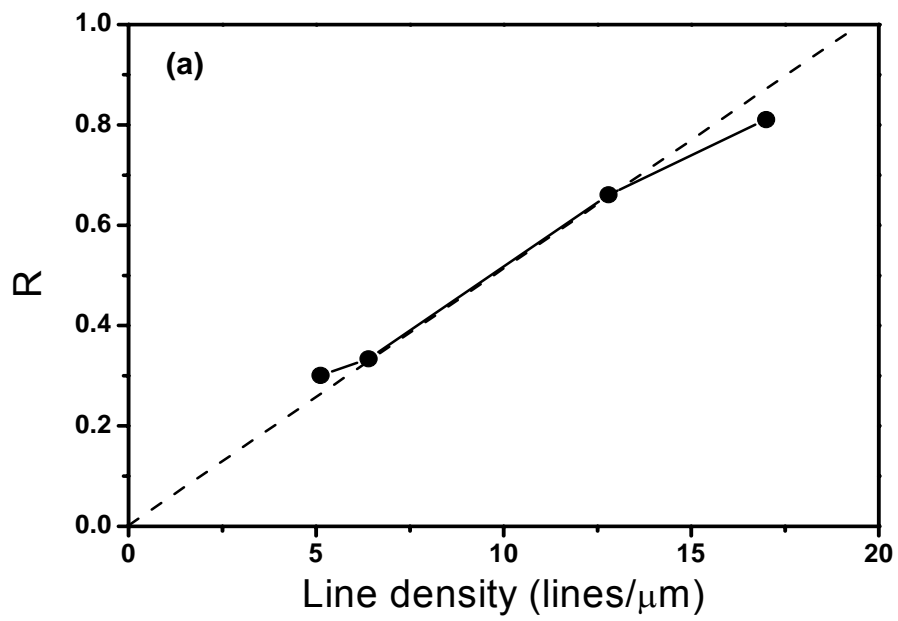


Fig.4-3-3. The transmission of two parallel cells between a pair of crossed polarizers vs. the angle of modifying direction with respect to the polarizer. The transmission is normalized at 1 for the case without sample and the two polarizers parallel to each other.

(a)



(b)

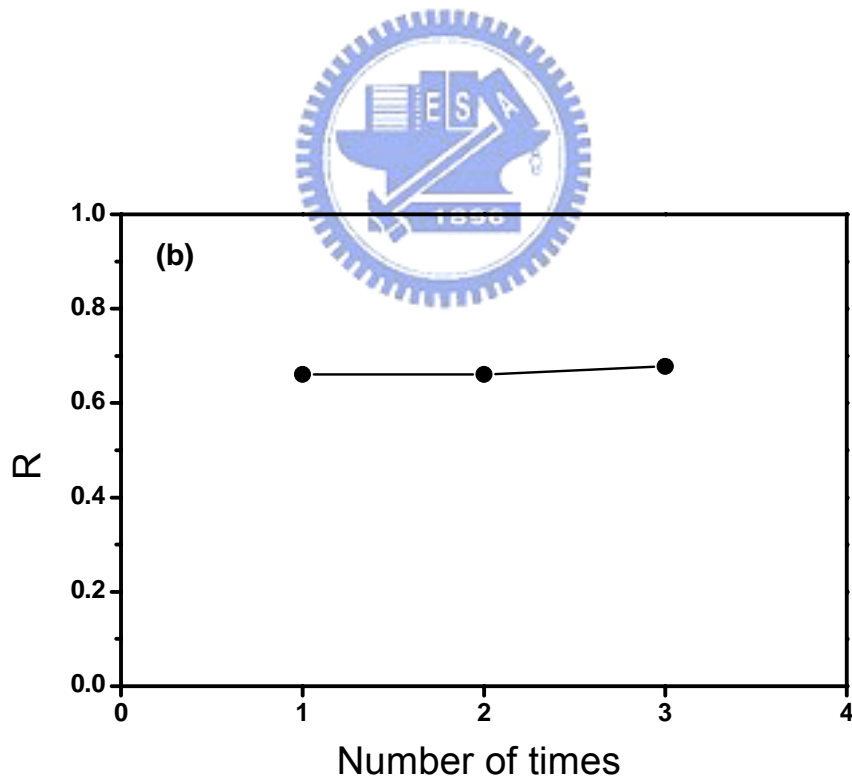
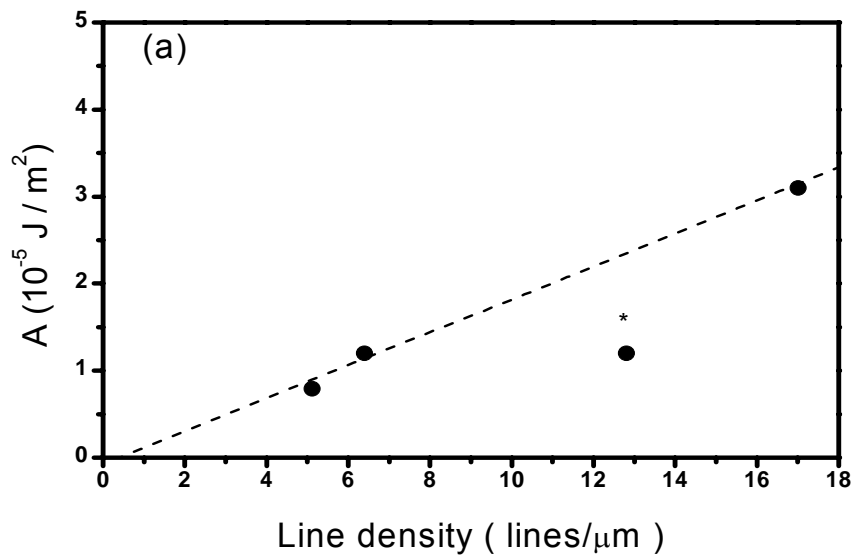


Fig.4-3-4. $R = (T_{max} - T_{min}) / (T_{max} + T_{min})$. (a) R vs. modifying density. The observing regions are modified only once. (b) The ratio R vs. number of times of modifying at same region. The modifying density is kept at 12.8 lines per μm .

(a)



(b)

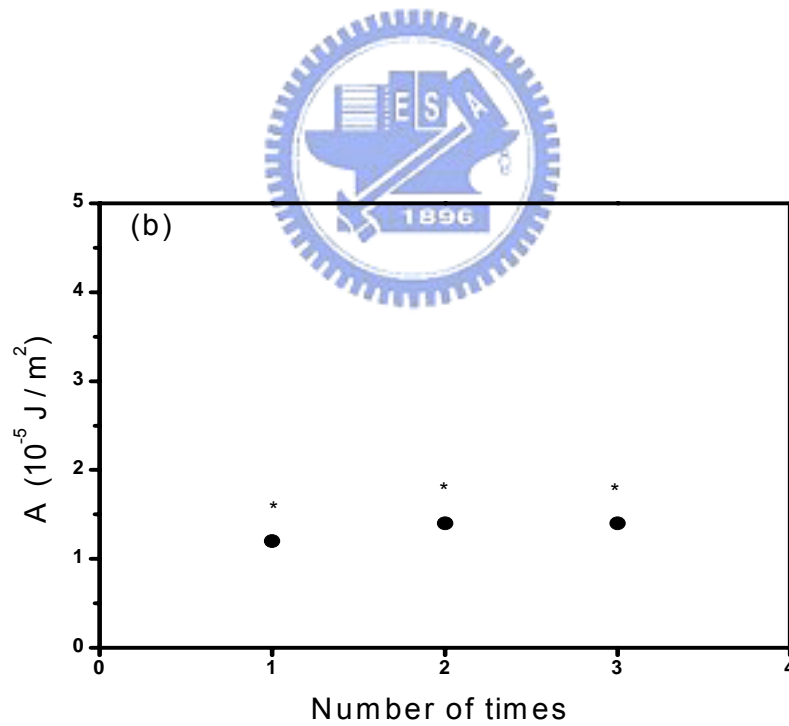
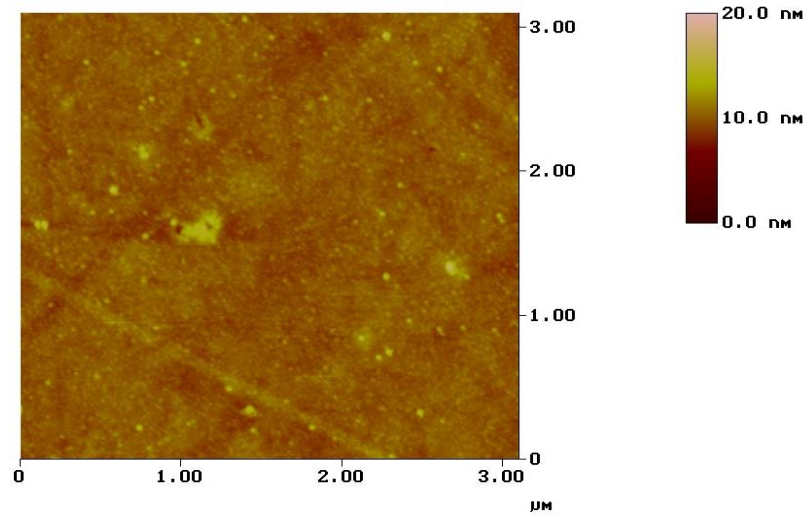


Fig.4-3-5. The anchoring strength, A . (a) The value of A vs. modifying density. The observed regions are modified only once. (b) The value of A vs. number of times of modifying at same region. The modifying density is kept at 12.8 lines per μm . The “*” mark by a data point indicates that point is measured with a parallel cell with chiral dopant in LC.

(a)



(b)

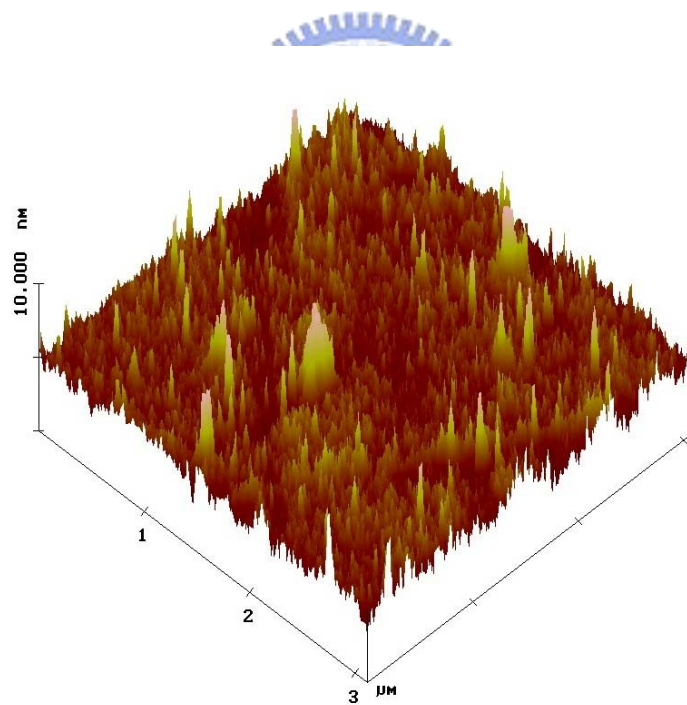


Fig.4-3-6. The AFM surface topology of the sample modified with line density 5.12 lines per μm . The scanning line density is 82.58 lines per μm , which is 16.1 times of the modify density. (a) 2-D surface topology (b) 3-D surface topology.

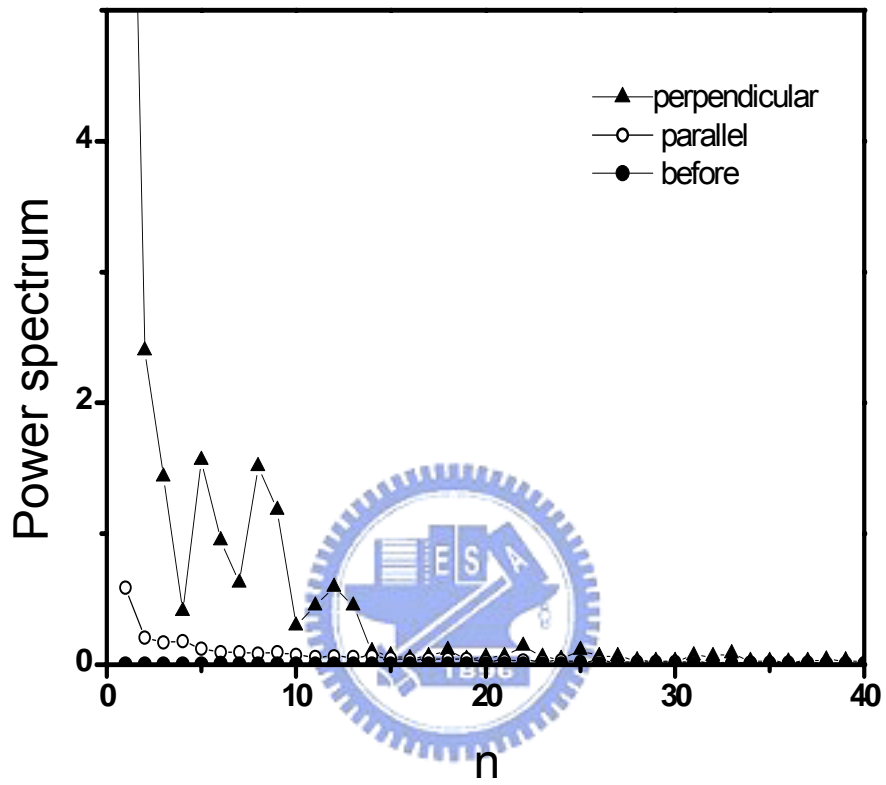


Fig.4-3-7. The Fourier analysis results for the sample shown in Fig. 6. If there were grooves formed by tip modifying, a peak for the “perpendicular” curve would appear at $n=16$.

Appendix A

Refractive Indices of 5CB as a Function of Temperature

In chapter 2, the refractive indices of 5CB used for fitting is published by R. G. Horn (reference in chapter 2, R. G. Horn, J. Physique., **39**, p.105, 1978). We used TABLE CURVE for fitting the data. The equation of the fitted curve is given as

$$n_e - n_o = 1.3727805 + 1.4580522E-1 T_n - 1.1831345E-4 T_n^2 \ln(T_n) - 1.5684267E-17 * e^{T_n} - 0.59246585 * T_n / \ln(T_n) \quad (A-1)$$

The fitted curve is shown in Fig.A-2, where $\Delta n = n_e - n_o$

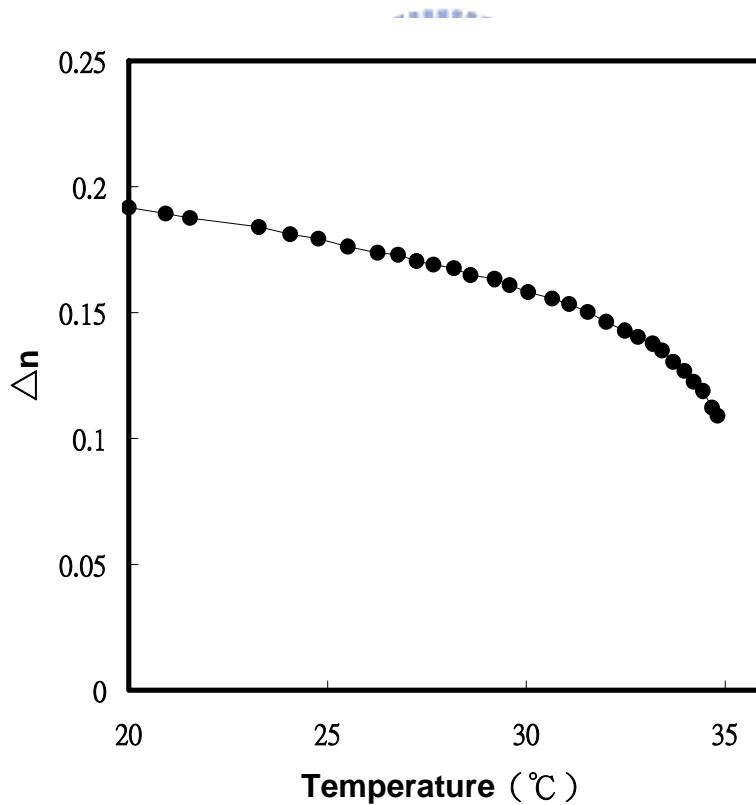


Fig.A-2 Fitted curve of Δn as a function of temperature.

Appendix B

Temperature Dependence of K_{11} , K_{22} , and K_{33} for 5CB

The data of temperature dependence of K_{11} , K_{22} , and K_{33} for 5CB have been published by J. D. Bunning *et al.* (reference in chapter 2, [8]).

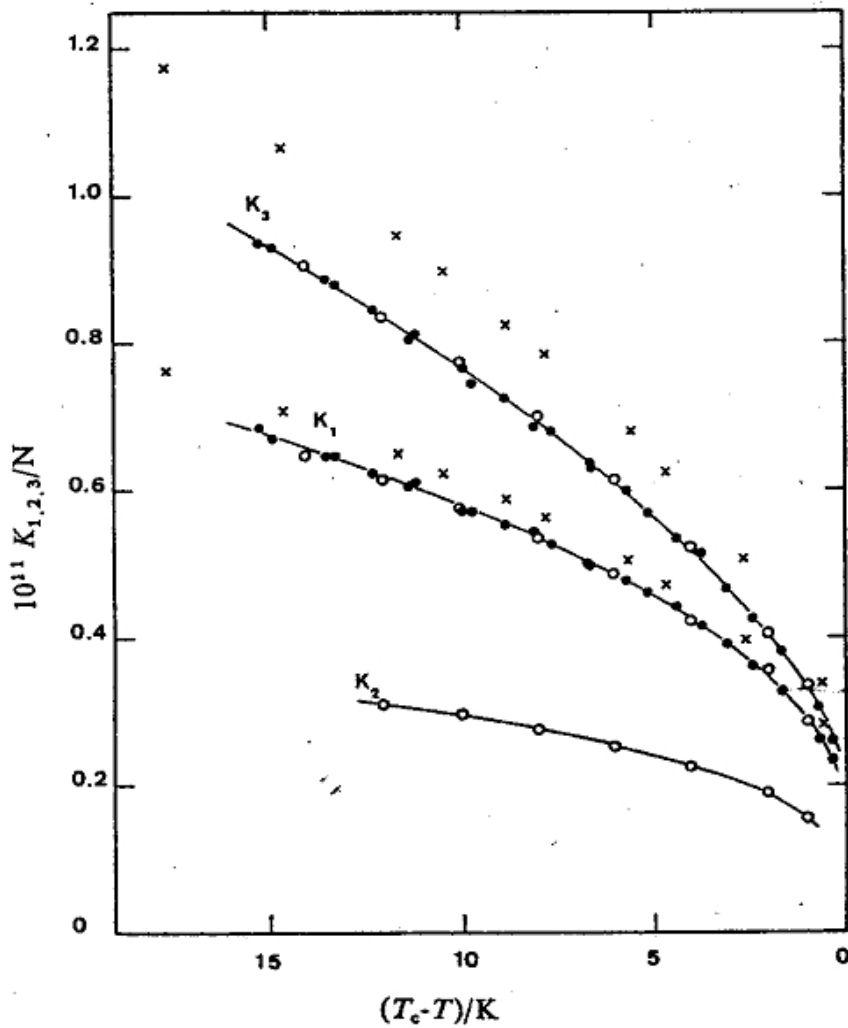


Fig. 4. — Temperature dependence of K_3 , K_1 and K_2 for 5CB : ●, specimens B and C ; ○, Karat and Madhusudana's results [1, 2] after scaling ; ×, unpublished data from Raynes *et al.*

Fig.B-1 Temperature dependence of K_{11} , K_{22} , and K_{33} for 5CB. J. D. Bunning, T. E. Faber, and P. L. Sherrell, "The Frank constants of nematic 5CB at atmospheric pressure", *J. Physique.*, **42**, pp.1175-1182 (1981).

Appendix C

Anchoring Strength for Different Depths and Periods

The periods of U-shape grooves were varied from 2 μm to 9 μm in this study. We obtained three different depths by changing the etching time in the RIE process. The depths were 21 ± 5 nm, 56 ± 6 nm, and 121 ± 5 nm for etching time 1 (Table C-1), 6 (Table C-2), and 20 (Table C-3) minutes, respectively.

Table C-1 RIE 1min

RIE 1min	Temp	A (J/m ²)	Average of A	Depth (nm)	Protrusion (μm)
2um	25.66	1.50E-06	1.50E-06	27.8	0.703
	25.68	1.50E-06			
	25.62	1.50E-06			
3um	25.5	1.89E-06	1.88E-06	27.55	0.821
	25.49	1.91E-06			
	25.48	1.84E-06			
4um	25.57	1.46E-06	1.46E-06	26.01	2.169
	25.5	1.45E-06			
	25.48	1.48E-06			
5um	25.23	1.68E-06	1.68E-06	26.6	2.636
	25.2	1.68E-06			
	25.12	1.68E-06			
6um	25.42	4.19E-07	4.19E-07	13.82	4.044
7um	25.49	1.27E-06	1.23E-06	13.84	4.91
	25.47	1.23E-06			
	25.43	1.19E-06			
8um	25.5	1.23E-06	1.21E-06	15.42	4.843
	25.36	1.20E-06			
	25.37	1.20E-06			
9um	25.39	2.26E-09	1.05E-08	13.75	5.357
	25.48	1.86E-08			
	25.52	1.05E-08			

Table C-2 RIE 6min

RIE 6min	Temp	A (J/m²)	Average of A	Depth (nm)	Protrusion (μm)
2um	25.7	1.49E-04	1.46E-04	52.29	0.782
	26.1	1.42E-04			
3um	25.49	1.29E-04	1.20E-04	50.95	1.406
	25.39	1.15E-04			
	25.3	1.16E-04			
4um	25.18	7.31E-05	7.83E-05	52.7	1.718
	25.32	7.60E-05			
	25.35	8.57E-05			
5um	25.52	4.75E-05	4.69E-05	62.27	2.364
	25.47	4.63E-05			

Table C-3 RIE 20min

RIE 20min	Temp	A (J/m²)	Average of A	Depth (nm)	Protrusion (μm)
2um	25.37	8.96E-05	8.99E-05	125.61	0.880
	25.28	9.02E-05			
3um	25.51	8.37E-05	8.45E-05	117.49	1.217
	25.52	8.61E-05			
	2.54	8.37E-05			
4um	25.51	6.36E-06	6.38E-06	126.36	2.246
	25.57	6.52E-06			
	25.72	6.26E-06			
5um	25.42	1.46E-05	1.48E-05	118.81	2.383
	25.44	1.49E-05			
	25.48	1.49E-05			

Appendix D

Refractive Indices of 5CB (for Wavelength 632.8nm and 532.55nm) as a Function of Temperature

The values of refractive indices (see Fig. 3-2-3) at various temperatures are interpolated from that measured by Wu et al. (reference in chapter 3, S. T. Wu, and C. S. Wu, “Refractive index dispersions of liquid crystals”, Opt. Eng. **32**(8), pp. 1775-1780 (1993)). We choice a power series as

$$n \approx c_1 + \frac{c_2}{\lambda^2} \quad . \quad (D-1)$$

Two appropriated wavelength at a fixed temperature to solve c_1 and c_2 (c_1 and c_2 are expansion coefficients). We obtained the relations of the refractive indices and temperature (Fig. 3-2-3). The values of refractive indices at various temperatures are interpolated from Table A1~A5 in the reference, and are shown in Table D-1~D-2.

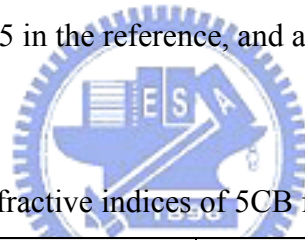


Table D-6 Refractive indices of 5CB for $\lambda=532.55\text{nm}$

$\lambda_1(\mu\text{m})$	$\lambda_2(\mu\text{m})$	n_{e1}	n_{e2}	$T(^{\circ}\text{C})$	532.55 n_e
0.5317	0.5361	1.7312	1.7298	25.1	1.730927
0.5294	0.5338	1.728	1.7267	27.2	1.727066
0.5288	0.5333	1.7199	1.7186	29.9	1.718814
0.5295	0.5341	1.7062	1.7049	32.6	1.705334
0.5292	0.5341	1.6839	1.6828	34.8	1.683145
$\lambda_1(\mu\text{m})$	$\lambda_2(\mu\text{m})$	n_{o1}	n_{o2}	$T(^{\circ}\text{C})$	532.55 n_o
0.5306	0.5373	1.539	1.5383	25.1	1.538794
0.5309	0.5374	1.5392	1.5384	27.2	1.538994
0.5263	0.5326	1.5418	1.5409	29.9	1.540907
0.5304	0.5367	1.546	1.5451	32.6	1.545689
0.5312	0.5374	1.5542	1.5532	34.8	1.553979

Table D-7 Refractive indices of 5CB for $\lambda=632.8\text{nm}$

$\lambda_1(\mu\text{m})$	$\lambda_2(\mu\text{m})$	n_{e1}	n_{e2}	$T(^{\circ}\text{C})$	632.8 n_e
0.6298	0.6367	1.7094	1.7084	25.1	1.708961
0.6273	0.6341	1.7065	1.7055	27.2	1.705689
0.6281	0.6351	1.6988	1.6978	29.9	1.698125
0.6318	0.6391	1.6854	1.6845	32.6	1.685275
0.6303	0.638	1.6664	1.6657	34.8	1.66617
$\lambda_1(\mu\text{m})$	$\lambda_2(\mu\text{m})$	n_{o1}	n_{o2}	$T(^{\circ}\text{C})$	632.8 n_o
0.6242	0.6339	1.5305	1.5299	25.1	1.529967
0.6243	0.6339	1.5306	1.5299	27.2	1.529979
0.6262	0.6358	1.5321	1.5315	29.9	1.531685
0.6308	0.6406	1.5361	1.5356	32.6	1.535996
0.6295	0.639	1.5437	1.543	34.8	1.543453



國立交通大學電子物理系 博士候選人資料

姓 名：林雅峰

性 別：男

出生年月日：53年3月6日

籍 貫：臺灣省新竹市

地 址：新竹市建功一路115號10樓

學歷：

畢 業 學 校	學 位	起 訖 年 月
文化大學物理系	學 士	75年9月 ~ 78年6月
淡江大學物理系	碩 士	78年9月 ~ 81年6月
交通大學電子物理系	博士(肄業)	83年9月 ~ 94年7月
交通大學電子物理系	博士	94年9月 ~ 96年7月

經歷：

服 務 單 位	職 位	起 訖 年 月
清華大學材料中心	研究助理	80年6月 ~ 83年7月
		年 月 ~ 年 月
		年 月 ~ 年 月
		年 月 ~ 年 月

論文題目：

中文：液態晶體表面配向之新方法及其特性研究

英文：Study of Liquid Crystal Surface Alignment: New Methods and the Properties

List of Publication

A. Journal Papers

1. Ru-Pin Pan, Hua-Yu Chiu, **Yea-Feng Lin**, and J. Y. Huan, “Surface topography and alignment effects in UV-modified polyimide films with micron size patterns”, Chinese Journal of Physics, Vol. 41, No. 2, pp. 177-184 (2003).
2. Chao-Yuan Chen, Cho-Fan Hsieh, **Yea-Feng Lin**, Ru-Pin Pan, Ci-Ling Pan, “Magnetically tunable room-temperature 2π liquid crystal terahertz phase shifter”, Optics Express, Vol. 12, No. 12, pp. 2625-2630 (2004).
3. Tsung-Sheng Shih, Yu-Ping Lan, **Yea-Feng Lin**, Ru-Pin Pan, Ci-Ling Pan, “Single-longitudinal-mode semiconductor laser with digital and mode-hop-free fine-tuning mechanism”, Optics Express, Vol. 12, No. 26, pp. 6434-6439 (2004).
4. **Yea-Feng Lin**, Ming-Chao Tsou, and Ru-Pin Pan, “Alignment of liquid crystals by ion etched grooving glass surfaces”, Chinese Journal of Physics, Vol. 43, No. 6, pp. 1066-1073 (2005).
5. **Yea-Feng Lin**, Shin-Ying Lu, and Ru-Pin Pan, “Temperature Dependence of Azimuthal Anchoring Strength of Liquid Crystal on Micro-grooved Glass Substrate”, Japanese Journal of Applied Physics, Vol. 44, No. 12, pp. 8552-8556 (2005).
6. Yu-Ping Lan, **Yea-Feng Lin**, Yu-Tai Li, Ru-Pin Pan, Chao-Kuei Lee, Ci-Ling Pan, “Intracavity measurement of liquid crystal layer thickness by wavelength tuning of an external cavity laser diode”, Optics Express, Vol. 13, No. 20, pp. 7905-7912 (2005).

B. International Conference Papers

1. Ru-Pin Pan, Sheng-Hsien Lin, Yih-Chuu Wu, **Yea-Feng Lin**, and Ray-Hung Huang, “Surface induced orientational ordering in liquid crystals with variable surface anchoring strength”, 17th International Liquid Crystal Conference, p.44 (1998)
2. Ru-Pin Pan, Yih-Chuu Wu, **Yea-Feng Lin**, and Ray-Hung Huang, “Surface induced

orientational ordering in liquid crystalline mixture”, 國際華人液晶研討會, pp. 37-40 (1998)

3. **Yea-Feng Lin**, Ming-Chao Tsou, Thunter Huang and Ru-Pin Pan, ” Alignment of liquid crystals by grooved glass surfaces”, 19th International Liquid Crystal Conference, p.368 (2002)

